

QUANTUM MECHANICAL CALCULATION OF
NITROUS OXIDE DECOMPOSITION ON TRANSITION METALS

A THESIS SUBMITTED TO
THE GRADUATE SCHOOL OF NATURAL AND APPLIED SCIENCES
OF
MIDDLE EAST TECHNICAL UNIVERSITY

BY

MUZAFFER KAAAN KARAÖZ

IN PARTIAL FULFILLMENT OF THE REQUIREMENTS
FOR
THE DEGREE OF MASTER OF SCIENCE
IN
CHEMICAL ENGINEERING

NOVEMBER 2007

Approval of the Thesis

**QUANTUM MECHANICAL CALCULATION OF NITROUS OXIDE
DECOMPOSITION ON TRANSITION METALS**

submitted by **MUZAFFER KAN KARAÖZ** in partial fulfillment of the requirements for the degree of **Master of Science in Chemical Engineering** by,

Prof. Dr. Canan Özgen
Dean, Graduate School of **Natural and Applied Sciences** _____

Prof. Dr. Gürkan Karakaş
Head of Department, **Chemical Engineering** _____

Prof. Dr. Işık Önal
Supervisor, **Chemical Engineering, METU** _____

Examining Committee Members:

Prof. Dr. Hayrettin Yücel
Chemical Engineering, METU _____

Prof. Dr. Işık Önal
Chemical Engineering, METU _____

Prof. Dr. Suzan Kıncal
Chemical Engineering, METU _____

Assoc. Prof. Dr. Naime Aslı Sezgi
Chemical Engineering, METU _____

Prof. Dr. Şakir Erkoç
Physics, METU _____

Date: November 9, 2007

I hereby declare that all information in this document has been obtained and presented in accordance with academic rules and ethical conduct. I also declare that, as required by these rules and conduct, I have fully cited and referenced all material and results that are not original to this work.

Name, Last name: MUZAFFER KAAN KARAÖZ

Signature:

ABSTRACT

QUANTUM MECHANICAL CALCULATION OF NITROUS OXIDE DECOMPOSITION ON TRANSITION METALS

Karaöz, Muzaffer Kaan

M.S., Department of Chemical Engineering

Supervisor: Prof. Dr. Işık Önal

November 2007, 116 pages

Nitrous oxide decomposition on Ag_{51} , Au_{51} , Pt_{22} , Rh_{51} and Ir_{51} clusters representing (111) surface were studied quantum mechanically by using the method of ONIOM with high layer DFT region and low layer of molecular mechanics region utilizing universal force field (UFF).

The basis set employed in the DFT calculations is the Los Alamos LANL2DZ effective core pseudo-potentials (ECP) for silver, gold, platinum, rhodium and iridium and 3-21G** for nitrogen, oxygen and hydrogen. Nitrous oxide was

decomposed on the all metal surfaces investigated in this study by leaving oxygen atom adsorbed as supported by experimental findings.

Activation energies of nitrous oxide decomposition on Ag₅₁, Au₅₁, Pt₂₂, Rh₅₁ and Ir₅₁ representing (111) surface are calculated as 14.48 kcal/mol, 15.72 kcal/mol, 7.02 kcal/mol, 3.76 kcal/mol and 5.51 kcal/mol, respectively. Based on these results, decomposition of nitrous oxide occurs on Rh more easily than other metals.

KEYWORDS: DFT, ONIOM, nitrous oxide decomposition, transition metals.

ÖZ

GEÇİŞ METALLERİ ÜZERİNDE DİAZOT MONOKSİT DEKOMPOZİSYONUNUN KUANTUM MEKANİKSEL OLARAK İNCELENMESİ

Karaöz, Muzaffer Kaan

Yüksek Lisans, Kimya Mühendisliği Bölümü

Tez Yöneticisi: Prof. Dr. Işık Önal

Kasım 2007, 116 sayfa

Ag₅₁, Au₅₁, Pt₂₂, Rh₅₁ and Ir₅₁ topakları temsili (111) yüzeyi üzerinde diazot monoksit dekompozisyonu, üst katmanı DFT bölgesinden ve alt katmanı evrensel kuvvet alanı (UFF) kullanılan moleküler mekanik bölgesinden mevcut ONIOM yöntemi kullanılarak kuantum mekaniksel olarak incelenmiştir.

Gümüş, altın, platin, rodyum ve iridyum için DFT hesaplamalarında uygulanan dalga fonksiyonu seti Los Alamos LANL2DZ etkin çekirdek pseudo-potansiyeli

(ECP) ve azot, oksijen ve hidrojen için 3-21G** kullanılmıştır. Diazot monoksit bu metal yüzeylerinin hepsinde, deneysel bulguların da desteğinde yüzeyde adsorplanan bir oksijen atomu bırakarak dekompoze olur.

Ag₅₁, Au₅₁, Pt₂₂, Rh₅₁ and Ir₅₁ topakları temsili (111) yüzeyi üzerinde diazot monoksit dekompozisyonu aktivasyon enerjileri her biri için sırasıyla 14,48 kcal/mol, 15,72 kcal/mol, 7,02 kcal/mol, 3,76 kcal/mol and 5,51 kcal/mol olarak hesaplanmıştır. Bu sonuçlara göre diazot monoksit Rh üzerinde daha kolay dekompoze olmaktadır.

Anahtar kelimeler: DFT, ONIOM, diazot monoksit dekompozisyonu, geçiş metalleri.

To My Mother

ACKNOWLEDGEMENTS

First of all, I would like to express my sincere appreciation to my supervisor Prof. Dr. Işık Önal for his guidance, valuable discussions, criticism and comments throughout this study.

I wish to thank my family for their encouragement and great support.

I would like to thank to Mehmet Ferdi Fellah and Derya Düzenli for their support and valuable friendship during this investigation.

TABLE OF CONTENTS

ABSTRACT	iv
ÖZ.....	vi
ACKNOWLEDGEMENTS	ix
TABLE OF CONTENTS	x
LIST OF TABLES	xii
LIST OF FIGURES.....	xiv
NOMENCLATURE.....	xvii
CHAPTERS	
1. INTRODUCTION.....	1
1.1. Nitrous Oxide	1
1.2. Uses of Nitrous Oxide as an Oxidant	3
1.3. Nitrous Oxide Decomposition Catalysts	4
1.4. Aim of This Study	9
2. LITERATURE SURVEY	12
2.1. Experimental Studies Regarding N ₂ O Decomposition	12
2.2. Theoretical Studies Regarding N ₂ O Decomposition.....	18
3. METHODOLOGY	20
3.1. ONIOM	20
3.2. Computational Procedure.....	38

4. RESULTS AND DISCUSSION	42
4.1. N ₂ O Decomposition Over Ag ₅₁ Cluster Representing (111) Surface ..	42
4.2. N ₂ O Decomposition Over Au ₅₁ Cluster Representing (111) Surface ..	50
4.3. N ₂ O Decomposition Over Pt ₂₂ Cluster Representing (111) Surface....	56
4.4. N ₂ O Decomposition Over Rh ₅₁ Cluster Representing (111) Surface...	62
4.5. N ₂ O Decomposition Over Ir ₅₁ Cluster Representing (111) Surface.....	67
5. CONCLUSIONS	72
REFERENCES	74
APPENDICES	
A. SAMPLE INPUT AND OUTPUT FILES OF GAUSSIAN 2003	89
B. DENSITY FUNCTIONAL THEORY	106

LIST OF TABLES

Table 1.1. Estimated amounts of N ₂ O emitted by various human activities.....	2
Table 3.1. Inclusion of Specific Interactions in the Standard (Mechanical Embedding) ONIOM (QM:MM) Energy Expression For The Specific Example of Histidine (Vreven, 2006)	31
Table 3.2. Inclusion of Specific Interactions in the Generic Electronic Embedding QM/MM Energy Expression, with the Charges on C3 and C5 Scaled to Zero in the Model System Calculations ^a	33
Table 3.3. Inclusion of Specific Interactions in the Electronic Embedding ONIOM (QM:MM) Energy Expression, with the Charges on C3 and C5 Scaled to Zero in the Model System Calculations ^a (Vreven, 2006) ^a	35
Table 4.1. Activation barrier (E _a) and enthalpy of reaction (ΔH) on Ag (in kcal/mol).....	47
Table 4.2. Ag-O bond distance in this investigation comparing to literature data (Å)	48
Table 4.3. Activation barrier (E _a) and enthalpy of reaction (ΔH) on Au (in kcal/mol).....	51
Table 4.4. Au-O bond distance in this investigation comparing to literature data (Å)	54

Table 4.5. Activation barrier (E_a) and enthalpy of reaction (ΔH) on Pt in kcal/mol).....	57
Table 4.6. Pt-O bond distance in this investigation comparing to literature data (\AA)	60
Table 4.7. Activation barrier (E_a) and enthalpy of reaction (ΔH) on Rh (in kcal/mol).....	64
Table 4.8. Rh-O bond distance in this investigation comparing to literature data (\AA)	65
Table 4.9. Activation barrier and enthalpy of reaction (ΔH) on Ir in (kcal/mol)	71
Table 4.10. Ir-O bond distance in this investigation comparing to literature data (\AA)	71
Table A.1 Gaussian input file for coordinate driving of nitrous oxide decomposition on Ag_{51} cluster representing (111) surface	89
Table A.2 Gaussian output file for coordinate driving of nitrous oxide decomposition on Ag_{51} cluster representing (111) surface	93

LIST OF FIGURES

Figure 1.1. N ₂ O molecule (Partington, 1989)	1
Figure 1.2. Reactant and model surface for nitrous oxide decomposition over TM ₅₁ cluster representing (111) surface (TM=Ag, Au, Ir, Pt, Rh)	9
Figure 1.3. Product and model surface for nitrous oxide decomposition over TM ₅₁ cluster representing (111) surface (TM=Ag, Au, Ir, Pt, Rh)	10
Figure 3.1. ONIOM terminology using ethane as an example (Vreven, 2006) ..	24
Figure 3.2. QM/MM terminology using ethane as an example (Vreven, 2006) .	25
Figure 3.3. Real system, QM/MM partitioning, and model system for the (H18) deprotonation of histidine (Vreven, 2006).	30
Figure 3.4. Error of ONIOM-EE and QM/MM-EE as a function of the charges scaled based on distance from the QM region. (Vreven, 2006)	37
Figure 3.5. Enlarged silver cluster.....	39
Figure 3.6. Reduced Silver (111) Surface	40
Figure 4.1. Ag ₅₁ cluster representing (111) surface and optimized N ₂ O i) Side view ii) Top view	43
Figure 4.2. Distances of O1 between the selected Ag atoms in the input geometry for N ₂ O decomposition.....	45
Figure 4.3. Energy profile of N ₂ O decomposition on Ag ₅₁ cluster representing (111) surface.....	46

Figure 4.4. Adsorbed oxygen atom on Ag ₅₁ cluster representing (111) surface and N ₂ molecule after N ₂ O decomposition from different two sides of view, i and ii.....	49
Figure 4.5. Distances of O1 between the selected Au atoms in the input geometry for N ₂ O decomposition.....	51
Figure 4.6. Energy profile of N ₂ O decomposition on Au ₅₁ cluster representing (111) surface.....	53
Figure 4.7. Adsorbed oxygen atom on Au ₅₁ cluster representing (111) surface and N ₂ molecule after N ₂ O decomposition from different two sides of view, i and ii.....	55
Figure 4.8. Distances of O1 between the selected Pt atoms in the input geometry for N ₂ O decomposition.....	57
Figure 4.9. Energy profile of N ₂ O decomposition on Pt ₂₂ cluster representing (111) surface.....	58
Figure 4.10. Adsorbed oxygen atom on Pt ₂₂ cluster representing (111) surface and N ₂ molecule after N ₂ O decomposition from different two sides of view, i and ii.....	61
Figure 4.11. Distances of O1 between the selected Rh atoms in the input geometry for N ₂ O decomposition	63
Figure 4.12. Energy profile of N ₂ O decomposition on Rh ₅₁ cluster representing (111) surface.....	65
Figure 4.13. Adsorbed oxygen atom on Rh ₅₁ cluster representing (111) surface and N ₂ molecule after N ₂ O decomposition from different two sides of view, i and ii.....	66

Figure 4.14. Distances of O1 between the selected Ir atoms in the input geometry for N ₂ O decomposition.....	68
Figure 4.15. Adsorbed oxygen atom on Ir ₅₁ cluster representing (111) surface and N ₂ molecule after N ₂ O decomposition from different two sides of view, i and ii.....	69
Figure 4.16. Energy profile of N ₂ O decomposition on Ir ₅₁ cluster representing (111) surface.....	70

NOMENCLATURE

E	Energy
H	Enthalpy
J	Projection of the atom gradients
P	Pressure
q	Cartesian coordinates of the system
T	Kinetic contribution to the ground state energy
TM	Transition metal
V	Potential
Subscripts:	
a	Activation barrier
el-el	Electron-electron interaction
Superscripts:	
ext	External
Greek Letters:	
Δ	Increment
\emptyset_i	Single-particle Kohn-Sham orbitals
Ψ	Wave function
λ	Wavelength
ρ	Electron density

Abbreviations:

AES	Auger electron spectroscopy
B3LYP	Becke 3-Parameter, Lee, Yang and Parr
DFT	Density functional theory
ECP	Effective core potentials
LA	Link atom
LAC	Link atom connection
LAH	Link atom host
LANL2DZ	Los Alamos National Laboratory 2-double-z
LEED	Low energy electron diffraction
MSC	Multiple scattering cluster
MM	Molecular mechanics
NEXAFS	Near edge X-ray absorption fine structure
ONIOM	Our own n-layer integrated molecular orbital molecular mechanics
QM	Quantum mechanics
SCF	Self-consistent field
TDS	Thermal desorption spectroscopy
TPD	Temperature programmed desorption
UV	Ultraviolet
UPS	Ultraviolet photoemission spectroscopy
UBI-QEP	Unity bond index quadratic exponential potential
XPS	X-ray photoemission spectroscopy
ZPE	Zero point energy

CHAPTER 1

INTRODUCTION

1.1. Nitrous Oxide

Nitrous oxide is a linear triatomic molecule in the gas phase, which is best described by the two canonical structures ${}^{-}\text{N}=\text{N}^{+}=\text{O}$ and $\text{N}\equiv\text{N}^{+}-\text{O}^{-}$ (Ceballos et al., 2001).

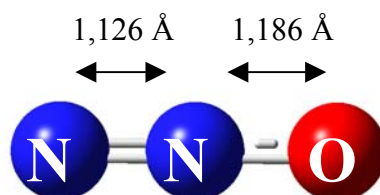


Figure 1.1. N₂O molecule (Partington, 1989)

Nitrous oxide, N₂O, has been long considered as a relatively harmless species and has suffered from a lack of interest from scientists, engineers and politicians, due to the underestimation and unawareness of the potential contribution of this species to

environmental problems. During the last decade a growing concern can be noticed since nitrous oxide has been identified as a relatively strong greenhouse gas (Crutzen, 1971; Kramlich et al., 1994; Wojtowicz, 1993). The estimated human contribution to the nitrous oxide emission to the atmosphere amounts to 4.7-7 million ton per year, (Choe, 1993; Wojtowicz, 1993) about 30-40% of the total emission including natural sources. Adipic acid production, nitric acid manufacture, fossil fuels and biomass combustion and land cultivation are reported as identified anthropogenic sources and estimated amounts of N₂O emitted by various human activities are given in Table 1.1 (Brem, 1990; Choe, Soete, Wojtowicz, 1993; Reimer 1994).

Table1.1. Estimated amounts of N₂O emitted by various human activities

Source	kton/year	Point sources	%Man made ^a
Adipic acid production	371 (545) ^b	23	5-8
Nitric acid production	280-370	255	4-8
Land cultivation, fertilizers	1000-2200		14-45
Fossil fuels (stationary)	190-520	>1000	4-10
Fossil fuels (mobile)	200, 400-850	>2.10 ⁸	4-15
Biomass burning	500-1000		10-20
FCC regeneration	?		
Waste incineration	?		
Other chemicals	?		

^a Total global man made emission taken 4.7-7*10⁹ kg N₂O per year (Choe et al., 1993)

^b Total industrial production (Reimer et al., 1994)

Wojtowicz et al. 1993 claimed that the human contribution has led to an imbalance between the total global sources and sinks, and a 70-80% reduction in the human emissions is necessary to stabilize the atmospheric N₂O concentration at the present level of about 310 ppb.

N₂O is potent greenhouse gas, exhibiting approximately 300 times the greenhouse activity of CO₂ according to Centi et al. 2000. Regarding this fact, the growing governmental awareness of the environmental impact of N₂O reached an important level in Kyoto, Japan December 11, 1997 that Kyoto Protocol declared the goal as lowering overall emissions of six greenhouse gases including nitrous oxide.

1.2. Uses of Nitrous Oxide as an Oxidant

During the last decades, one of the most intriguing new reagents for the selective oxidation has appeared to be nitrous oxide, N₂O. This compound is used in medicine due to its light narcotic effect (“laughing gas”) but in chemistry it was considered mostly as a not very toxic but practically useless compound. Moreover, in the last two decades even some special environmental restrictions were issued to prevent the emission of N₂O into the atmosphere, since the compound has been recognized as a both greenhouse and ozone depleting agent (Parmon et al., 2005).

In the late 1970s–early 1980s, nitrous oxide has attracted a significant attention of researchers involved in searching for new ways in selective transformation of methane. In particular, research groups of Lunsford, (1982, 1984) and Somorjai (1985) showed that application of N₂O oxidant over supported MoO₃ and V₂O₅ oxides provided high selectivity of methane oxidation to methanol and formaldehyde, especially at low conversions.

In 1983, Iwamoto et al. were the first to use N₂O for the oxidation of benzene. In the light of this view considering N₂O as an oxygen donor, there has been significant progress in the reaction of oxidation of benzene to phenol (Panov, 2000). The decomposition of N₂O can be expected to generate oxygen species with an electrophilic characteristic on an appropriate catalyst for giving a chance of highly selective reaction e.g. epoxidation of propylene according to Zhang et al., 2006.

According to Parmon et al., 2005 generally, N₂O is considered as an expensive and quite “exotic” compound which application in chemical industry is economically unreasonable. At the thorough consideration it appeared to be not correct. Indeed, the production of inexpensive N₂O seems to be easy arranged as a large-scale catalytic process too, the starting materials being widely available and inexpensive ammonia and air. The economic estimations based on the results of the pilot unit tests demonstrated that the specific cost of active oxygen in N₂O obtained by the new technology, is about four times lower than the cost of active oxygen in the widely accepted oxidant H₂O₂ (Uriarte, 2000). No doubt this finding will provide an additional driving force for searching new applications of nitrous oxide in various fields of chemistry.

1.3. Nitrous Oxide Decomposition Catalysts

The metal catalysts include Pt, Pd, Ag, Au and Ge where decomposition generally occurs above 650 K (Kalback, 1978; Meyer, 1936). Especially the early studies focused on Pt (Lintz, 1981 and 1984) has been studied most amongst metals. The reaction rate is proportional to P_{N₂O} and oxygen has an inhibiting effect (Hinshelwood, 1925; Steacie, 1934) up to a certain partial pressure, above which the rate becomes independent of P_{O₂} (Riekert, 1965). Also N₂ inhibits the reaction, although much less than O₂ according to Hinshelwood, 1925. The apparent activation energy is around 135 kJ/mol (Meyer, 1936). Takoudis and Schmidt (1983) studied the reaction at low N₂O pressures (1-65Pa) and arrived at an activation energy for the N₂O dissociation at the surface of 146 kJ/mol, with a heat of adsorption of 89 kJ/mol. The activity of Au has been studied up to 70 bar, yielding a first order P_{N₂O} dependency and activation energy around 142 kJ/mol.

Pure oxides have been collected and reviewed in (Golodets 1983; Winter 1969, 1970,1974). The highest activities are exhibited by the oxides of the transition metals of group VIII (Rh, Ir, Co, Fe, Ni) by CuO and by some rare earth oxides (La) (Li, 1992; Zhang 1994). High activities per unit surface area are also claimed for CaO, SrO, V₂O₃ and HfO₂ (Soete 1993; Winter 1969, 1970). Moderate activities are found for elements of group III-VII (Mn, Ce, Th, Sn, Cr) and of group II (Mg, Zn, Cd). The valency of an element is also important. For manganese which can have various oxidation states the activity order (per unit surface area) was MnO<MnO₂< Mn₃O₄< Mn₂O₃ (Yamashita, 1996); thus 3+ seems the optimal oxidation state. For vanadium V₂O₃ is much more active than the nearly inactive V₂O₅ (Soete, 1993). It should be mentioned that, depending on the experimental conditions, some oxides are not stable and are partially converted, like MnO₂, MnO (Yamashita, 1996), Cu₂O (Dell et al., 1953) and CoO (Amphlett, 1954). The apparent activation energies range between 80 and 170 kJ/mol. The rate is usually proportional to P_{N₂O} or has a slightly lower order due to the inhibition of produced oxygen. The order in P_{O₂} for strong inhibition amounts to -0.5. (Yamashita, 1996).

Much work has been done on mixed oxidic systems, like doped oxides or solid solutions, spinels and perovskites, not only for the N₂O decomposition reaction as such, but also predominantly for a better mechanistic understanding of catalytic phenomena over oxidic transition metal (TM) systems in general. Nowadays the studies are focused more on the development of more active and stable systems (Kapteijn et.al, 1996). Cimino (1966, 1969, 1972), Stone (1974, 1975) and others have systematically studied the effect of various transition metal ion concentrations in relatively inert oxide matrices like MgO, Al₂O₃, MgAl₂O₄ (Indovina, 1979; Keenan, 1966) on N₂O decomposition. The catalytic activity develops strongly already in very dilute solutions (<1 TM ion per 100 cations), where the activity per TM ion is the highest at the lowest dilution.

The TM ions act specifically, i.e. the activity of different oxidation states varies widely. An example of the former is the study of Cimino and Indovina (1970) who

demonstrated that Mn^{3+} ions dispersed in a MgO matrix had the most active oxidation state compared to Mn^{2+} and Mn^{4+} , in agreement with the results for the pure oxides (Yamashita, 1996).

Swamy et al. (1994,1995,1996) reported very high activities of mixed oxide catalysts, prepared from thermal decomposition (ca. 700K) of transition metal (Co, Cu, Ni, Rh, Ru, Pd, La) containing hydrotalcites, belonging to the class of clay minerals. Some of them are even more active than the zeolitic catalysts. A typical reaction order found is $\text{Co-Rh} > \text{Co-La} > \text{Co-Mg} > \text{Co-ZSM-5}$. Conversion of N_2O already occurs below 500 K. The apparent activation energies amount to 45-55 kJ/mol and the reaction is first order in $\text{P}_{\text{N}_2\text{O}}$. The oxygen inhibition is not high, water inhibits strongly. The Co containing calcined samples exhibit a sustained life at temperatures above 900 K in a wet and oxygen containing atmosphere with 10% N_2O (Armor, 1996); thus, keep promises for practical application.

Supported oxides are not as frequently studied as the pure and mixed oxides, but for practical applications they might be better studied due to the higher dispersion by combination with the larger specific surface area of the support. Often their behaviour is compatible with that of the pure oxides. On the other hand, the loading, the way of preparation and the temperature history determine the final catalyst performance and the distinction between supported oxide and solid solution may vanish. Most reports deal with alumina as carrier for Pd and oxides of Cu, Co, Mn, Rh, Ru, Fe, Cr (Dandl, 1995; Li, 1992; Lolacano, 1975), some with silica-supported oxides of Ni, Fe, Cr, Cu and Co (Panov, 1990; Rebenstroff, 1978; Silinkin, 1979), but an observed trend is that zirconia is applied more and more in combination with, e.g. Rh, Co/Ni, Cu (Centi, 1995; Zeng, 1994), with as important property the hydrophobic character.

Although the decomposition of N_2O over zeolite catalysts was already known for some time for Fe-systems (Akbar, 1981; Fu, 1981; Leglise, 1984), in recent years numerous catalysts have been identified with high activities for the reaction. They are

mostly based on transition metal ion (Fe, Co, Ni, Cu, Mn, Ce, Ru, Rh, Pd) exchange procedure with a suited zeolite (ZSM-5, ZSM-11, Beta, Mordenite, USY, Ferrierite, A, X) (Chang, 1994; Rodriguez-Mirasol, 1995), and some already exhibit activities below 600 K (Chang, 1994; Li, 1992).

The combination of metal ion and zeolite type determines the activity for N₂O decomposition. The activity order for the different elements can deviate considerably from that of the pure oxides. Pt itself has a good activity as a metal, but in zeolite is hardly active. Co is very active in ZSM-5, Beta, ZSM-11, Ferrierite and Mordenite (MOR), moderately in L and Erionite, but hardly active in Y. Fe in ZSM-5 is much more active than in MOR and Y (Hall, 1982; Panov, 1990). For ZSM-5, the most studied zeolite, the activity order is Rh, Ru >Pd>Cu>Co>Fe>Pt>Ni>Mn (Chang, 1994; Li, 1992)

The reaction rate is mostly first order in P_{N₂O}, with apparent activation energies ranging between 75 and 170 kJ/mol, although for Ru values ranging between 46 (ZSM-5) and 220 kJ/mol (USY) were reported (Chang, 1994).

The oxygen inhibition varies from catalyst to catalyst. In ZSM-5, Pd, Fe and Co show hardly any, Rh a moderate, and Ru and Cu a strong inhibition, although a high concentration of oxygen does not seem to lower the rate any further, a result also observed for Pt (Riekert, 1965) and for Co-perovskite (Wang, 1995). On the other hand, for Fe-ZSM-5 and Fe-MOR the complete absence of oxygen inhibition (Leglise, 1984; Panov, 1990) and for Fe-ZSM-5 even a positive effect is reported (Chang, 1995). For Ru zeolite systems apparent orders in oxygen of -0.5 for Ru-USY and -0.2 for Ru-ZSM-5 are reported (Chang, 1994).

A Cu-ZSM-5 catalyst has been reported to be active in the photocatalytic decomposition of N₂O. UV irradiation ($\lambda < 300$ nm) of the catalyst stimulates the reaction already at ambient conditions (Yamazoe, 1990; Ebitani, 1993, 1994), whereby

oxygen is evolved. In earlier studies on this type of reaction over ZnO, TiO₂, and Pt/TiO₂ oxygen was not always observed (Anpo, 1985; Connigham, 1971). It is noted that N₂O itself can decompose (Meyer, 1936) under UV radiation ($\lambda < 200$ nm). It is proposed that in the Cu-ZSM-5 catalyst the charge donation to the N₂O is triggered by excited Cu⁺-Cu⁺ dimers, resulting in fast decomposition (Ebitani, 1994). The reaction turned out to be proportional to the Cu⁺ concentration (Ebitani, 1993), independent of N₂O pressure, but it is inhibited by oxygen to a certain level.

While evaluating the activity data on the reported N₂O decomposition catalysts, it is noticed that of the first row of transition metals Co and Cu generally exhibit a very high activity, while Rh and Ru are the most active of the second row. Very active catalysts are based on calcined hydrotalcites, zeolites and alumina supported noble metals (Kapteijn et al., 1996).

It should be highlighted again that the human contribution to N₂O emissions has long been underestimated as a serious problem. Catalysis offers opportunities to reduce the emissions of various sources. Although much research has been performed in the past for mechanistic studies, activities are still going on, focusing on the development of new catalysts for N₂O decomposition. Like NO decomposition, the reaction is thermodynamically feasible, but also, contrary to NO decomposition, it has clearly been demonstrated to be practically feasible. Research is now targeting on catalysts active at low temperatures as required by several applications. Each application imposes specific requirements for the catalyst and it is felt that the suitable catalyst for each application is either not completely optimized or still identified (Kapteijn et al., 1996).

1.4. Aim of This Study

Nitrous oxide decomposition is the model reaction placed in the main core of this thesis and nature of this reaction and trend of the reaction progress represented by figures based on the data obtained by the quantum chemical methods constitute the essential parts of this thesis.



Nitrous oxide decomposition over a transition metal cluster representing (111) surface can be demonstrated in Fig. 1.2. and Fig. 1.3. including both model reaction, reactant, product and model cluster as studied in this thesis.

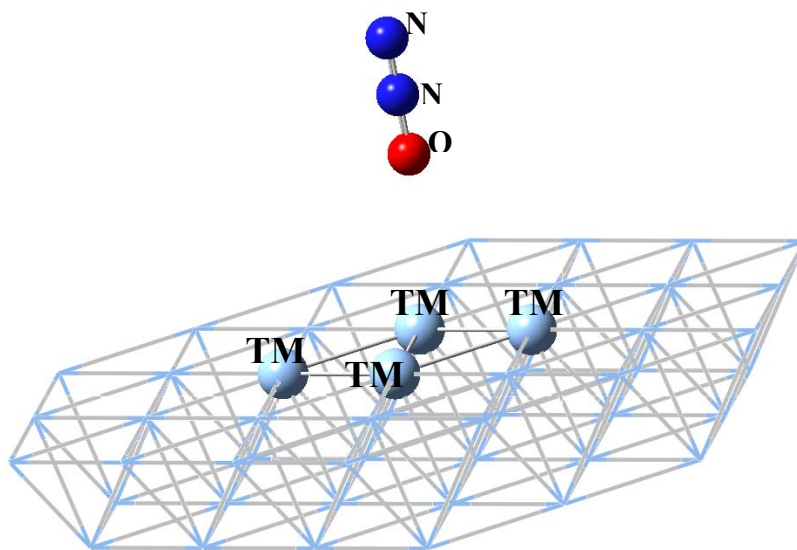


Figure 1.2. Reactant and model surface for nitrous oxide decomposition over TM_{51} cluster representing (111) surface (TM=Ag, Au, Ir, Pt, Rh)

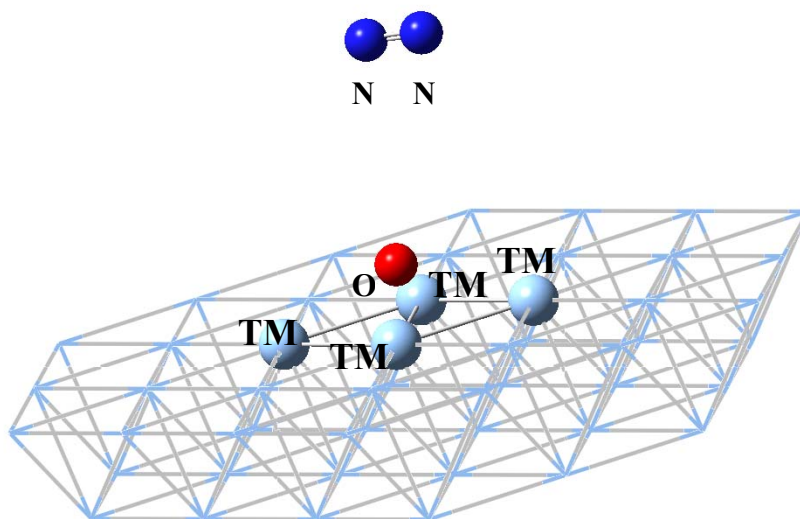


Figure 1.3. Product and model surface for nitrous oxide decomposition over TM_{51} cluster representing (111) surface (TM=Ag, Au, Ir, Pt, Rh)

In this study it is desired to analyze the behaviour of nitrous oxide decomposition over (111) surfaces of five different transition metals, Ag, Au, Ir, Pt and Rh by means of quantum chemical simulation methods. In the literature there do not exist many studies examining the nitrous oxide decomposition over surfaces of single crystal from both experimental and theoretical sides. Hence, in order to highlight this point nitrous oxide decomposition is analyzed over (111) crystal planes of the transition metals and obtained results are compared with the data in the literature by focusing on the reaction behaviour whether it acts on the same line with studies in the literature.

It should be also mentioned that nitrous oxide decomposition follows a way in which nitrous oxide leaves atomic oxygen on the surface of all these metals by leaving N_2 gas and a deliberate analysis is aimed to be completed by considering five different transition metals by concentrating on this fact.

Furthermore, to have far clearer results input geometry of reactant, final geometry of products, reaction path and relative energy diagrams of the model reaction of nitrous oxide decomposition are obtained and taken into consideration for making a better comparison of the nature of the reaction on representing surfaces by using quantum chemical methods.

The relationship between the geometry of reactant during the progress of reaction and representing (111) surfaces of the transition metals is another point aimed for studying and reaching some conclusions in order to determine the profiles of reaction energy. With respect to this profiles and final geometry of products, a detailed analysis is also desired for examining the results by comparing the data in the literature and also taking into consideration of the geometry of products to compare with each other representing (111) surfaces of metals.

Within the scope of this thesis, representing (111) surfaces are taken as model surface of Ag, Au, Ir, Pt and Rh metals of nitrous oxide decomposition reaction for having a general view from the side of reaction progress and a more detailed view from the side of dissociation nature on these various metals.

Quantum chemical methods are used for this analysis by Gaussian (Frisch et al., 2004) in order to reach a goal of specifying the decomposition reaction completely by theoretical means and observing the trends of the results obtained at the end of calculation with respect to the studies in the literature concerning important data e.g. activation barrier, enthalpy of reaction and final geometries. In the light of these investigations, an elaborate study regarding a systematic approach for determining the progress of nitrous oxide decomposition over transition metals representing (111) surfaces and obtaining energy values of the model reaction for each metal respectively occupy the center of this thesis.

CHAPTER 2

LITERATURE SURVEY

2.1. Experimental Studies Regarding N₂O Decomposition

As a recent experimental study, Boissel et al. (2006) studied the catalytic decomposition of N₂O over monolithic noble metal-transition metal oxides and demonstrated that the addition of IrO₂ and RhO₂ to monolithic supported transition metals can set the catalytic activity for N₂O decomposition and vice versa to a higher level.

In another article published recently (Santiago et al., 2007), catalytic N₂O decomposition has been studied over metal-substituted hexaaluminates with the general formula ABA₁₁O₁₉, where A = La, Ba, and B = Mn, Fe, Ni. Santiago and coworkers concluded that the Fe- and Mn-substituted hexaaluminates exhibit high activity and stability for N₂O decomposition in mixtures simulating the outlet of the Pt-Rh gauzes in ammonia oxidation reactors, containing N₂O, NO, O₂, and H₂O and these materials are promising for high-temperature abatement of nitrous oxide in the chemical industry, particularly in nitric acid and caprolactam production.

From a different side of view, it is estimated that 10% of nitrous oxide released every year into the atmosphere originates from the production of adipic acid. With this respect, Alini et al. (2007) focused on the issue of development of new catalysts for N₂O decomposition from adipic acid plant. In their study, direct decomposition of N₂O was investigated using simulated and real industrial gas stream coming from an adipic acid plant. The importance of copper on catalytic activities is confirmed by the investigation on CaMn_{1-x}Cu_xO₃ samples on which highest value of N₂O conversion is reached.

Studies of Russo et al. 2007 are aimed at the development of catalytic systems based on spinel-type oxides because of their good stability and intrinsic catalytic activity. They focused on the concerns of the synthesis, characterization, catalytic activity test and reaction mechanism assessment of a series of Co spinels, whose performance towards N₂O decomposition, evaluated both in presence and in absence of oxygen, is compared with that of other spinels (ferrite and chromites). They reach some conclusions concerning either the role of each single constituting element on the activity of the most promising catalyst (MgCo₂O₄), or its reaction mechanism, thereby pointing out the way to the development of new, more active catalysts.

2.1.1. Zeolites as Catalyst

Sugawara et al. (2007) studied the importance of Fe loading on the N₂O reduction with NH₃ over Fe-MFI and the effect of acid site formation on Fe species. The results of this study suggest that the acid sites were formed on the bridge oxide ions in binuclear Fe species and adsorbed NH₃ on the strong acid sites inhibited N₂O dissociation, which can be related to the low activity of N₂O + NH₃ reaction over Fe-MFI with high Fe loading.

Coq and co-workers, (1999, 2003) concluded that pentasyl-type frameworks (BEA, FER, MFI) loaded with iron are more efficient catalysts for direct N₂O decomposition than other zeolites such as MOR, FAU, MAZ, and OFF. Evaluation of zeolite frameworks with traces of iron could constitute a suitable approach to investigate matrix effects in direct N₂O decomposition. All the zeolites (except USY) experienced a substantial increase in activity upon steam treatment. This is attributed to the creation of highly active iron species in extra-framework positions, involving both extraction of lattice iron and/or formation of oligonuclear oxo-cations (Øygarden, 2006).

Sun et al., 2006 investigated the effect of high-temperature treatment of Fe/ZSM-5 prepared by solid-state ion exchange on the mechanism of nitrous oxide decomposition. They proposed that nitrous oxide decomposition over calcined Fe/ZSM-5 is catalyzed by clustered iron species, most likely by coordinatively unsaturated Fe³⁺ sites. Upon high-temperature treatment, a new type of active site-Fe²⁺ sites stabilized by extra-framework Al species in the micropore of zeolite is formed. These sites are able to decompose nitrous oxide at a higher rate.

Ramirez et al., 2006 studied the ex-framework method comprising the isomorphous substitution of iron in the zeolite framework followed by calcination and steam treatment. In their work it is stated that extra-framework iron species in Fe-MFI prepared via an ex-framework route are essential for the formation of reactive oxygen species in direct catalytic decomposition of N₂O, while Lewis or Bronsted acid sites play a minor role in this reaction.

In another experimental investigation, Kawi et al., (2001) reported the results of the effects of Ru precursors, the amount of Ru loading on MCM-41, impregnation method, the presence of oxygen and carbon monoxide and moisture in the feed stream on the catalytic performance of the catalyst for N₂O conversion by catalytic decomposition and reduction. According to the results obtained they concluded that

the Ru/MCM-41 catalyst prepared from Ru(OH)₃ as the catalyst precursor and having a 5 wt.% Ru loading is promising for the catalytic decomposition and reduction of N₂O.

Wood and co workers (2002) studied the mode and strength of N₂O adsorption on Fe–ZSM-5 and the activity of this catalyst for N₂O decomposition. Samples of Fe–ZSM-5 were prepared with Fe loadings significantly lower than Fe/Al=1, in order to assure that all of the exchanged Fe was present as isolated cations. The roles of Fe/Al ratio and oxidative versus reductive pretreatment were also examined in their study.

2.1.2. Studies Over Single Crystals

Using the method of thermal desorption spectroscopy (TDS), chemisorbed and multilayer physisorbed nitrous oxide has been observed. According to TDS data, the binding energies of multilayer and submonolayer N₂O are rather close. Physically adsorbed N₂O desorbs from the Ir(111) surface at 93 K (multilayer adsorption) and chemisorbed N₂O desorbs at 102 K (<1 monolayer, ML) (Cornish, 1990). Similar data have been reported for Ag(111) (Schwaner, 1996). For this surface, two thermal desorption peaks were observed: at 98 K (multilayer adsorption) and 94–102 K (chemisorbed N₂O). In the case of multilayer adsorption on Pt(111), N₂O desorbs at 86 K (Avery, 1983). Kiss et al., 1991 observed two thermal desorption peaks of N₂O: at 75–87 K (multilayer adsorption) and 97–102 K (chemisorption).

On some of the surfaces studied, N₂O adsorption has not been detected. Thus, on the Rh(111) surface, N₂O adsorbs neither molecularly nor dissociatively at temperatures from room temperature to 900 K (Li, 1996). Li and Bowker, 1996 assumed that adsorption requires overcoming a high activation barrier, but this assumption seems highly improbable because the activation energy of adsorption is usually low or equal to zero on clean surfaces. According to Spitzer and Luth, 1984 the temperature range

90–300 K, nitrous oxide is not adsorbed on Cu(111). We cannot exclude that molecular adsorption of N₂O is possible on almost all surfaces, but researchers do not always explore wide ranges of temperatures and exposures.

In another experimental study concentrating on single crystal surfaces, the interaction of monolayer and submonolayer N₂O with the Cu(100) and Ag(110) surfaces have been studied using near-edge X-ray absorption fine structure spectroscopy. Based on the results of angular dependent intensity of the molecular resonances Ceballos et al., 2001 derived a substrate and coverage dependent bent of the N₂O molecules upon adsorption. From the comparison of the π^* resonance intensity from the terminal N_t and central N_c nitrogen atoms it is concluded that the N₂O molecules couple with the Cu surface through the terminal N_t atom in contrast to the Ag surface where the N_c atom is involved.

N₂O has been examined on Pt(111) (Avery, 1983) as well as other metals. N₂O adsorbs molecularly on Pt(111) (Avery, 1983) and Ir(111) (Cornish, 1990). It partly dissociates, leaving oxygen on the surface on Ag(111) (Grimblot, 1990).

In a similar issue to the previous mentioned article concerning N₂O decomposition on single crystal surfaces, N₂O adsorbed on a Pt(111) surface was irradiated by UV light from a mercury arc lamp. The photochemistry of N₂O was studied by XPS, UPS, and TPD. Upon irradiation at 50 K, adsorbed N₂O undergoes dissociation and desorption. Photon energies exceeding 4.35 eV are required. The cross section is in the range of 10⁻¹⁹-10⁻²⁰ cm². The data are adequately described with a model involving subvacuum hot electrons (Kiss, 1991).

In another experimental study within the concept covering single crystal plane and nitrous oxide interactions Wu et al., 2006 studied the nitrogen 1s near-edge X-ray absorption fine structure (NEXAFS) spectra of the N₂O adsorbed on Ag(110) by the multiple-scattering cluster (MSC) and self-consistent field (SCF) DV-Xa methods.

Two adsorption models, in which the N_2O molecule attached to the Ag substrate through the central nitrogen (N_C) atom and the terminal nitrogen (N_T) atom, respectively, have been checked up thoroughly. The MSC calculation and the R-factor analysis show that the N_2O molecule is attached to the Ag substrate through the terminal nitrogen atom with the adsorption height $h = 3.4 \pm 0.1 \text{ \AA}$. In the overlayer the N_2O molecules arrange themselves into a tilted chain due to the interaction between the cations and the anions in the molecules. The physical cause of the resonances in the NEXAFS spectra mentioned above has been discussed by the DV-Xa method, which confirms the MSC calculations.

Gomez et al., 2002 investigated the reduction of nitrous oxide on Ir(hkl) electrodes in contact with an acidic medium constitutes a striking example of sensitivity to the structure. Whereas the process occurs apace at Ir(111) and Ir(110) electrodes within the hydrogen potential region, the Ir(100) electrode is inert. A mechanism is proposed in order to explain, at least in a semiquantitative way, the shape and location of the voltammetric waves. It is based on the dissociative adsorption of nitrous oxide originating oxygen adatoms, which are reduced by coadsorbed hydrogen resulting from the electrosorption of protons. This simple kinetic model implies that, under certain experimental conditions, the maximum activity of the electrode is attained when the electrode surface is half-covered by hydrogen. Hydrogen adsorption on Ir(100) occurs as a phase transition, and therefore there does not seem to exist an extended potential region where the coverage is around 0.5, which explains its lack of activity.

According to Li et al., 1996, the adsorption and decomposition behaviours of N_2O on the (110) and (111) faces of rhodium, using molecular beam adsorption and reaction, LEED and XPS. A striking difference is observed. There is a clear structural dependence of nitrous oxide adsorption and rhodium single crystals. On the (111) surface, at or above 160 K adsorption and dissociation only take place on defects. On the (110) surface dissociative adsorption takes place over a wide range of

temperatures. With respect to the big differences found with the two planes two reasons are suggested: the different heights of the potential barriers, and the different supplies of surface sites available.

2.2. Theoretical Studies Regarding N₂O Decomposition

Kobayashi and coworkers (1997) applied the density functional method to investigate the mechanism of deNO_x reaction. They focused on the structure and role of the active site composed of Al, O, and Cu atoms and the energetics during the reaction. A density functional method was applied to investigate the electronic structures of Cu ion adsorbed ZSM-5 zeolite and the interactions of NO molecules with zeolite. Two types of models were considered, the pentameric cluster model and the 5-membered ring cluster model. In the former, the Cu ion was bound to the two O atoms with larger stabilization energy (52 kcal/mol) than the single O atom. For the 5-membered ring model, a much smaller stabilization energy (38 kcal/mol) was calculated. The deNO_x reaction mechanism was simulated as the reactions between two NO molecules or between NO and HNO (or NOH) molecules. The former did not produce N₂ and O₂ smoothly due to the activation barrier, whereas the latter is found to lead to N₂O and OH more easily.

In another theoretical study, Karlson et al., 2003 investigated the activity of O²⁻ in the N₂O decomposition process, and in particular, they considered the mechanisms in which O and O³⁻ species are involved in the decomposition process.

In a study of the dissociation of N₂O on platinum catalysts by combined transient and computational approaches, the energetics of the low-temperature adsorption and decomposition of nitrous oxide, N₂O, on flat and stepped platinum surfaces were calculated using density-functional theory (DFT). The results show that the preferred adsorption site for N₂O is an atop site, bound upright via the terminal nitrogen. The

molecule is only weakly chemisorbed to the platinum surface. The decomposition barriers on flat (111) surfaces and stepped (211) surfaces are similar. While the barrier for N₂O dissociation is relatively small, the surface rapidly becomes poisoned by adsorbed oxygen. These findings are supported by experimental results of pulsed N₂O decomposition with 5% Pt/SiO₂ and bismuth-modified Pt/C catalysts. At low temperature, decomposition occurs but self-poisoning by O(ads) prevents further decomposition. At higher temperatures some desorption of O₂ is observed, allowing continued catalytic activity. The study with bismuth-modified Pt/C catalysts showed that, although the activation barriers calculated for both terraces and steps were similar, the actual rate was different for the two surfaces. Steps were found experimentally to be more active than terraces and this is attributed to differences in the preexponential term (Burch, 2004).

As a theoretical study regarding N₂O decomposition, Scagnelli et al., 2006 studied that the catalytic activity of pure and Ni-doped MgO surfaces in N₂O decomposition with DFT B3LYP cluster model calculations. Scope of their work is to investigate the role of Ni impurities on Ni-doped MgO in increasing the activity of the catalyst. For this reason, they considered also the N₂O decomposition on pure MgO. They considered also the reaction on low-coordinated edge sites, which are quite abundant on high-surface area polycrystalline materials.

CHAPTER 3

METHODOLOGY

3.1. ONIOM

Hybrid methods allow the combination of two or more computational techniques in one calculation and make it possible to investigate the chemistry of very large systems with high precision. The region of the system where the chemical process takes place, for example bond breaking or bond formation, is treated with an appropriately accurate method, while the remainder of the system is treated at a lower level. The most common class of hybrid methods is formed by the QM/MM methods, which combine a quantum mechanical (QM) method with a molecular mechanics (MM) method (Field, 1990; Maseras, 1995; Singh, 1986; Warshel, 1976). The ONIOM (our Own N-layer Integrated molecular Orbital molecular Mechanics) scheme is more general in the sense that it can combine any number of molecular orbital methods as well as molecular mechanics methods (Dapprich, 1999; Hopkins, 2003; Humbel, 1996; Karadakov, 2000; Rega, 2004; Svensson, 1996; Vreven, 2000, 2001, 2003) Hybrid methods in general have been the subject of a number of recent reviews (Froese, 1998; Gao, 1996, 1998; Merz, 1998; Ruiz-López, 1998; Tomasi, 1998; Ujaque, 2004; Warshel, 2003)

3.1.1. Combining Quantum Mechanics Methods with Molecular Mechanics Methods in ONIOM

A variety of QM/MM schemes have been reported in the literature. Although the main concepts are similar, the methods differ in a number of details. One major distinction is in the treatment of covalent interaction between the two regions. The resulting dangling bonds in the QM calculation need to be saturated, and the simplest approach is to use link atoms (Field, 1990; Derat, 2003). These are usually hydrogen atoms but can, in principle, be any atom that mimics the part of the system that it substitutes. Link atoms are used in a large proportion of QM/MM implementations as well as our ONIOM scheme. The main alternative to link atoms is the use of frozen orbitals, which can through parametrization and use of p and d orbitals describe a more accurate charge density than link atoms (Gao, 1998; Reuter, 2000; They, 1994; Warshel, 1976). Although the few studies that directly compare link atom methods with frozen orbital methods show that both schemes perform well, (Nicoll, 2000; Reuter, 2000), it appears generally accepted that the latter can provide a better description of the boundary. However, due to the required parametrization of the frozen orbitals, they lack the flexibility and generality of link atoms. In our implementation we exclusively use link atoms because we consider generality one of the key aspects of our ONIOM scheme, and it is not feasible to parametrize frozen orbitals for every possible method combination. It must be noted that to some extent also the accuracy of link atoms can be improved by parametrization. The electronegativity can be modified through the use of a shift operator (Koga, 1990) or, in the case of semiempirical QM methods, the parameters involving link atoms can be adjusted (Antes, 1999). We have not included this limited parametrization in our current method but may do so in the future. Besides frozen orbitals and link atoms, several QM/MM methods use pseudopotentials to handle the covalent interactions between the QM and MM regions.(Zhang, 1999; DiLabio, 2002).

The second main difference between various QM/MM methods is the way the electrostatic interaction between the two layers is treated (Bakowies, 1996). In its simplest form, the interaction between the QM and MM region is completely described by MM style terms. This includes the electrostatic interaction, which is then evaluated as the interaction of the MM partial charges with partial (point) charges assigned to the atoms in the QM region. This approach is usually referred to as *classical* or *mechanical embedding*. In the second approach, the charge distribution of the MM region interacts with the actual charge distribution of the QM region. In this case, the partial charges from the MM region are included in the QM Hamiltonian, which provides a more accurate description of the electrostatic interaction and, in addition, allows the wave function to respond to the charge distribution of the MM region. This approach is referred to as *electronic embedding*. In the original version of ONIOM, the QM region and MM region interact via mechanical embedding.

3.1.2. MM Force Fields

An example of a typical force field, in this case Amber, (Cornell, 1995) is of the form:

$$\begin{aligned}
 E^{total} = & \sum_{bonds} K_r (r - r_{eq})^2 + \sum_{angles} K_\theta (\theta - \theta_{eq})^2 + \\
 & \sum_{dihedrals} \frac{V_n}{2} [1 + \cos(n\phi - \gamma)] + \sum_{i < j} \left[S_{ij}^{vdw} \left(\frac{A_{ij}}{r_{ij}^{12}} - \frac{B_{ij}}{r_{ij}^6} \right) + S_{ij}^q \frac{q_i q_j}{\epsilon r_{ij}} \right]
 \end{aligned}
 \tag{3.1}$$

The first three terms describe the *bonded interactions*, formed by all the (chemical) bonds, angles, and dihedrals (including out-of-plane deformations) that are present in the system. The number of bonded terms scales linearly with the size of the system. The last term describes the *nonbonded interaction* between each pair of atom in the system. The van der Waals interaction, $(A_{ij}/r_{ij}^{12} - B_{ij}/r_{ij}^6)$, and the Coulomb

interaction, $q_i q_j / \epsilon r_{ij}$, are scaled by factors s^{VdW}_{ij} and s^q_{ij} , respectively. The factors only differ from unity when the centers i and j are separated by three bonds or fewer, and the argument for using them is that the van der Waals and electrostatic interactions are already included in the bonded terms. The number of nonbonded terms scales quadratically with the size of the system and would be the bottleneck in MM calculations if computed as written in Eq. 3.1. Most implementations, however, use either distance based cutoffs or linear scaling methods for the evaluation of the nonbonded interaction. In our implementation we use cutoffs and a boxing algorithm to evaluate with the van der Waals interaction (Vreven, 2006) and the Fast Multipole Method to deal with the electrostatic interaction (Greengard, 1987, Kudin, 1998; 1988; Strain, 1996; Vreven, 2006).

3.1.3. ONIOM and QM/MM Energy Expressions

In a two-layer ONIOM(QM:MM) calculation, the total energy of the system is obtained from three independent calculations:

$$E^{\text{ONIOM}} = E^{\text{real, MM}} + E^{\text{model, QM}} - E^{\text{model, MM}} \quad (3.2)$$

The *real* system contains all the atoms and is calculated only at the MM level. The *model* system contains the part of the system that is treated at the QM level. Both QM and MM calculations need to be carried out for the model system.

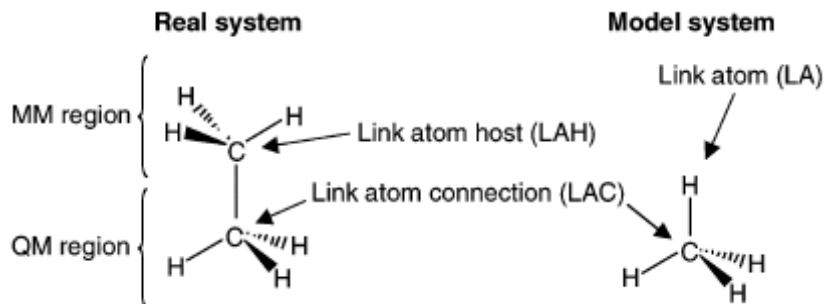


Figure 3.1. ONIOM terminology using ethane as an example (Vreven, 2006)

In Figure 3.1 Vreven et al., 2006 illustrated the terminology using ethane, where they include one methyl group in the QM region and the remainder in the MM region. Because there is bonded interaction between the two regions, the model system includes a hydrogen link atom to saturate the open valence. The atoms that occur in both the model system and the real system have identical geometrical coordinates. The link atom (LA) is placed on the line that connects the center to which it is connected (the *Link Atom Connection*, LAC) with the atom that it substitutes (the *Link Atom Host*, LAH). The LAC-LA distance is obtained by scaling the original LACLAH distance with a constant factor, g , which is chosen so that a (chemically) reasonable LAC-LAH distance yields a reasonable LAC-LA distance (Dapprich, 1999).

$$q_{LA} = q_{LAC} + g(q_{LAH} - q_{LAC}) \quad (3.3)$$

ONIOM(QM:MM) expression is related to the generic QM/MM scheme. The latter can be written as

$$E^{QM/MM} = E^{MM\text{-only},MM} + E^{\text{model},QM} + E^{MM\text{-only}*\text{model-only},MM} \quad (3.4)$$

Vreven et al., 2006 illustrated the QM/MM terminology. In Figure 3.2 the QM/MM terminology is illustrated. It is assumed that the position of the link atom is the same

as in the ONIOM scheme. $E^{\text{MM-only,MM}}$ is the MM energy of the part of the system that only involves MM atoms (thus excluding the LA's).

$E^{\text{MM-only*model-only,MM}}$ describes the interaction between the QM region and the MM region and contains all the MM terms that have at least one center in the MM-only region and at least one center in the model only region. The QM/MM equation reflects a different approach than the ONIOM equation: Equation 3.4 is a summation scheme. It adds the QM energy of the QM region, the MM energy of the MM region, and the MM interaction energies between the two regions. The ONIOM expression 2, on the other hand, is cast as an extrapolation scheme. Note that in the ONIOM expression all three subcalculations are on 'complete systems', whereas in the QM/MM expression two of the terms are on partial systems, which is the reason for only ONIOM allowing the combination of QM methods with QM methods.

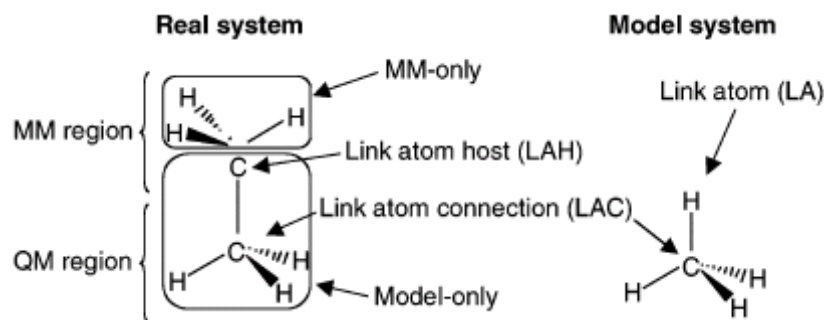


Figure 3.2. QM/MM terminology using ethane as an example (Vreven, 2006)

In the ONIOM scheme, most of the MM terms in the model system exist in the real system as well and cancel exactly in the full expression. The difference between the real system and model system MM calculations, the S -value, describes the contribution from the MM region, which includes both the energy of the MM region as well as the interaction between the QM region and the MM region (Vreven, 2006).

$$S^{\text{MM}} = E^{\text{real,MM}} - E^{\text{model,MM}} \quad (3.5)$$

S^{MM} plays the same role as the $E^{\text{MM-only,MM}} + E^{\text{MM-only*model-only,MM}}$ terms in the QM/MM expression. In fact, when no bonded interactions are present between the regions, S^{MM} is identical to $(E^{\text{MM-only,MM}} + E^{\text{MM-only*model-only,MM}})$, and also the ONIOM and QM/MM energies become identical (Vreven, 2006).

When bonded interactions are present in the system, the ONIOM and QM/MM functions are not identical. The terms involving LA in the model system calculation are not identical to the terms involving LAH in the real system calculation and do not cancel. The difference between the terms describes the difference between the LA and the LAH and can be interpreted as the MM extrapolation (or correction) of the link atoms in the model system QM calculation to the corresponding LAH atoms in the real system. In the generic QM/MM scheme, this extrapolation (or any other way to correct the QM link atom) is not present, although several QM/MM methods deal with this issue in other ways (Vreven, 2006).

It is clear that when the ONIOM scheme is applied in its original formalism, as in Eq. 3.2, the interaction between the QM and MM regions is included via the MM calculations and therefore follows the *mechanical embedding* formalism. For this reason we also presented the generic QM/MM method in its mechanical embedding form. Later the *electronic embedding* formalisms should be presented for both ONIOM and QM/MM (Vreven, 2006).

3.1.4. Derivatives and Three-Layer ONIOM

Derivatives with respect to geometrical coordinates and other properties can be obtained with the ONIOM formalism (Dapprich, 1999). For example, the gradient is written as

$$\frac{E^{ONIOM}}{\partial q} = \frac{E^{real,MM}}{\partial q} + \frac{E^{model,QM}}{\partial q_{QM}^M} J_{QM} - \frac{E^{model,MM}}{\partial q_{MM}^M} J_{MM} \quad (3.6)$$

\mathbf{q} is a vector that contains the Cartesian coordinates of the real system, and q_{QM}^M and q_{MM}^M are the Cartesian coordinates of the QM and MM model systems, respectively. The Jacobian \mathbf{J} projects the gradients of the link atoms onto the link atom host (LAH) and connection (LAC) coordinates. Because the positions of the link atoms is a function of the geometry of the real system, there are no additional (or fewer) degrees of freedom in the ONIOM scheme, and the potential function is well-defined. ONIOM can therefore be used in standard geometry optimization schemes and almost every other technique for the investigation of potential energy surfaces.

In principle, ONIOM can handle any number of layers, although the current implementation is limited to three. This facilitates QM/QM/MM calculations, which can for a given accuracy handle much larger QM regions than regular QM/MM methods. The combined QM/QM region in ONIOM- (QM:QM:MM) is obtained in a similar manner as in ONIOM(QM:QM), using three independent QM subcalculations. This is conceptually different from the QM/QM/MM implementation using CDFT, in which only two QM subcalculations are carried out, and the wave functions are directly coupled (Strajbl, 2002). The expression for ONIOM(QM-high: QM-low:MM), where QM-high and QM-low denote a high-level QM method and a low-level QM method, respectively, contains five terms:

$$E^{\text{ONIOM3}} = E^{\text{real,MM}} + E^{\text{intermediate, QM-low}} - E^{\text{intermediate,MM}} + E^{\text{model, QM-high}} - E^{\text{model, QM-low}} \quad (3.7)$$

Intermediate denotes the intermediate model system. Gradients and properties can be obtained for a three-layer system in the same way as for a two-layer system (Vreven, 2006).

3.1.5. Link Atom Placement and Link Atom Extrapolation

When Vreven and coworkers, 2006 first presented the ONIOM formalism, they also assumed all the geometrical coordinates of the two model system calculations to be identical. The link atom scale factors are then the same for the QM and MM model systems, and also \mathbf{JQM} and \mathbf{JMM} in Eq. 3.6 are identical. In the most recent implementation we generalized the link atom placement and allow different scale factors g for the QM model system and the MM model system. The initial reason for lifting the restriction was to be able to minimize the error resulting from the link atom. In ONIOM(QM:MM) calculations, however, they mentioned that this mechanism can be used for a different purpose, illustrated in Figure 3.2. The QM model system calculation is obtained in the usual way with ‘chemically reasonable scale factors’, but the MM model system is obtained with unit scale factors, and \mathbf{JMM} is a unit matrix. In addition, the MM atom type of the link atom is kept the same as the LAH in the real system. Carrying out an ONIOM(QM:MM) calculation in this way has the advantage that no MM parametrization for the link atoms is required and that therefore any system for which MM parameters are available can also be treated with ONIOM- (QM:MM).

However, close inspection of the MM terms in the ONIOM energy expression shows that all the MM terms from the model system occur in the real system as well and therefore cancel. Since the terms involving LAH and LA are now identical, the

extrapolation of the LA to the LAH is no longer present. In fact, the ONIOM (QM:MM) expression with unit scale factors for the MM model system becomes in this case identical to the QM/MM Eq. 3.4. Since the advantages of ONIOM(QM:MM) over QM/MM are removed with unit scale factors, this could not be taken as favor according to Vreven et al., 2006.

3.1.6. Electronic Embedding

In QM/MM methods, there are two choices for dealing with the electrostatic interactions between the QM layer and the MM layer. The first, *classical embedding* or *mechanical embedding*, treats the cross-region electrostatic interactions at the molecular mechanics level. The second, *electronic embedding*, incorporates the crossregion electrostatic interaction in the QM Hamiltonian. The latter avoids the approximation of the QM charge distribution by point charges and allows the wave function to be polarized by the charge distribution of the MM region. From the original formulation, as outlined in the previous sections, it follows that ONIOM uses mechanical embedding by default (Vreven, 2006),

Vreven and coworkers, 2006 illustrated different embedding approaches, by using the deprotonation of Histidine in Figure 3.3 as an example. The ONIOM expression contains two molecular mechanics terms, of which $E^{\text{model,MM}}$ includes the electrostatic interaction for the QM region, while $E^{\text{real,MM}}$ includes the electrostatic interaction for the *full* system. The latter includes the electrostatic interactions between atoms within the MM region, atoms within the QM region, and atoms in the QM region with atoms in the MM region. Electrostatic interactions between atoms that are separated by three bonds or less are scaled according to the MM force field definition, because they are (partially) implicit in the stretch, bend, and torsional terms (For example, Amber uses a factor of zero for one and two bond separated electrostatic interactions and a factor of 1/1.2 for three bond separated interactions.).

Using Figure 3.3, Vreven et al., 2006 showed a number of specific interactions to illustrate which terms are included in Table 3.1.

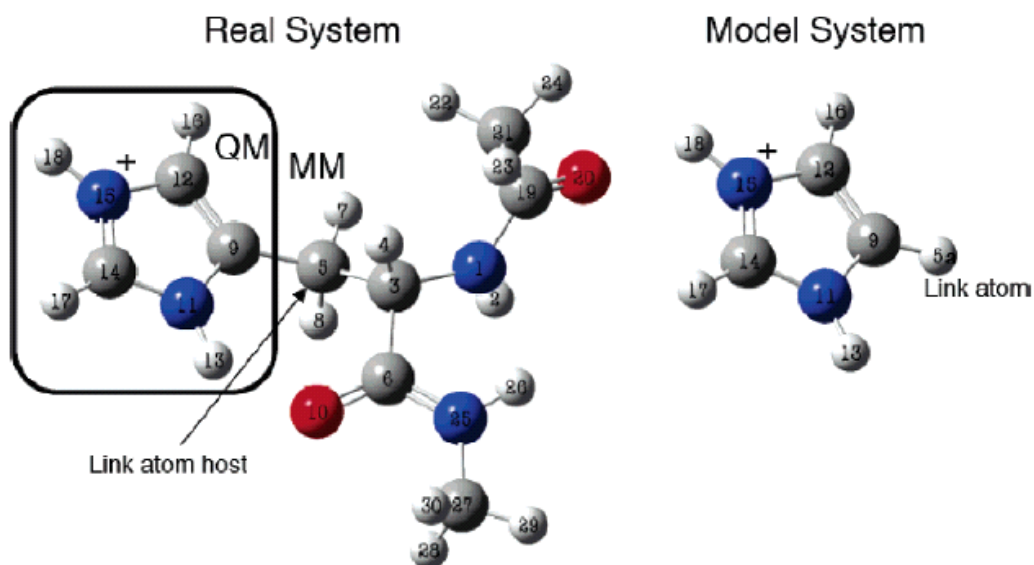


Figure 3.3. Real system, QM/MM partitioning, and model system for the (H18) deprotonation of histidine (Vreven, 2006).

Table 3.1. Inclusion of Specific Interactions in the Standard (Mechanical Embedding) ONIOM (QM:MM) Energy Expression For The Specific Example of Histidine (Vreven, 2006)

centers	included in MM model system?	included in MM real system?	in QM model?
N1-C6	no (centers not in model)	no (2 bond separation)	no
N1-N25	no (centers not in model)	scaled (3 bond separation)	no
N1-C27	no (centers not in model)	yes	no
C3-C9	no (C3 not in model)	no (2 bond separation)	no
C3-C12	no (C3 not in model)	scaled (3 bond separation)	no
C3-N15	no (C3 not in model)	yes	no
C6-C9	no (C6 not in model)	scaled (3 bond separation)	no
C6-N11	no (C6 not in model)	yes	no
C6-C14	no (C6 not in model)	yes	no
C6-H17	no (C6 not in model)	yes	no
H16-C9	no (2 bond separation)	no (2 bond separation)	yes
H16-N11	scaled (3 bond separation)	scaled (3 bond separation)	yes
H16-H13	yes	yes	yes
C5-N11	no (C5 not in model system)	no (2 bond separation)	no
C5-C14	no (C5 not in model system)	scaled (3 bond separation)	no
C5-H17	no (C5 not in model system)	yes	no
H5a-N11	no (2 bond separation)	no (H5a not in real system)	yes
H5a-C14	scaled (3 bond separation)	no (H5a not in real)	yes
H5a-H17	yes	no (H5a not in real system)	yes

Because the interactions between QM and QM atoms (for example between H16 and H13) are included in *both* the $E^{\text{model,MM}}$ and the $E^{\text{real,MM}}$ terms, they cancel in the ONIOM energy expression. It follows that the only electrostatic interactions at the MM level that are retained in eq 3.1 are those between MM atoms and MM atoms and those between MM atoms and QM atoms. Hence, the electrostatic interaction between the two layers is described by the MM component of the energy expression, which is referred to as mechanical embedding. The point-charge electrostatic interactions involving LA and LAH are a special case. The interactions of the QM atoms with both LAH (C5) and LA (H5a) are retained but with different value, sign, and position. Their difference represents the extrapolation of the hydrogen link atom in the QM

calculation to the carbon atom as it is in the real system, similar to the bonded terms involving LA and LAH as presented and discussed in the previous pages (Vreven, 2006).

For the discussion of how the generic QM/MM scheme is extended to electronic embedding. The equation of 3.4. QM/MM energy expression is modified to

$$E^{QM/MM-EE} = E^{MM-only,MM} + E_v^{model,QM} + E_{noQ}^{MM-only*model-only,MM} \quad (3.9)$$

where

$$\hat{H}_v^{model,QM} = \hat{H}^{model,QM} - \sum_i \sum_N \frac{s_N q_N}{r_{iN}} + \sum_J \sum_N \frac{Z_j s_N q_N}{r_{jN}} \quad (3.10)$$

N , J , and i refer to the atoms from the MM region, atoms from the QM region, and electrons, respectively. The subscript noQ indicates that the electrostatic terms are excluded. The scaling factor s_N is used to avoid overpolarization of the wave function due to large charges close to the QM region. Usually s_N is zero for charges less than three bonds away from the QM region, and unit for the remaining charges. The scaling factor also avoids ‘overcounting’. For example, for the C3-C5-C9 angle there are molecular mechanics bending (C3-C5-C9) and stretching terms (C3- C5 and C5-C9) in $E_{noQ}^{MM-only*model-only,MM}$ as mentioned in Table 3.2.

Table 3.2. Inclusion of Specific Interactions in the Generic Electronic Embedding QM/MM Energy Expression, with the Charges on C3 and C5 Scaled to Zero in the Model System Calculations^a

centers	included in MM model system?	included in MM real system?	in QM model?
N1-C6	no (centers not in model)	no (2 bond separation)	no
N1-N25	no (centers not in model)	scaled (3 bond separation)	no
N1-C27	no (centers not in model)	yes	no
C3-C9	<i>no (C3 scaled to zero)</i>	<i>no (excluded)</i>	<i>no (C3 scaled)</i>
C3-C12	<i>no (C3 scaled to zero)</i>	<i>no (excluded)</i>	<i>no (C3 scaled)</i>
C3-N15	<i>no (C3 scaled to zero)</i>	<i>no (excluded)</i>	<i>no (C3 scaled)</i>
C6-C9	yes	<i>no (excluded)</i>	yes
C6-N11	yes	<i>no (excluded)</i>	yes
C6-C14	yes	<i>no (excluded)</i>	yes
C6-H17	yes	<i>no (excluded)</i>	yes
H16-C9	no (2 bond separation)	no (2 bond separation)	yes
H16-N11	scaled (3 bond separation)	scaled (3 bond separation)	yes
H16-H13	yes	yes	yes
C5-N11	<i>no (C5 scaled to zero)</i>	<i>no (excluded)</i>	<i>no (C5 scaled)</i>
C5-C14	<i>no (C5 scaled to zero)</i>	<i>no (excluded)</i>	<i>no (C5 scaled)</i>
C5-H17	<i>no (C5 scaled to zero)</i>	<i>no (excluded)</i>	<i>no (C5 scaled)</i>
H5a-N11	<i>no (excluded)</i>	no (H5a not in real system)	yes
H5a-C14	<i>no (excluded)</i>	no (H5a not in real system)	yes
H5a-H17	<i>no (excluded)</i>	no (H5a not in real system)	yes

^aEntries in italics are different from those in Table 3.2.

The electrostatic and van der Waals interactions between these three centers are implicit in these bending and stretching terms and are therefore excluded from the list of nonbonded interactions in MM calculations. However, if the partial charge of C3 were included in the QM Hamiltonian, the electrostatic interaction of this center with the charge density of C9 would be fully included via the term $E_v^{\text{model, QM}}$. The electrostatic interaction would then be included twice: once through the C3-C5-C9 bending term and once through the inclusion of the charge on C3 in the Hamiltonian. Vreven et al., 2006 referred to this as ‘overcounting’, and scaling the charge on C3 to zero ensures that it does not take place. This solution, however, is not satisfactory, because scaling the charge on C3 to zero results in the exclusion of the electrostatic

interaction of this center with all the other QM atoms (C14, N15, etc.). Since these interactions should in fact be included, we refer to this as ‘undercounting’. In short, standard QM/ MM will always result in either undercounting or overcounting, which is ultimately the result of the incompatibility between the QM charge density and the MM atom centered charges (Vreven, 2006).

Some QM/MM implementations deal with the overpolarization and overcounting problem by using delocalized charges instead of point charges,(Amara, 2003; Das, 2002) or by redistributing the charges close to the QM region (Lin,2005). For electronic embedding in ONIOM we follow an approach that differs from standard QM/MM schemes. Following the spirit of ONIOM, the model system calculations were performed on the same system, which includes the charges that come from the MM region. In the QM model system these point charges are then incorporated in the Hamiltonian, while in the MM model system calculation they are evaluated at the classical level. Furthermore, only the model system calculations are modified, while the real system MM term remains identical to that in the ONIOM-ME (ONIOM-Mechanical Embedding) expression 1. The expression for ONIOM-EE (ONIOM Electronic Embedding) becomes

$$E^{ONIOM-EE} = E_v^{model,QM} + E^{real,MM} - E_v^{model,MM} \quad (3.11)$$

where

$$E_v^{model,MM} = E^{model,MM} + \sum_J \sum_N \frac{q_J s_N q_N}{r_{JN}} \quad (3.12)$$

The QM calculation in Eq. 3.11 is identical to that in Eq. 3.9. Since the model systems must be identical, Vreven et al., 2006 used the same scale factor s_N in both the QM and the MM model system calculations.

It must be noted that the use of delocalized or redistributed charges, as in other QM/MM schemes, is not mutually exclusive with the ONIOM implementation of electronic embedding. Applying both methods simultaneously might provide a superior scheme. Furthermore, from a practical point of view, a major difference between the QM/MM and ONIOM electronic embedding schemes is that in the latter the user must specify charges for the QM region (Vreven, 2006).

In Table 3.3 the specific electrostatic interactions in the MM terms are given, with the entries in italic being different from the corresponding Table 3.1 for ONIOM-ME. The specific electrostatic interactions between standard QM/MM-EE and ONIOM-EE are now compared. With QM/MM-EE, the interaction between C3 and N15 is undercounted because the charge on C3 is scaled to zero in the QM calculation, and the C3-N15 interaction is excluded from the MM calculations (Vreven, 2006).

Table 3.3. Inclusion of Specific Interactions in the Electronic Embedding ONIOM (QM:MM) Energy Expression, with the Charges on C3 and C5 Scaled to Zero in the Model System Calculations^a (Vreven, 2006)^a

centers	included in MM model system?	included in MM real system?	in QM model?
N1-C6	no (centers not in model)	no (2 bond separation)	no
N1-N25	no (centers not in model)	scaled (3 bond separation)	no
N1-C27	no (centers not in model)	yes	no
C3-C9	<i>no (C3 scaled to zero)</i>	no (2 bond separation)	<i>no (C3 scaled)</i>
C3-C12	<i>no (C3 scaled to zero)</i>	scaled (3 bond separation)	<i>no (C3 scaled)</i>
C3-N15	<i>no (C3 scaled to zero)</i>	yes	<i>no (C3 scaled)</i>
C6-C9	yes	scaled (3 bond separation)	yes
C6-N11	yes	yes	yes
C6-C14	yes	yes	yes
C6-H17	yes	yes	yes
H16-C9	no (2 bond separation)	no (2 bond separation)	yes
H16-N11	scaled (3 bond separation)	scaled (3 bond separation)	yes
H16-H13	yes	yes	yes
C5-N11	<i>no (C5 scaled to zero)</i>	no (2 bond separation)	<i>no (C5 scaled)</i>
C5-C14	<i>no (C5 scaled to zero)</i>	scaled (3 bond separation)	<i>no (C5 scaled)</i>
C5-H17	<i>no (C5 scaled to zero)</i>	yes	<i>no (C5 scaled)</i>
H5a-N11	no (2 bond separation)	no (H5a not in real system)	yes
H5a-C14	scaled (3 bond separation)	no (H5a not in real system)	yes
H5a-H17	yes	no (H5a not in real system)	yes

Entries in italics are different from those in Table 3.1.

In the ONIOM-EE scheme, however, this interaction is still present in the $E^{\text{real,MM}}$ term. The electrostatic interaction between C3 and N15 is therefore still included in the ONIOM expression, albeit at the classical level. Another example is the interaction between C6 and C9. The MM torsional term C9-C5-C3- C6 already contains implicitly part of the electrostatic interaction, which is why the three-bond separated nonbonded interactions are scaled. However, the C6-C9 electrostatic interaction is without scaling included in the QM term in equation $E_v^{\text{model,QM}}$. In QM/MM-EE this leads to overcounting, but in ONIOM-EE this particular interaction is included fully in the model system MM term $E_v^{\text{model,MM}}$ and scaled in the real system MM term $E_{\text{real,MM}}$. The difference between the MM terms can be regarded as a correction to the overcounting at the QM level. In other words, in ONIOM-EE the overcounting or undercounting introduced at the QM level is always corrected automatically at the classical level. This follows naturally from the ONIOM expressions and does not require any of the corrections that generic QM/MM-EE schemes need (Vreven, 2006).

In Figure 3.4 the error of the ONIOM-EE and QM/MM-EE calculations are shown on the example of deprotonation of histidine, compared to full QM calculations. The focus on this specific example is not on the absolute performance of the hybrid schemes but rather on the difference in behavior between ONIOM and the generic QM/MM method. The graph shows the error as a function of the number of bonds away from the QM region that have the charges scaled to zero. The charge on C5 is always scaled to zero. At $x = 1$, only charges one bond out (C5) are scaled. At $x = 2$, charges up to two bonds out (C5, H7, H8, and C3) are scaled, and so forth (Vreven, 2006).

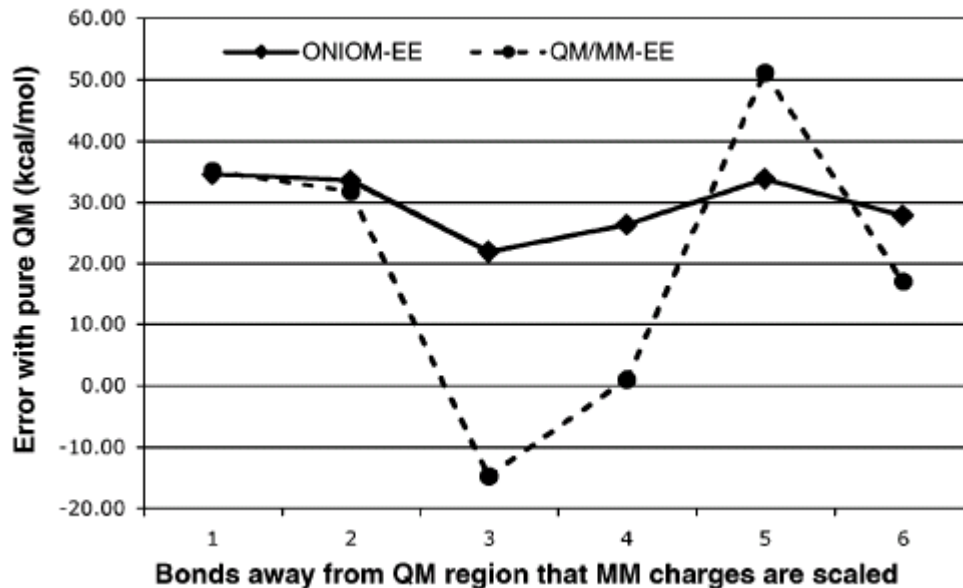


Figure 3.4. Error of ONIOM-EE and QM/MM-EE as a function of the charges scaled based on distance from the QM region. (Vreven, 2006)

Even though the QM/MM-EE has the smallest absolute error (at $x=4$), its behavior is much more erratic than ONIOM-EE. The reason is that, in this particular example, the sign of the charges in the MM region is alternating with each step further away from the QM region and that therefore the total charge included in the set of (nonzero) point charges changes strongly with each increasing x -value. In ONIOM-EE the total charge is always the same, because the error at the QM level is corrected at the MM level, and the graph is much less erratic (Vreven, 2006).

At $x=6$, all the charges in the MM region are scaled to zero in the model system calculations, and ONIOM-EE becomes identical to ONIOM-ME. It can be observed that the result is quite similar to the ONIOM-EE results, which indicates that the partial charges assigned to the QM region describe the real QM charge density quite well. Note that ONIOM-EE and QM/MM-EE are not identical to each other when all the charges are scaled to zero, at $x=6$. In that case, QM/MM-EE completely ignores

all the electrostatic interactions between the two layers, while QM/MM-EE becomes ONIOMME and still includes the electrostatic interactions at the classical level, through the $E^{\text{real,MM}}$ calculation (Vreven, 2006).

Finally, in this specific example of histidine deprotonation Vreven et al, 2006 stressed that the example is intended primarily to demonstrate that correct charge balancing follows naturally from the electronic embedding version of ONIOM. Their generic QM/MM implementation is crude in many ways, and the unfavorable comparison to ONIOM-EE in Figure 3.4. is not typical for state-of-the-art QM/MM implementations, which have incorporated other methods for dealing with the charge-balancing. These methods, however, are complimentary with ONIOM, and using both approaches simultaneously may provide the superior QM/MM scheme.

3.2. Computational Procedure

With respect to the specific examples of ethane and histidine (Vreven, 2006), the calculation methods followed in this research could be understood more easily.

In this investigation, preliminary calculations of nitrous oxide decomposition on 51 atoms of Ag, Au, Ir, Rh and 22 atoms of Pt ONIOM cluster which simulates (111) surfaces were carried out using DFT/B3LYP method with basis sets composed of Los Alamos LANL2DZ effective core pseudo-potentials (ECP) for silver, gold, iridium, platinum and rhodium and 3-21G** for nitrogen, oxygen and hydrogen as implemented in Gaussian 2003 (Appendix A). Relative energy profiles as functions of chosen reaction coordinate pathways were calculated and two distinct pathways, one leading to N₂ gas and the other forming atomic oxygen identified.

3.2.1. Surface Model

Quantum chemical calculations employing DFT (Kohn and Sham, 1965) are carried out to investigate the energetics of nitrous oxide decomposition on a 51 atom Ag, Au, Ir, Rh and a 22 atom Pt cluster representing (111) surface. All calculations are conducted using the Gaussian 2003 suite of programs (Frisch et al. 2003). DFT calculations are carried out using Becke's (1988,1989) three-parameter hybrid method involving the Lee, Yang, and Parr (1988) correlation functional (B3LYP) formalism (Appendix B). Ag, Au, Ir, Pt and Rh atom 2 layer ONIOM method is used to simulate (111) surface where 14 Ag atoms, 4 Au, Ir, Pt and Rh atoms are in high layer DFT region and the rest of the cluster (37 Ag atoms, 47 Au, Ir, and Rh atoms and 18 Pt atoms) is in low layer molecular mechanics region utilizing universal force field (UFF).

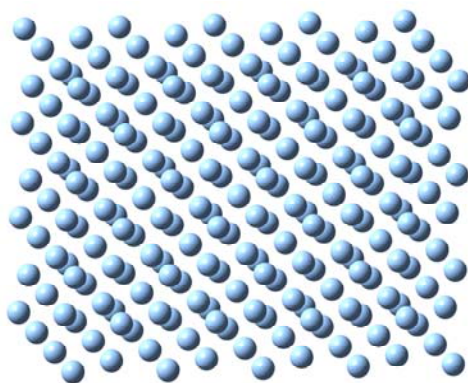


Figure 3.5. Enlarged silver cluster

Silver unit cell is taken as an example for demonstrating the construction of all metals investigated in this study. Silver unit cell has a face centered cubic lattice structure with lattice parameter $a=4.08 \text{ \AA}$ and space group number 225. It is constructed using

this data and it is first enlarged three times in X, Y and Z directions (Fig.3.5). Ag(111) surface is then obtained by reduction from the enlarged cluster and finally the 2 layer 51 Ag atom ONIOM cluster is formed as shown in Figure 3.6.

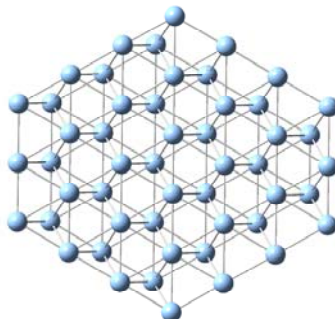


Figure 3.6. Reduced Silver (111) Surface

3.2.2. Computational Method

The basis set employed in the DFT calculations is the Los Alamos LANL2DZ effective core pseudo-potentials (ECP) for silver and 3-21G** for nitrogen, oxygen and hydrogen as implemented in Gaussian 2003. The LANL2DZ pseudo-potential is chosen particularly because of the advantage of doing faster calculations with relatively little compromise on accuracy. All energies and energy differences are calculated for 0 K without zero point energy (ZPE) corrections. The ZPE corrections would likely be similar for each of these cluster systems and thus would not influence conclusions based on the relative energies.

The following general computational procedure is followed in the calculations of this research: Initially, the adsorbing molecules are optimized geometrically by means of the equilibrium geometry calculations. The total energy of the fixed Ag, Au, Ir, Pt and Rh cluster is obtained by single point geometry calculations. Then, the adsorbing molecule is located over the active site of the cluster at a selected distance and a coordinate driving calculation is performed by selecting a reaction coordinate in order to obtain the variation of the relative energy with a decreasing reaction coordinate to get an energy profile as a function of the selected reaction coordinate distance. All of the adsorption calculations are carried out by considering the Ag, Au, Pt, Rh and Ir cluster systems as neutral with quartet, singlet, singlet, doublet and triplet spin multiplicity, respectively.

The relative energy is defined as:

$$\Delta E = E_{\text{System}} - (E_{\text{Cluster}} + E_{\text{Adsorbate}})$$

where E_{System} is the calculated energy of the given geometry containing cluster and the adsorbing molecule at any interatomic distance, E_{Cluster} is the energy of the cluster itself and $E_{\text{Adsorbate}}$ is that of the adsorbing molecule.

After having obtained the energy profile for the desired reaction, the geometry with the minimum energy on the energy profile is re-optimized by means of the equilibrium geometry calculations to obtain the final geometry for the reaction. Furthermore, from the energy profile, the geometry with the highest energy is taken as the input geometry for the transition state geometry calculations. Starting from these geometries, the transition state structures with only one negative eigenvalue in Hessian matrix are obtained.

CHAPTER 4

RESULTS AND DISCUSSION

The behaviour of nitrous oxide decomposition over representing (111) surfaces of five different transition metals, Ag, Au, Ir, Pt and Rh is desired to be studied by means of quantum chemical simulation methods as mentioned in earlier chapters. With respect to the computational procedure described in Chapter 3, the reaction of nitrous oxide decomposition on five transition metals is analyzed deliberately from the sides of activation barrier, reaction enthalpy and equilibrium geometries in sub-headlines.

4.1. N₂O Decomposition Over Ag₅₁ Cluster Representing (111) Surface

Firstly, Ag₅₁ cluster was constructed by using a lattice parameter of 4.08 Å and space group number 225, the bond lengths of Ag-Ag were 2.885 Å (Wyckoff, 1965), and then representing (111) surface was selected as the face where the reaction of N₂O decomposition should occur. As mentioned in Chapter 3, ONIOM method was used to determine the sites where atomic oxygen was adsorbed. For the case of Ag₅₁ cluster, 14 atoms were selected as DFT region (represented as balls), the basis set employed in DFT calculations for silver was LANL2DZ, and the remaining 37 atoms were appointed as Molecular Mechanics region (represented as wireframe). Optimized N₂O molecule by using 3-21 G^{**} basis set at B3LYP level was selected as reactant and placed over the representing (111) surface as demonstrated clearly in Figure 4.1.

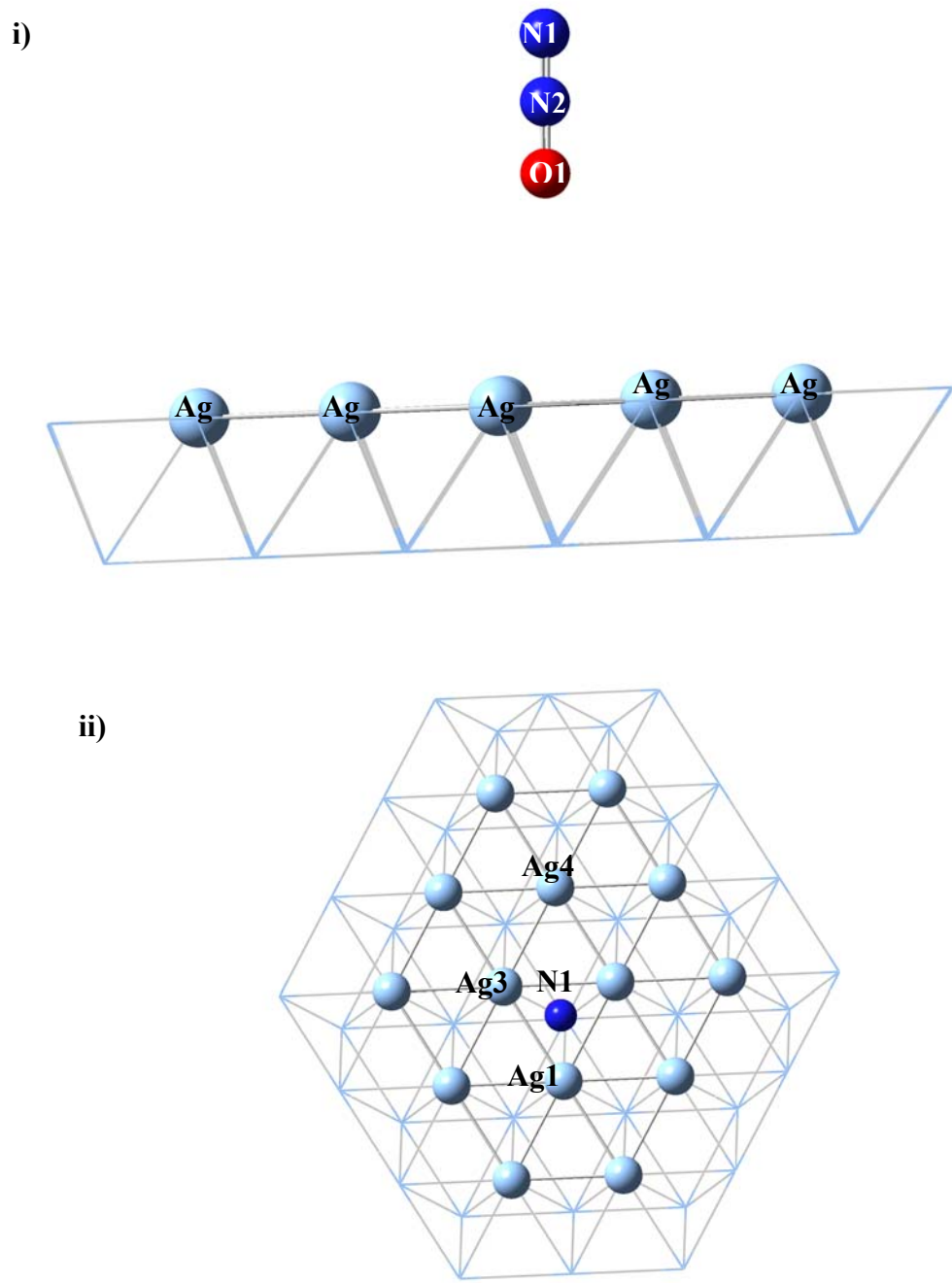


Figure 4.1. Ag₅₁ cluster representing (111) surface and optimized N₂O
 i) Side view ii) Top view

Single-crystal measurements show that N₂O decomposition is significantly activated on atomically clean Ag(111) (Tan et al., 1987).

Schwamer and coworkers, 1996 investigated the dissociation of N₂O over Ag(111) single crystal experimentally. In this research, the thermal and electron-induced chemistry of N₂O on Ag(111) was examined using temperature programmed desorption (TPD) and Auger electron spectroscopy (AES). N₂O adsorbs and desorbs molecularly with multilayer and monolayer desorption temperatures of 86 and 94-102 K, respectively. No thermal decomposition was observed. Irradiation with 50 and 2500 eV electrons at 83 K causes partial decomposition of multilayers; N₂ desorbs during irradiation, O₂ desorption, at 530 K, is observed in post-irradiation TPD. Only O and Ag are detected by AES after flashing irradiated samples to 500 K; O disappears above 700 K. Incident and secondary electrons can account for the observed surface chemistry and the latter can account for reported N₂O decomposition in X-ray photoelectron measurements. For monolayer coverages, irradiated with 50 eV electrons, there is no dissociation, an effect attributed to substrate quenching.

The results of Schwamer et al., 1996 indicate the decomposition of N₂O on Ag(111) reported earlier in the investigation of Grimblot et al., 1990, was not due to thermally activated dissociation but, in all likelihood, was the result of secondary electrons generated by the X-rays either at the anode itself or upon photon absorption by the Ag(111) substrate.

Based on the data presented in literature by Tan et al., 1987; Schwamer, 1996 and Grimblot, 1990 it is clear that the nitrous oxide decomposition on Ag(111) surface occurs as leaving an oxygen atom on the surface and with respect to this findings the input of coordinate driving for nitrous oxide decomposition over representing Ag(111) surface was prepared for loading to Gaussian 2003.

In order to determine spin multiplicity of the system illustrated in Figure 4.1, single point energy calculations were performed for different spin multiplicities; and by comparing these results spin multiplicity for the system of N₂O and Ag₅₁ cluster was obtained as four. By taking spin multiplicity as four, the reaction coordinate input was loaded by taking the basis sets for silver, nitrogen and oxygen into consideration as mentioned earlier.

The O1 of N₂O was placed at distance of 4.148 Å far from Ag1 atom of Ag₅₁ cluster in the input geometry as illustrated in Figure 4.2. in detail. The distance was chosen for the reason that any interaction of N₂O with Ag₅₁ cluster should be prevented in order to observe the physical adsorption of N₂O onto the surface.

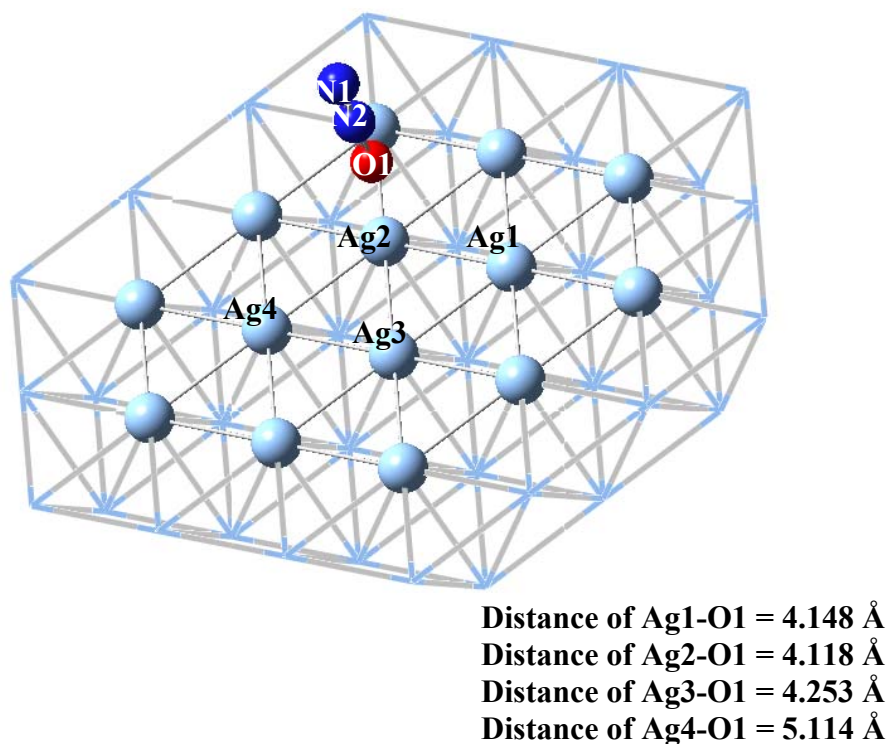


Figure 4.2. Distances of O1 between the selected Ag atoms in the input geometry for N₂O decomposition

Regarding the geometry of reactant and cluster as input, reaction coordinate calculations were started and the distances between the O1 atom of N₂O and Ag1, Ag2, Ag3 and Ag4 atoms in the Ag₅₁ cluster were analyzed especially. The reaction profile was drawn with respect to the energies of optimized geometries of reactant and Ag₅₁ cluster for each distance of O1 and Ag4 in the Figure 4.3. By using the results of the reaction profile the activation barrier, reaction enthalpy, interatomic distances in the final geometry of reaction complex are determined for N₂O decomposition reaction:

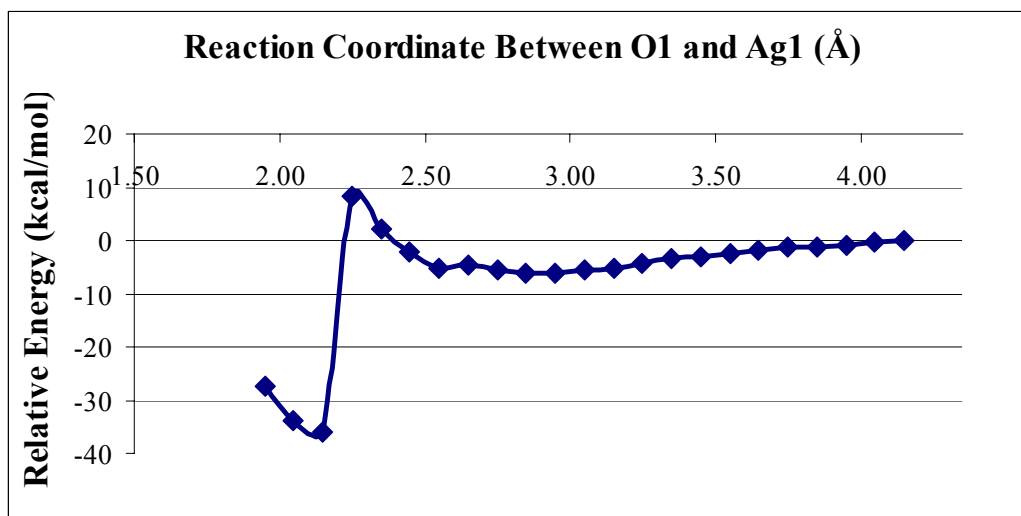


Figure 4.3. Energy profile of N₂O decomposition on Ag₅₁ cluster representing (111) surface

Table 4.1. Activation barrier (E_a) and enthalpy of reaction (ΔH) on Ag (in kcal/mol)

Catalyst	E_a	ΔH
Ag ₅₁ Cluster Representing (111) Surface	14.48	-29.79
Ag(111) (Zeigarnik, 2002)	0.00	-41.2

For calculating activation barrier and reaction enthalpy, the energy of input system in Figure 4.2. was taken as reference and the energies for each step of reaction coordinate was calculated as indicated below.

Energy at each reaction step starting from the distance between Ag1 and O1 of 4.148 Å to 2.166 Å was calculated as:

$$\text{Relative Energy} = \text{Energy at the reaction step} - \text{Energy of the reactant system}$$

By using the data of relative energy, activation barrier and enthalpy were calculated simply by taking the energy differences of reactant and transition complex and reactant and product complex, respectively and presented in Table 4.1 by comparing with the data in the literature.

Activation barrier (E_a) and reaction enthalpy (ΔH) values are reported in Table 4.1, and it could be noticed that these values do not coincide with the data reported by Zeigarnik, 2002. The method followed in the investigation of Zeigarnik, 2002, unity bond index-quadratic exponential potential (UBI-QEP), makes use of the data on the energies of two-center metal-adsorbate bonds. Within the framework of UBI-QEP method, by using the binding energies of adsorbed oxygen atom and nitrogen atom as

initial data, the binding energy of adsorbed N₂O is calculated in the investigation of Zeigarnik, 2002. With respect to our approach executed in this investigation, the value of activation barrier for nitrous oxide decomposition is far more different than the value obtained in the literature. This difference originates from application of different calculation methods; thus, an experimental investigation in the future covering nitrous oxide decomposition on Ag (111) would give us the chance of comparing the reliability of the method applied in this study and the method used by Zeigarnik, 2002 for the reaction of nitrous oxide decomposition, especially.

The distance between O1 and Ag1, Ag2, Ag3 and Ag4 in the reaction complex were found in the Figure 4.4., final geometry of N_{2(g)}, O_(ads) and Ag₅₁ cluster as 2.166 Å, 2.156 Å, 2.255 Å, and 3.656 Å, respectively. The comparison of the values of Ag-O bond is presented in the Table 4.2.

Table 4.2. Ag-O bond distance in this investigation comparing to literature data (Å)

System	Ag-O Bond Distance (Å)
This Investigation	2.166
Nakatsuji et al., 1993	2.160
Dubiel et al., 1997	2.150

As demonstrated in the Table 4.2, the bond distance between silver and oxygen has a very near value to the distances reported in other investigations. This shows the accuracy of the coordinate driving calculations following the ONIOM method and also it should be noted that nitrous oxide decomposes as leaving oxygen atom on the surface. This point also supports the values of activation energy and reaction enthalpy values reported in Table 4.1.

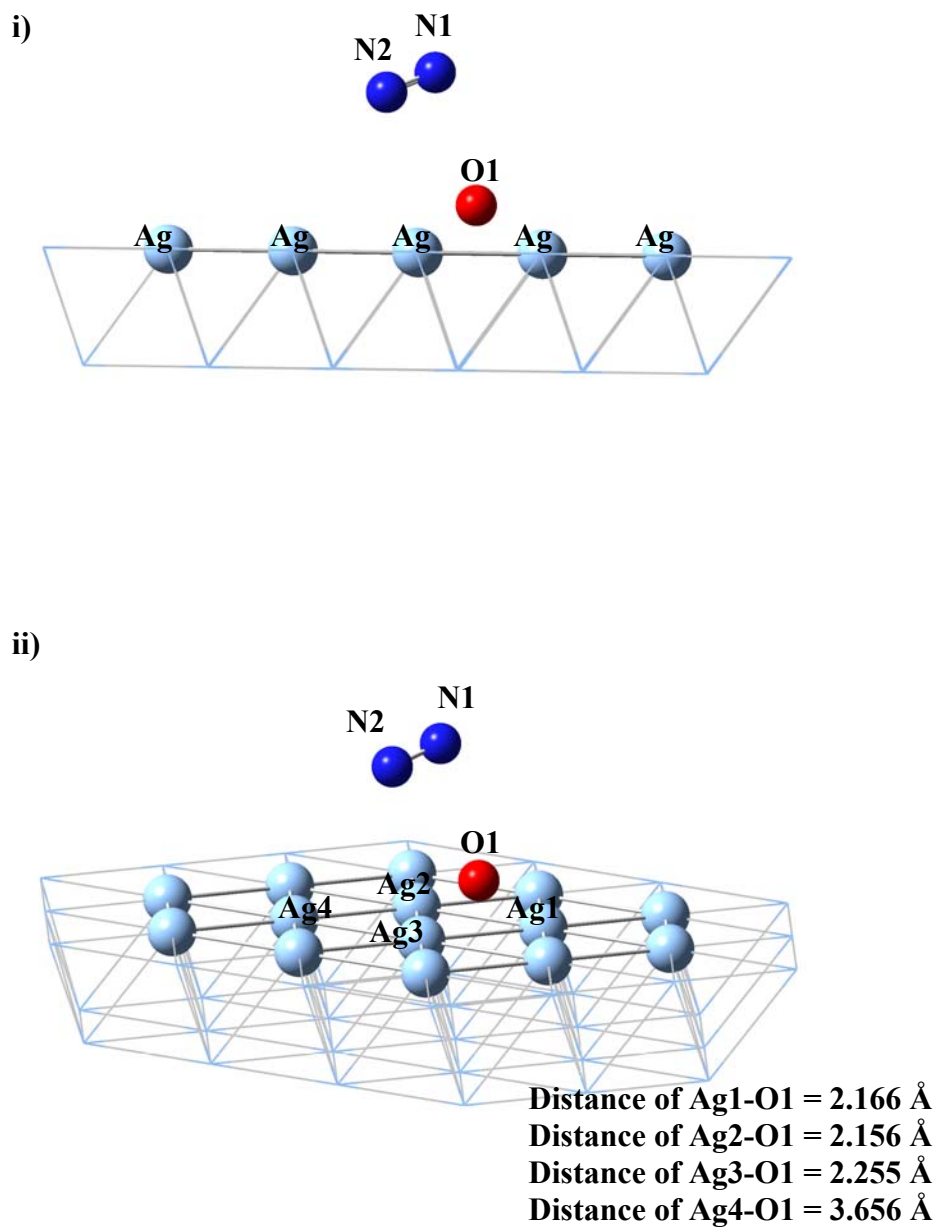


Figure 4.4. Adsorbed oxygen atom on Ag₅₁ cluster representing (111) surface and N₂ molecule after N₂O decomposition from different two sides of view, i and ii

4.2 N₂O Decomposition Over Au₅₁ Cluster Representing (111) Surface

Au₅₁ cluster was constructed by using space group number 225 with a lattice parameter of 4.08 Å (Wyckoff, 1965). The bond lengths of Au-Au were 2.88 Å. The plane of (111) was assigned as the representing surface over which N₂O decomposition should proceed. By using ONIOM method, the active sites of representing (111) surface was clearly observed as demonstrated in the Figure 4.5. Contrast to Ag₅₁ cluster, for the case of Au₅₁ cluster 4 atoms were selected as DFT region with LANL2DZ appointed as basis set for gold in the calculations performed, and the remaining 47 atoms were selected as Molecular Mechanics region. Same as the previous case N₂O molecule was optimized by using 3-21 G** basis set at B3LYP level and played a role as reactant. In the Figure 4.5 N₂O molecule was located at a distance of 4.186 Å considering the atoms O1 and Au1. Then Gaussian 03 was used as a software tool for performing calculations of N₂O decomposition and reaction profile was obtained with important information of activation barrier, reaction enthalpy and final geometry of reaction complex.

The acquired information based on the reaction progress gave us the chance of comparing the similar type of data from literature as listed in Table 4.3. When comparing with the data in the literature, it could be observed that the values of activation energy and reaction enthalpy do not follow the parallel lines. According to Zeigarnik, 2002, the activation barrier was calculated as zero for gold case likewise to the previous case. Also, it should be noted that the binding is via the terminal nitrogen atom in the investigation of Zeigarnik, 2002, unlike to this study in which nitrous oxide adsorbs by oxygen atom.

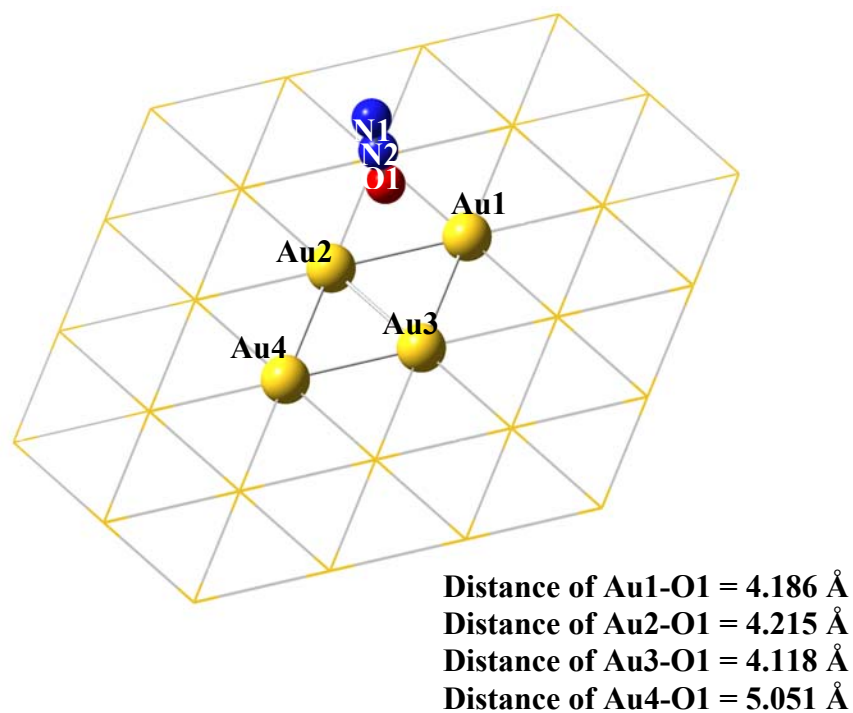


Figure 4.5. Distances of O1 between the selected Au atoms in the input geometry for N₂O decomposition

Table 4.3. Activation barrier (E_a) and enthalpy of reaction (ΔH) on Au (in kcal/mol)

Catalyst	E_a	ΔH
Au ₅₁ Cluster Representing (111) Surface	15.72	-18.82
Au(111) (Zeigarnik. 2002)	0.00	-35.9

Spin multiplicity of the reaction complex of N₂O and Au₅₁ cluster in Figure 4.5 was reached as one depending on the single point energy calculations performed for each different probable spin multiplicities. Concerning the basis sets for gold, nitrogen and oxygen stated previously and spin multiplicity of one, the reaction coordinate input was applied by using Gaussian 2003.

The location of O1 of N₂O was far from Au1 atom of Au₅₁ cluster in the reaction input as drawn in Figure 4.5 with each distances of Au1-O1, Au2-O1, Au3-O1 and Au4-O1. In the same manner of the previous case, N₂O was inserted at an adequate distance from the representing (111) surface of Au₅₁ cluster in order to prevent any interactions and any confusing behaviour of the decomposition trend and reach the line of existed phenomena in regard with increasing energy of reaction complex for each step in reaction coordinate calculations.

Input geometry was applied as the reactant, N₂O, and the cluster, Au₅₁ by using Gaussian 2003. The distances between the O1 atom of N₂O and Au1, Au2, Au3 and Au4 atoms in the Au₅₁ cluster were determined after performing coordinate calculations of N₂O decomposition.

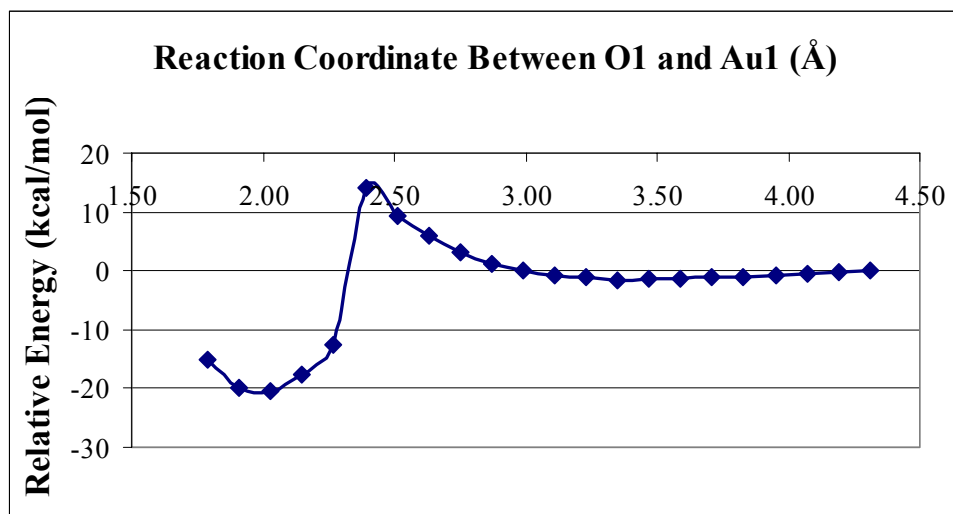


Figure 4.6. Energy profile of N₂O decomposition on Au₅₁ cluster representing (111) surface

In the Figure 4.6 the relative energy diagram was obtained by using the data of nitrous oxide decomposition over Au₅₁ cluster representing (111) surface for each step between O1 and Au1 in the Figure 4.5. In addition, important data of the activation barrier, reaction enthalpy, interatomic distances in the final geometry of reaction system was acquired for N₂O decomposition reaction, N₂O_(g) → N_{2(g)} + O_(ads) by using the results of the reaction profile.

In parallel with the method applied in the previous case, activation barrier and reaction enthalpy, the energy of input system in Figure 4.5. was selected as reference energy and the energies for each step of reaction coordinate was obtained as indicated below. In other words, energy at each reaction step starting from the distance between Au1 and O1 of 4.186 Å to 2.250 Å was determined as:

$$\text{Relative Energy} = \text{Energy at the reaction step} - \text{Energy of the reactant system}$$

Activation barrier and enthalpy values for gold were calculated as same as in silver case simply by taking the energy differences of reactant and transition complex and reactant and product complex, respectively by the help of relative energy data and detailed presentation of the results can be observed in Table 4.3 in previous pages.

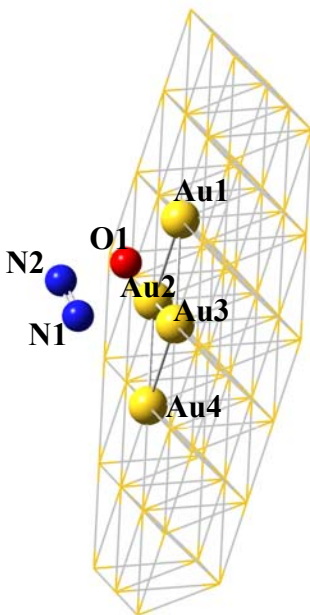
Furthermore, in the Figure 4.7 Au1-O1, Au2-O1, Au3-O1 and Au4-O1 distances in the final reaction system were observed as 2.250 Å, 2.359 Å, 2.209 Å, and 3.701 Å, respectively in the form of bridge composed of Au1, Au2, Au3 and O1.

Comparison of the bond distance with the one reported in literature is presented in Table 4.4. It can be easily noticed that the results of this study are reasonable like the energy values.

Table 4.4. Au-O bond distance in this investigation comparing to literature data (Å)

System	Au-O Bond Distance (Å)
This Investigation	2.250
Zharkova et al.. 2006	2.071
Salama et al.. 1996	2.164

i)



ii)

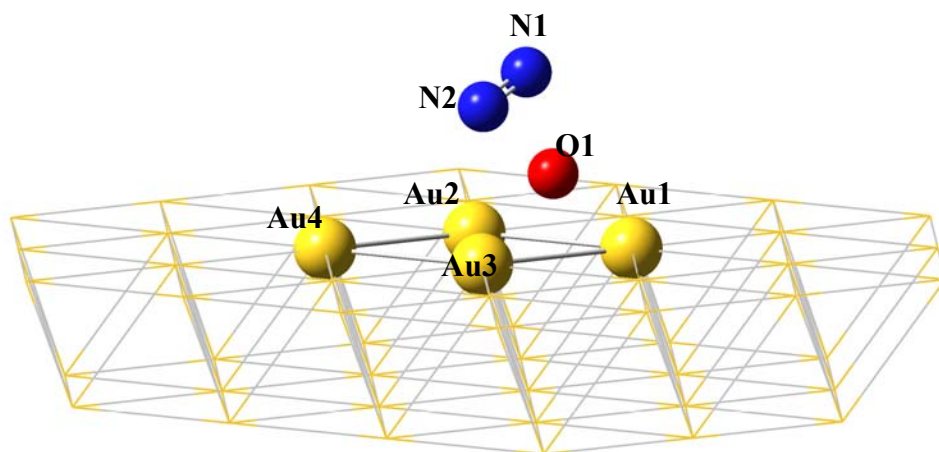


Figure 4.7. Adsorbed oxygen atom on Au₅₁ cluster representing (111) surface and N₂ molecule after N₂O decomposition from different two sides of view, i and ii

4.3. N₂O Decomposition Over Pt₂₂ Cluster Representing (111) Surface

The unit cell of platinum with a lattice parameter of 3.923 Å was constructed by using space group number 225 (Wyckoff, 1965), then the representing plane of (111) was chosen as model cluster then assigned as Pt₂₂. The bond lengths of Pt-Pt were 2.774 Å in Pt₂₂ model cluster and then layers in this model cluster representing plane (111) was appointed. The detailed demonstration of the model cluster and N₂O is in Figure 4.8. The plane where the decomposition of nitrous oxide should proceed and the atoms of DFT region (represented as balls) and the atoms of Molecular Mechanics region (represented as wireframe) was drawn as the input of reaction coordinate. By using ONIOM method, the active sites of representing (111) surface was indicated in the following figures. Likewise to Au₅₁ cluster case, 4 atoms were selected as DFT region with LANL2DZ were taken as basis set for platinum for performance of calculations, and the remaining 18 atoms were decided as Molecular Mechanics region. Optimization of reactant N₂O molecule was completed by using 3-21 G** basis set at B3LYP level. In the Figure 4.8. N₂O molecule was placed at a distance of 4.327 Å as taking into consideration of the atoms of O1 and Pt1. It should be mentioned again that Gaussian 03 was applied as a tool for accomplishment of coordinate driving for N₂O decomposition and based on the results obtained by coordinate driving calculations reaction profile was drawn and important information of activation barrier, reaction enthalpy and final geometry of reaction complex were acquired.

The results were listed in Table 4.5 and compared with the data in the literature by considering both model catalyst and model reaction.

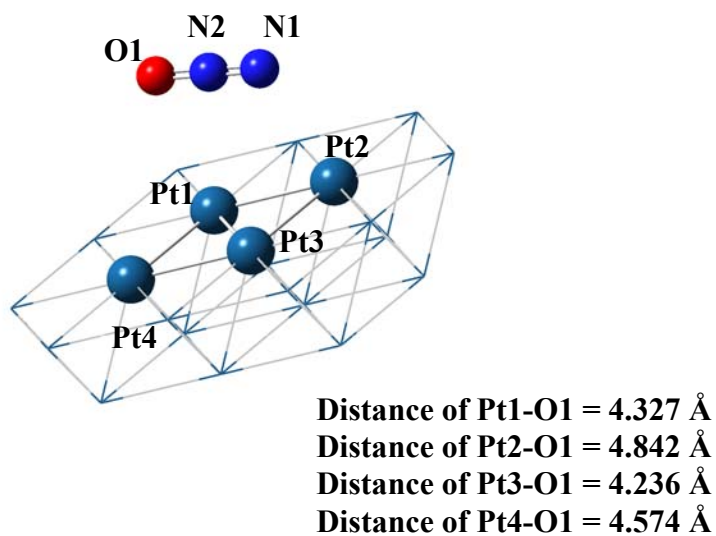


Figure 4.8. Distances of O1 between the selected Pt atoms in the input geometry for N₂O decomposition

Table 4.5. Activation barrier (E_a) and enthalpy of reaction (ΔH) on Pt in kcal/mol)

Catalyst	E_a	ΔH
Pt ₂₂ Cluster Representing (111) Surface	7.02	-32.82
Pt(111) (Burch et al., 2004)	7.38	not reported
Pt(111) (Zeigarnik, 2002)	0.00	-46.10

After performing of the single point energy calculations considering all possible spin multiplicities, the information of spin multiplicity of the reaction complex of N₂O and Pt₂₂ cluster in Figure 4.8 was found as one same as the case of Au₅₁ cluster. Coordinate driving calculations were started after preparing the input as demonstrated in Figure 4.8 N₂O was placed over Pt₂₂ cluster in the form of initial reaction complex with distances of Pt1-O1, Pt2-O1, Pt3-O1 and Pt4-O1. Any risk of possible interactions between P₂₂ cluster representing (111) surface and N₂O was eliminated by settling down of the reactant molecule at remote distance from the cluster. Hence, the physical adsorption can be easily examined on the reaction profile meaning that the reaction started at the natural level of reactant energies. For each reaction step, smooth energy increase of reaction complex underlines the natural trend of decomposition reaction and this trend could be observed in Figure 4.9.

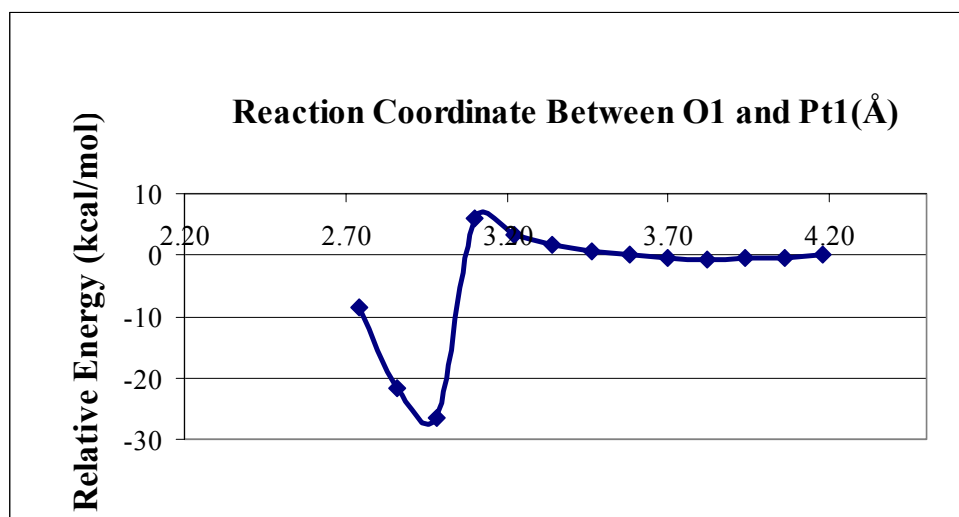


Figure 4.9. Energy profile of N₂O decomposition on Pt₂₂ cluster representing (111) surface

Detailed reaction input composed of the reactant, N_2O , and the cluster of Pt_{22} representing (111) surface was applied. After performing of the coordinate driving calculations for N_2O decomposition reaction the distances of Pt1-O1, Pt2-O1, Pt3-O1 and Pt4-O1 were determined as drawn in Figure 4.10.

For every each step of nitrous oxide decomposition over Pt_{22} cluster representing (111) surface, energy of the reaction complex was obtained and with respect to this data the reaction profile was drawn in the Figure 4.9. Depending on data obtained by this graph activation barrier and reaction enthalpy were reported then final representation of the system was drawn by using the atomic coordinates concerning the overall progress of N_2O decomposition.

With respect to the information given in Table 4.5, the comparison of activation barrier and enthalpy values with the data reported by Zeigarnik, 2002 does not coincide; on the other hand, the value of activation barrier presented by Burch et al., 2004 is nearly the same as the one calculated in this study. Contrary to the method of Zeigarnik, 2002, all calculations were carried out within the DFT framework in the investigation of Burch et al.

In the light of the approach mentioned in earlier cases, the referred energy while determining relative energy levels was the input geometry of reaction complex and depending on this selection energy of every reaction step was calculated by subtracting the reference from the energy of each step.

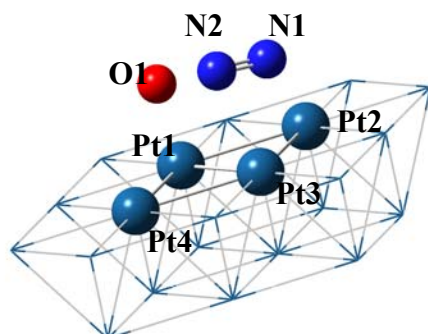
Table 4.6. Pt-O bond distance in this investigation comparing to literature data (Å)

System	Pt-O Bond Distance (Å)
This Investigation	2.049
Jacob et al., 2003	2.110

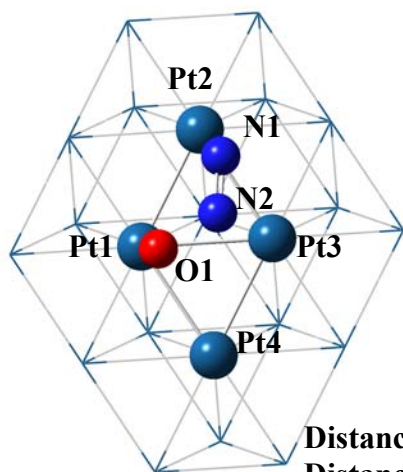
As mentioned in previous pages, calculation of activation barrier and enthalpy was achieved by considering the energy levels of reactant and transition complex and reactant and product complex, and reported as in Table 4.5. Moreover, Pt1-O1, Pt2-O1, Pt3-O1 and Pt4-O1 distances in the reaction system was simulated as 2.049 Å, 3.371 Å, 3.297 Å and 3.376 Å, respectively by adsorbing onto the site of Pt1. Comparison of bond distances with literature data are presented in Table 4.6.

Based on the comparison in Table 4.6, the calculated bond distance in this investigation follows a line parallel with the one reported in literature (Jacob et al., 2003). This also supports the phenomena of oxygen atom adsorption onto the cluster by considering the nature and path of nitrous oxide decomposition. As demonstrated in the Figure 4.10, nitrous oxide leaves an oxygen atom onto the Pt1 atom over the surface.

i)



ii)



Distance of Pt1-O1 = 2.049 Å
Distance of Pt2-O1 = 3.371 Å
Distance of Pt3-O1 = 3.297 Å
Distance of Pt4-O1 = 3.376 Å

Figure 4.10. Adsorbed oxygen atom on Pt₂₂ cluster representing (111) surface and N₂ molecule after N₂O decomposition from different two sides of view, i and ii

4.4. N₂O Decomposition Over Rh₅₁ Cluster Representing (111) Surface

First of all, rhodium unit cell with a lattice parameter of 3.803 Å was built by using space group number 225 and atomic coordinates (Wyckoff, 1965). Rh cluster containing 51 atoms representing (111) surface was used as the model plane. There existed 4 atoms in DFT region and 47 atoms were selected as Molecular Mechanics region atoms in the ONIOM model of Rh₅₁ cluster with bond lengths of Rh-Rh. It could be clearly seen the drawing of Rh₅₁ model cluster and reactant of N₂O molecule in Figure 4.11. This figure also represents both the plane where the decomposition of nitrous oxide should take place and the atoms of DFT region and the atoms of Molecular Mechanics region demonstrating the coordinate driving of nitrous oxide. The sites of representing (111) surface where the main core of the subject reaction was realized could be seen in the following figures.

Basis set of rhodium was appointed as LANL2DZ same as the previous three clusters of silver, gold and platinum. Before performing the calculations 4 atoms were selected as DFT region and the remaining 47 atoms were decided as Molecular Mechanics region in ONIOM configuration of layers. It should be highlighted that reactant N₂O molecule was optimized by using 3-21 G** basis set at B3LYP level. During performing calculations of coordinate driving Gaussian 03 was the software tool achieving the simulation of N₂O decomposition. Connecting to the results obtained by each step of reaction coordinate relative energy diagram was represented and activation barrier, reaction enthalpy data were stated in Table 4.7 comparing the results reached in the literature.

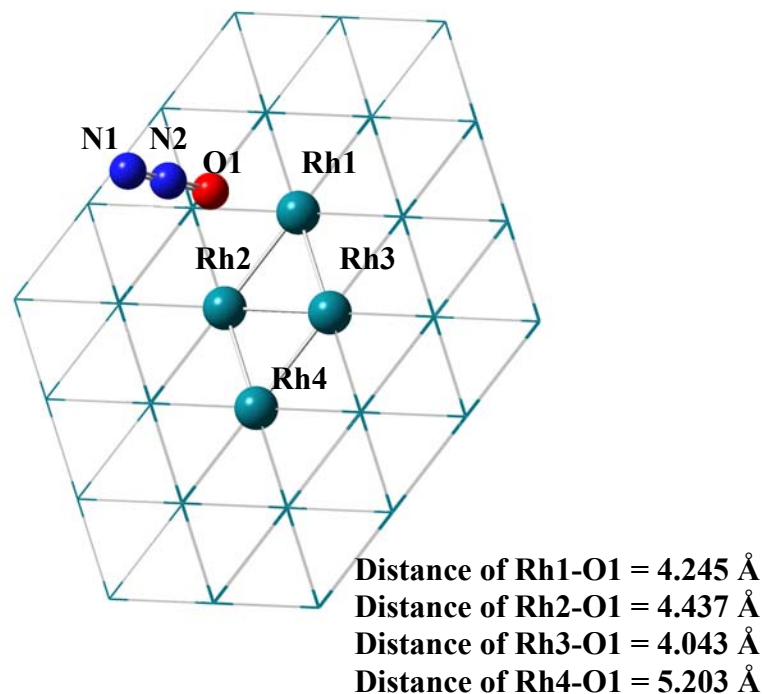


Figure 4.11. Distances of O1 between the selected Rh atoms in the input geometry for N₂O decomposition

Single point energies of Rh₅₁ cluster and reactant of N₂O for various different spin multiplicities were calculated and with respect to outcomes of these calculations the spin multiplicity was determined as two. Reaction coordinate calculations were applied with the help of Gaussian 03 by taking the input illustrated in Figure 4.11 as a starting point. The three important distances of Rh1-O1, Rh2-O1, Rh3-O1 and Rh4-O1 of this reaction input were clearly indicated in Figure 4.11 just for the same reason mentioned in previous cases that N₂O should be located at quite far from the Rh₅₁ cluster representing (111) surface. Thus, it should be again taken into consideration that reaction progress follows a smooth trend without any pre-increased level of reactant N₂O due to interactions with the surface atoms of Rh₅₁ cluster. For each reaction step, energy increase with decreasing atomic distance between Rh1 and O1 showed clearly the phenomena of N₂O decomposition starting from the initial

condition of reactant and cluster complex to the final condition representing $N_{2(g)}$ and $O_{(ads)}$ over the cluster surface. The calculated energy values and similar data in the literature are presented in Table 4.7 and the reaction profile is illustrated in Figure 4.12.

Table 4.7. Activation barrier (E_a) and enthalpy of reaction (ΔH) on Rh (in kcal/mol)

Catalyst	E_a	ΔH
Rh ₅₁ Cluster Representing (111) Surface	3.76	-58.08
Rh(111) (Zeigarnik. 2002)	0.00	-64.20

The reactant of nitrous oxide and Rh₅₁ cluster representing (111) surface were the main two elements to be loaded for accomplishing the coordinate driving and with respect to outcome of these calculations the interatomic distance between Rh1-O1, Rh2-O1, Rh3-O1 and Rh4-O1 as indicated in Figure 4.13 and the distances are compared with the data in the literature as presented in Table 4.8, and the calculated value in this study is consistent with the experimental value (Padberezkaya et al., 1997).

Regarding the values in Table 4.7, the dissimilarity of barrier and enthalpy values between the literature data reported by Zeigarnik, 2002, is obvious comparing to the calculated values in previous cases.

Table 4.8. Rh-O bond distance in this investigation comparing to literature data (Å)

System	Rh-O Bond Distance (Å)
This Investigation	2.187
Padberezkaya et al., 1997	2.001

Furthermore, it should be highlighted that a bridge was formed in an imaginary pyramidal top composing of O1 and Rh1, Rh2, Rh3 as the base corners clearly illustrated in Figure 4.13.

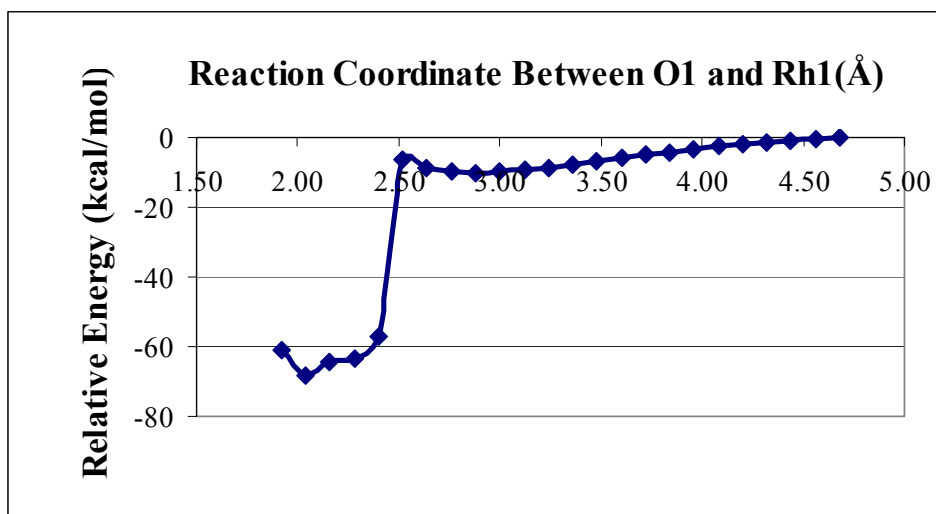


Figure 4.12. Energy profile of N₂O decomposition on Rh₅₁ cluster representing (111) surface

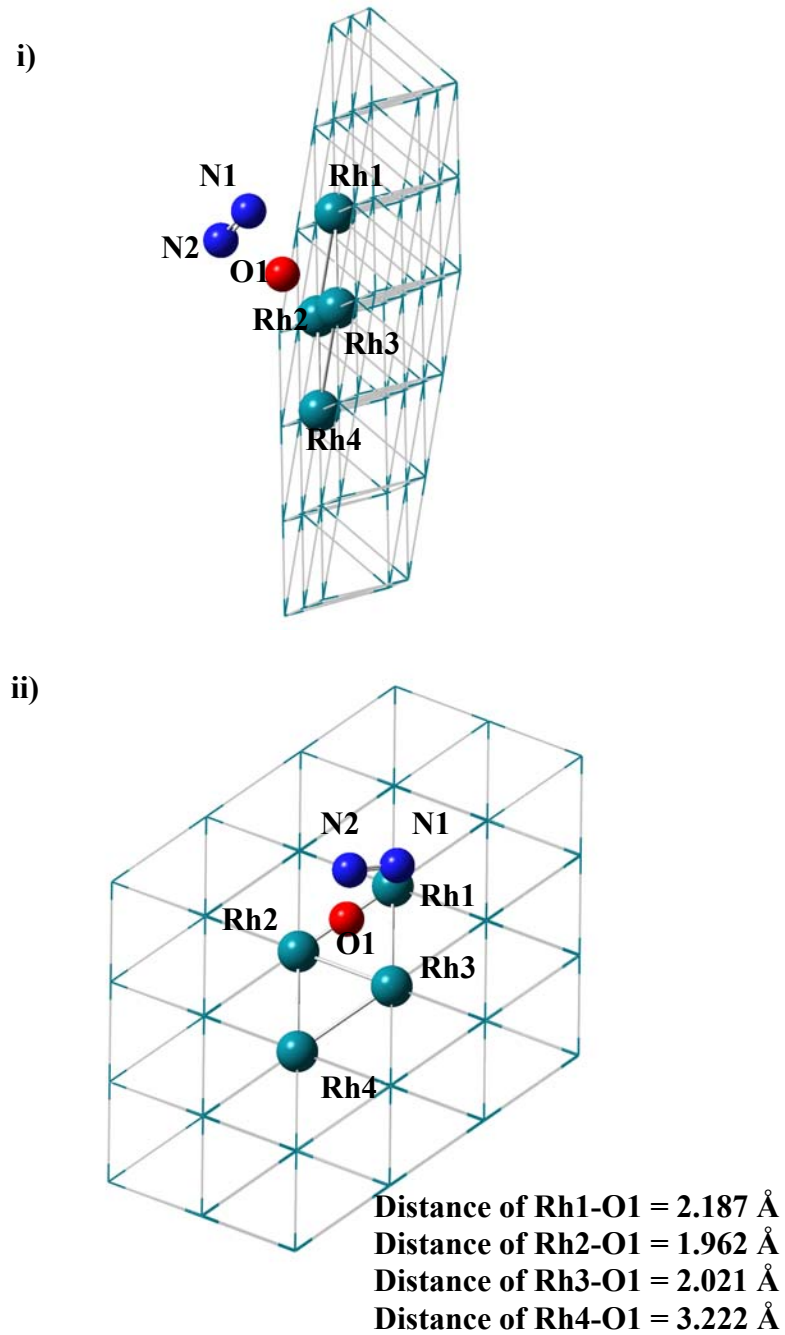


Figure 4.13. Adsorbed oxygen atom on Rh₅₁ cluster representing (111) surface and N₂ molecule after N₂O decomposition from different two sides of view, i and ii

4.5. N₂O Decomposition Over Ir₅₁ Cluster Representing (111) Surface

The final investigation of nitrous oxide decomposition over transition metals is Ir₅₁ cluster representing (111) surface constructed by using a lattice parameter of 3.839 Å and space group number 225 as the same for the other cases (Wyckoff, 1965), and based on the cluster bond lengths of Ir-Ir were 2.715 Å. Depending on the approach for construction unit cell representing (111) surface was assigned as the plane where the progress of N₂O decomposition was realized. ONIOM method was the method of attack for investigation of the decomposition reaction resulting one adsorbed oxygen atom on the surface and nitrogen gas.

In DFT region there existed 4 DFT atoms and it should be clearly stated that the basis set employed in DFT calculations for iridium was LANL2DZ as the same as the other cases in this investigation and the remaining 47 atoms were appointed as Molecular Mechanics region. In the Figure 4.14 it could be clearly observed the optimized N₂O molecule by using 3-21 G^{**} basis set at B3LYP level as located over the catalyst representing (111) surface.

The spin multiplicity was three after the investigations of single point energy for the subject reaction complex of Ir₅₁ and N₂O. By the help of Gaussian 03 the input illustrated in Figure 4.14 as the initial step was the beginning of the processing.

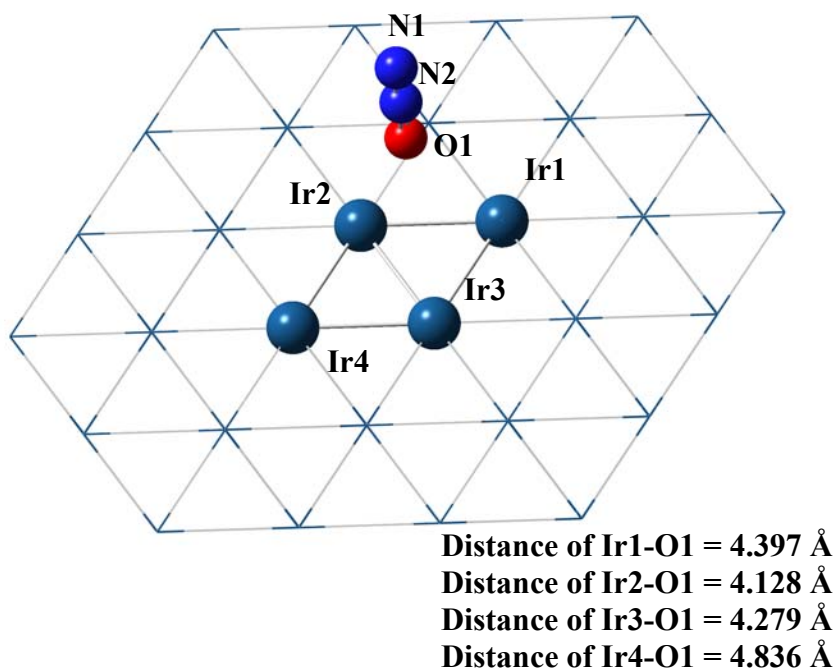
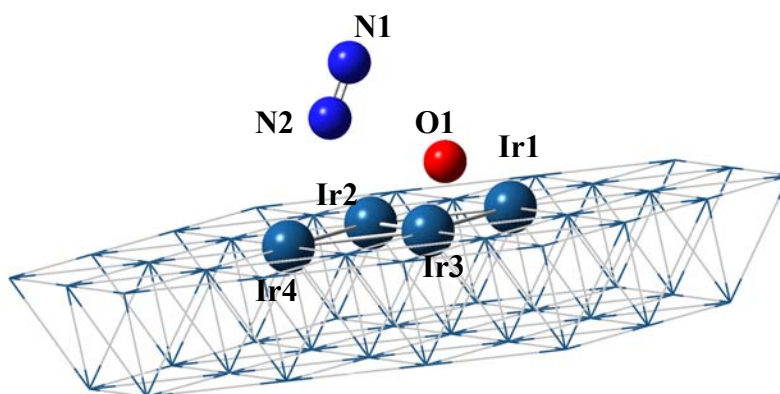


Figure 4.14. Distances of O1 between the selected Ir atoms in the input geometry for N₂O decomposition

Also, there are four important distances of Ir1-O1, Ir2-O1, Ir3-O1 and Ir4-O1 of this reaction input drawn in Figure 4.14. The natural tendency of N₂O decomposition was obtained by locating the N₂O at a distance of 4.397 Å enough far from the catalyst surface in order to prevent any extraordinary interactions of Ir₅₁ cluster representing (111) surface. Hence, the reaction proceeded in a line without sharp increase or decrease in the energy level of reaction system. As same as the other cases the reactant of N₂O left an adsorbed oxygen atom on the representing (111) plane as illustrated in Figure 4.15.

i)



ii)

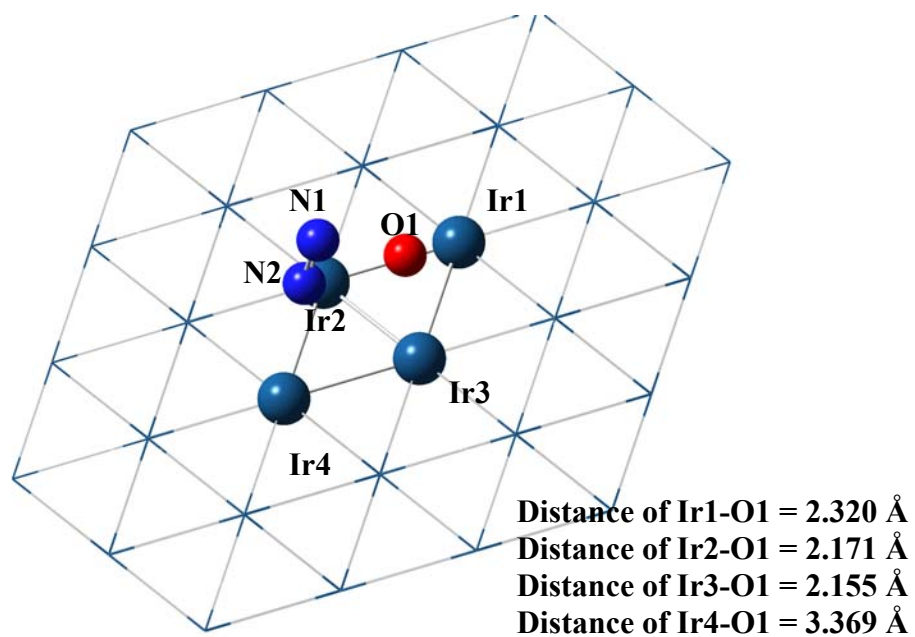


Figure 4.15. Adsorbed oxygen atom on Ir₅₁ cluster representing (111) surface and N₂ molecule after N₂O decomposition from different two sides of view, i and ii

Regarding coordinate driving calculation of nitrous oxide decomposition, the final geometry of reaction complex with adsorbed oxygen atom on the surface was clearly demonstrated in Figure 4.15, ii) with distances of Ir1-O1, Ir2-O1, Ir3-O1 and Ir4-O1.

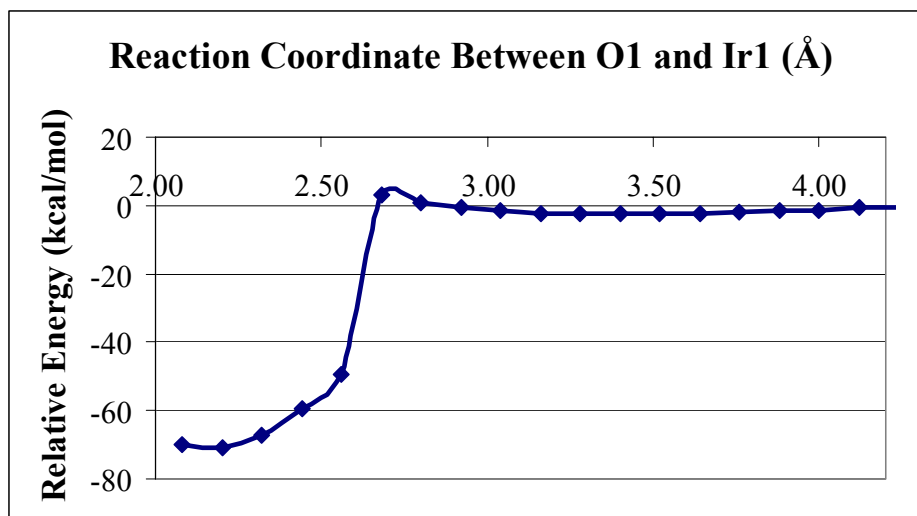


Figure 4.16. Energy profile of N₂O decomposition on Ir₅₁ cluster representing (111) surface

Through the investigation and analysis of reaction profile as in Figure 4.16 activation energy and reaction enthalpy were presented in Table 4.9. Comparing to the data reported by Zeigarnik, 2002, activation barrier and enthalpy values do not coincide very well similar to the cases of Ag, Au, Pt and Rh. At that point, it should be noted that there is no appropriate UBI-QEP formula, method followed by Zeigarnik, 2002, for calculating such binding of linear triatomic molecules like N₂O; furthermore, underlined again that for reaching a specific conclusion in order to compare the reliability of the results, an elaborate experimental analysis in future is needed then reliability of the method in this investigation and the one followed by Zeigarnik, 2002 could be appreciated in a definite way.

Table 4.9. Activation barrier and enthalpy of reaction (ΔH) on Ir in (kcal/mol)

Catalyst	E_a	ΔH
Ir ₅₁ Cluster Representing (111) Surface	5.51	-68.47
Ir(111) (Zeigarnik, 2002)	0.00	-54.60

As a result of this elaborate studies, a bridge formation can be observed in Figure 4.15 the bond distances iridium and adsorbed oxygen atom is presented in the Table 4.10. Like the other cases the reported distance is in parallel with the one experimentally reported.

Table 4.10. Ir-O bond distance in this investigation comparing to literature data (\AA)

System	Ir-O Bond Distance (\AA)
This Investigation	2.155
Ladipo et al., 1993	2.109

CHAPTER 5

CONCLUSIONS

In this study, nitrous oxide decomposition on representing (111) surface of Ag₅₁, Au₅₁, Pt₂₂, Rh₅₁ and Ir₅₁ clusters were investigated by means of quantum chemical calculations using ONIOM method.

In ONIOM calculations for nitrous oxide decomposition basis set of LANL2DZ is employed for the metal atoms in DFT region and 3-21 G** basis set at B3LYP level is selected for N₂O. Main core of this investigation is the understanding of the natural trend of nitrous oxide decomposition on transition metals representing (111) surface and determining the activation barrier, reaction enthalpy and interatomic distance between the metal and adsorbed oxygen atom.

With respect to the aim of this study, nitrous oxide decomposition is simulated and activation barrier values are reported. Activation energies for Ag, Au, Pt, Rh and Ir are calculated as 14.48 kcal/mol, 15.72 kcal/mol, 7.02 kcal/mol, 3.76 kcal/mol and 5.51 kcal/mol, respectively. It is concluded that decomposition of nitrous oxide occurs more easily on Rh metal comparing to other ones. The values in literature do not

follow the same trend in parallel with the reported barrier values in this investigation, except the case of Pt.

The calculated values for activation barrier and enthalpy of reaction do not coincide with the ones in literature except Pt. While there exists a clear dissimilarity in the cases of Ag, Au, Rh and Ir, the calculated value of activation barrier in Pt case coincides exactly with the data reported by literature.

Considering activation energies for both forward and reverse reaction, enthalpies on Ag, Au, Pt, Rh and Ir are calculated as -29.79 kcal/mol, -18.82 kcal/mol, -32.82 kcal/mol, -58.08 kcal/mol and -68.47 kcal/mol respectively. It should be concluded that exothermic nature of nitrous oxide decomposition can easily be observed on the reported values of reaction enthalpy in this study.

As a final point to conclude, nitrous oxide decomposition occurs as leaving the oxygen atom adsorbed on representing (111) surface. For on all clusters, this phenomena is observed as the natural trend of nitrous oxide decomposition.

REFERENCES

- Akbar, S. And Joyner, R.W., J. Chem. Soc. Faraday Trans. 1, 77, 803 (1981).
- Alini, S., Basile, F., Blasioli, S., Rinaldi C. and Vaccari, A., Applied Catalysis B:Environmental 70, 323 (2007).
- Amara, P.; Field, M. J. Theor. Chem. Acc., 109, 43- 52 (2003).
- Amphlett, C.B., Trans. Faraday Soc., 50, 273 (1954).
- Anpo, M., Aikawa, N., Kubokawa, Y., Che, M., Louis, C. and Giamello E., J. Phys. Chem., 89, 5017 (1985).
- Antes, I.; Thiel, W. J. Phys. Chem. A, 103, 9290- 9295 (1999).
- Armor, J.N., Braymer, T.A., Farris, T.S., Li, Y., Petrocelli, F.P., Weist, E.L., Kannan, A. and Swamy, C.S., Appl. Catal. B, 7, 397 (1996).
- Avery, N. R. Surf, Sci., 235, 501 (1983).
- Avery, N.R., Surf. Sci., 131, 501, (1983).
- Bakowies, D.; Thiel, W. J. Phys. Chem., 100, 10580-10594 (1996).

Becke, A. D., Phys. Rev., B., 38, 3098 (1988).

Boissel, V., Tahir, S. and Koh, C. A., Applied Catalysis B: Environmental 64, 234 (2006).

Brem G., Onderzoek naar N₂O emissies door verbranding (Investigations into N₂O emissions from combustion), Report 90-411 /8726-22254, MT-TNO, Leidschendam, 1990 (in Dutch).

Burch, R., Daniells, S. T., Breen, J. P., Hu, P., J. Catal. 224, 252–260 (2004).

Ceballos, G., Wende, H., Baberschke, K., Arvanitis, D., Surf. Sci., 482-485, 15-20 (2001).

Centi, G., Cerrato, G., D'Angelo, S., Finardi, U., Giamello, E., Morterra, M. And Perathoner, S., in Proceedings of Environmental Catalysis: 1st World Conference, Pisa, Italy, pp.175-178, (2001).

Centi, G., Dall'Olio, L., Perathoner, S., Appl. Catal. A 194-195, 79 (2000).

Centi, G., Dall'Olio, L., Perathoner, S., J.Catal. 192, 224 (2000).

Centi, G., Galli, B., Montanari, B., Perathoner, S., Vaccari, A., Catal. Today 35, 113 (1997).

Ceperley, D.M., Alder, B.J. Phys. Rev. Lett., 45, 566 (1980).

Chang, Y.F., McCarty, J.G. and Zhang, Y.L., Catal. Lett. 34, 163 (1995).

Chang, Y.F., McCarty, J.G., Wachsman, E.D. and Wong, V.L., Appl.Catal.B, 4 283 (1994).

- Choe, J.S., Cook P.J. and Petrocelli F.P., Presented at ANSPG Conference,
Cimino, A. And Indovina V., J. Catal., 17, 54 (1970).
- Cimino, A., Bosco, R., Indovina, V. And Schiavello, M., J.Catal., 5, 271 (1966).
- Cimino, A., Indovina, V., Pepe, F. and Schiavello, M., J.Catal., 14, 49 (1969).
- Cimino, A. and Pepe, F. J.Catal., 25, 362 (1972).
- Conningham, J., Kelly, J.J. and Penny, A.L., J.Phys. Chem., 75, 617 (1971).
- Cornell, W. D.; Cieplak, P.; Bayly, C. I.; Gould, I. R.; Merz, K. M.; Ferguson, D. M.; Spellmeyer, D. C.; Fox, T.; Caldwell, J. W.; Kollman, P. A. J. Am. Chem. Soc., 117, 5179 (1995).
- Cornish, J. C. L.; Avery, N. R. Surf, Sci.. 235, 209 (1990).
- Cornish, J.C.L. and Avery, N.R., Surf. Sci., vol.235, p. 209 (1990).
- Crutzen, P.L., J.Geophys. Res., 76, 7311 (1971).
- Dandl, H. And Emig G., in Proceedings of Environmental Catalysis: 1st World Conference, Pisa, Italy, pp.615-618 (1995)
- Dapprich, S.; Koma'romi, I.; Byun, K. S.; Morokuma, K.; Frisch, M. J. J. Mol. Struct. (THEOCHEM) 461-462, 1-21 (1999).
- Das, D.; Eurenus, K. P.; Billings, E. M.; Sherwood, P.; Chatfield, D. C.; Hodoscek, M.; Brooks, B. R. J. Chem. Phys., 117, 10534-10547 (2002).

- Dell, R.M., Stone, F.S. and Tiley P.F., *Trans. Faraday Soc.*, 49, 201 (1953).
- Derat, E.; Bouquant, J.; Humbel, S. *J. Mol. Struct. (THEOCHEM)*, 632, 61-69 (2003).
- Destin FL, USA, 6, pp.1-13 (October 1993)
- DiLabio, G. A.; Hurley, M. M.; Christiansen, P. A. *J. Chem.Phys.*, 116, 9578-9584 (2002).
- Dubiel, M., Brunsch, S., Kolb, U., Gutwerk, D. And Bertagnolli, H., *J. Non-Crys. Sol.*, 220, 30-44 (1997).
- Ebitani K., Morokuma, M. and Morikawa A., *Bull. Chem. Soc. Jpn.*, 66, 3811 (1993).
- Ebitani K., Morokuma, M. and Morikawa A., *Stud.Surf. Sci. Catal.*, 84, 1501-1506 (1994).
- Ebitani K., Morokuma, M., Kim, J.H. and Morikawa A., *J. Catal.*, 141, 725 (1993).
- Field, M. J.; Bash, P. A.; Karplus, M. *J. Comput. Chem.*, 11, 700-733 (1990).
- Framework Convention on Climate Change (FCCC), Report of the Conference of the Parties on its 3rd Session, Held at Kyoto, 1(11) Retrieved December 1997, FCCC/CP/1997/7/Add.1, from <http://www.unfccc.de/> (1997).

Frisch, M. J.; Trucks, G. W.; Schlegel, H. B.; Scuseria, G. E.; Robb, M. A.; Cheeseman, J. R.; Montgomery, J. A., Jr.; Vreven, T.; Kudin, K. N.; Burant, J. C.; Millam, J. M.; Iyengar, S. S.; Tomasi, J.; Barone, V.; Mennucci, B.; Cossi, M.; Scalmani, G.; Rega, N.; Petersson, G. A.; Nakatsuji, H.; Hada, M.; Ehara, M.; Toyota, K.; Fukuda, R.; Hasegawa, J.; Ishida, M.; Nakajima, T.; Honda, Y.; Kitao, O.; Nakai, H.; Klene, M.; Li, X.; Knox, J. E.; Hratchian, H. P.; Cross, J. B.; Adamo, C.; Jaramillo, J.; Gomperts, R.; Stratmann, R. E.; Yazyev, O.; Austin, A. J.; Cammi, R.; Pomelli, C.; Ochterski, J. W.; Ayala, P. Y.; Morokuma, K.; Voth, G. A.; Salvador, P.; Dannenberg, J. J.; Zakrzewski, V. G.; Dapprich, S.; Daniels, A. D.; Strain, M. C.; Farkas, O.; Malick, D. K.; Rabuck, A. D.; Raghavachari, K.; Foresman, J. B.; Ortiz, J. Frisch, M. J.; Trucks, G. W.; Schlegel, H. B.; Scuseria, G. E.; Robb, M. A.; Cheeseman, J. R.; Montgomery, J. A., Jr.; Vreven, T.; Kudin, K. N.; Burant, J. C.; Millam, J. M.; Iyengar, S. S.; Tomasi, J.; Barone, V.; Mennucci, B.; Cossi, M.; Scalmani, G.; Rega, N.; Petersson, G. A.; Nakatsuji, H.; Hada, M.; Ehara, M.; Toyota, K.; Fukuda, R.; Hasegawa, J.; Ishida, M.; Nakajima, T.; Honda, Y.; Kitao, O.; Nakai, H.; Klene, M.; Li, X.; Knox, J. E.; Hratchian, H. P.; Cross, J. B.; Adamo, C.; Jaramillo, J.; Gomperts, R.; Stratmann, R. E.; Yazyev, O.; Austin, A. J.; Cammi, R.; Pomelli, C.; Ochterski, J. W.; Ayala, P. Y.; Morokuma, K.; Voth, G. A.; Salvador, P.; Dannenberg, J. J.; Zakrzewski, V. G.; Dapprich, S.; Daniels, A. D.; Strain, M. C.; Farkas, O.; Malick, D. K.; Rabuck, A. D.; Raghavachari, K.; Foresman, J. B.; Ortiz, J. Froese, R. D. J.; Morokuma, K. In *Encyclopedia of Computational Chemistry*; Schleyer, P. v. R., Allinger, N. L., Kollman, P. A., Clark, T., Schaefer, H. F., III, Gasteiger, J., Schreiner, P. R., Eds.; Wiley: Chichester; Vol. 2, pp 1244-1257 (1998).

Fu, C.M., Korchak, V.N. and Hall, W.K., *J.Catal.*, 68, 166 (1981).

Gao, J. In *Encyclopedia of Computational Chemistry*; Schleyer, P. v. R., Allinger, N. L., Kollman, P. A., Clark, T., Schaefer, H. F., III, Gasteiger, J., Schreiner, P. R., Eds.; Wiley: Chichester, Vol. 2, pp 1257-1263 (1998).

Gao, J. In *ReViews in Computational Chemistry*; Lipkowitz, K. B., Boyd, D. B., Eds.; VCH Publishers: New York; Vol. 7, pp 119-301 (1996).

Gao, J.; Amara, P.; Alhambra, C.; Field, M. J. *J. Phys. Chem. A*, 102, 4714-4721 (1998).

Golodets, G.I., *Stud. Surf. Sci. Cat.*, 15 200 (1983).

Gomez, R., Weaver, M.J., *Langmuir*, 18, 4426-4432 (2002).

Greengard, L. *The rapid eValuation of potential fields in particle systems*; MIT Press: Cambridge, MA, (1988).

Greengard, L.; Rokhlin, V. *J. Comput. Phys.*, 73, 325 (1987).

Grimblot, J.; Alnot, P.; Bchm, R. J.; Brundle, C. R. *J. Electron Spectrosc. Relat. Phenom.*, 52, 175 (1990).

Guzma'n-Vargas, A., Delahay, G., Coq, B., *Appl. Catal.*, B 42, 369 (2003).

Heyden, A, Ph.D. Dissertation, Hamburg University of Technology, Hamburg (2005).

Hinshelwood, C.N. and Prichard, C.R., *J.Chem.Soc.*, 127, 327 (1925).

Hohenberg, P., Kohn, W., *Phys. Rev.*, 136, B864 (1964).

Hopkins, B. W.; Tschumper, G. S. *J. Comput. Chem.*, 24, 1563 (2003).

Humbel, S.; Sieber, S.; Morokuma, K. *J. Chem. Phys.*, 105, 1959-1967 (1996).

- Indovina, V., Cordischi, D., Occhiuzzi, M. And Arieti, A., J. Chem.Soc. Faraday Trans. 1, 75 2177 (1979).
- Iwamoto, M., Matsukami, K., Kagawa, S., J. Phys. Chem. 87 903 (1983).
- Jacob T., Muller R.P., Goddard W.A., J.Phys.Chem., 107, pp.9465-9476 (2003).
- Kalback, W.M. and Sliepcevich, C.M., Ind. Eng. Chem. Fundam., 17, 165 (1978).
- Kannan, S. And Swamy, C.S., Appl.Catal., 3 109 (1994).
- Kapteijn, F., Rodrigues-Mirasol, J., Moulijn, J.A., Appl.Catal. B., 9, 25-64 (1996).
- Karadakov, P. B.; Morokuma, K. Chem. Phys. Lett., 317, 589-596 (2000).
- Karlsen E.J. and Pettersson, L. G. M., J. Phys. Chem. A, 107, 1641 (2003).
- Kawi, S., Liu S.Y. and Shen, S.C., Catalysis Today 68, 237 (2001).
- Keenan, A.G. and Iyengar, R.D., J.Catal., 5, 301 (1966).
- Khan, M.M., Somorjai, G.A., J. Catal. 91, 263 (1985).
- Kim, Y.; Schreifels, J. A.; White, J. M. Surf. Sei. 1982, 111 , 349. Spectrosc. Relat. Phenom., 52, 175 (1990).
- Kiss, J., Lennon, D., Jo, S.K., White, J.M., J. Phys. Chem., 95, 8054-8059 (1991).
- Kobayashi H.and Ohkubo, K., Applied Surface Science 121/122, 111 (1997).

- Koga, N.; Morokuma, K. Chem. Phys. Lett., 172, 243-248 (1990).
- Kohn, W., Sham, L. J., Phys. Rev., 140, A1133 (1965).
- Kramlich, J.C. and Linak, W.P., Prog. Energy Combust Sci., 20, 149 (1994).
- Kudin, K. N.; Scuseria, G. E. Chem. Phys. Lett., 283, 61-68 (1998).
- Ladipo, F.T., Kooti, M., Merolo, J.S., Inorg.Chem., 32, pp.1681-1688, (1993)
- Lee, C., Yang, W., Parr, R. G. Phys. Rev., B, 37, 785, (1988).
- Leglise, J., Petunchi, J.O. and Hall, W.K., J.Catal., 86, 392 (1984).
- Li, Y. And Armor, J.N., Appl. Catal. B, 1, L21 (1992).
- Li, Y. And Armor, J.N., Catal. B, 1, L31 (1992).
- Li, Y. and Bowker, M., Surf. Sci., vol. 348, p. 67 (1996).
- Li, Y., Bowker, M., Surf. Sci 348, 67-76 (1996).
- Lin, H.; Trulahr, D. G. J. Phys. Chem. A, 109, 3991-4004 (2005).
- Lintz, H.G., Surf. Sci. 108 L481, (1981).
- Lintz, H.G. and Riekert, L., J.Catal., 88, 244 (1984).

Liu, H.F., Liu, R.S., Liew, K.Y., Johnson, R.E., Lunsford, J.H., J. Am. Chem. Soc. 106, 4117 (1984).

Liu, R.S., Iwamoto, M., Lunsford, J.H., J. Chem. Soc. Chem. Commun. 78, 78 (1982).

Lolacano, M., Schiavello M., Cordischi D. And Mercati, G., Gazz. Chim. Ital., 105, 1165 (1975).

Madey, T. E.; Avery, N. R.; Anton, A. B.; Toby, B. H.; Weinberg, Maseras, F.; Morokuma, K. J. Comput. Chem., 16, 1170-1179 (1995).

Mauvezin, M., Delahay, G., Kisslich, F, Coq, B., Kieger, S., Catal. Lett. 62, 41 (1999)

Merz, K. M.; Stanton, R. V. In Encyclopedia of Computational Chemistry; Schleyer, P. v. R., Allinger, N. L., Kollman, P. A., Clark, T., Schaefer, H. F., III, Gasteiger, J., Schreiner, P. R., Eds.; Wiley: Chichester; Vol. 4, pp 2330-2343 (1998).

Meyer, R.J. and Pietsch (Editors), Gmelins Handbuch der Anorganischen Chemie, Vol., 4, Verlag Chemie, Berlin, pp.558-597 (1936)

Nakatsuji, H. And Nakai, H., J. Chem. Phys, Vol.98, pp.2423-2436, (1993).

Nicoll, R. M.; Hindle, S. A.; MacKenzie, G.; Hillier, I. H.; Burton, N. A. Theor. Chem. Acc., 106, 105-112 (2000).

Øy garden, A.H., Ramirez, J. P., Applied Catalysis B: Environmental 65, 163 (2006).

P. M. W.; Johnson, B.; Chen, W.; Wong, M. W.; Gonzalez, C.; Pople, J. A. Gaussian 03 ReVision C.01 ed.; Gaussian, Inc.: Wallingford, CT, (2004).

P. M. W.; Johnson, B.; Chen, W.; Wong, M. W.; Gonzalez, C.; Pople, J. A. Gaussian DeVelopment Version ReVision C.02 ed.; Gaussian, Inc.: Wallingford, CT, (2004).

Panov, G.I., CATTECH 4, 18 (2000).

Panov, G.I., Sobolev, V.I. and Kharitanov, A.S., J. Mol. Catal., 61, 85 (1990).

Partington, J. R., A Short History of Chemistry, Dover, New York, (1989)

Parmon, V.N., Panov, G.I., Uriarte, A., Noskov, A.S., Catal. Today 100, 115-131 (2005).

Padberezkaya, N.V., Romanenko G.V., Khranenko S.P, Belyaev, A.V., J.Struct. Chem., 38, pp.620-625 (1997).

Penunchi, J.O. and Hall, W.K., J. Catal., 78, 327 (1982).

Perdew, J.P., Wang, Y., Phys. Rev. B, 45, 13244 (1992).

Ramirez, J.P., Kapteijn, F., Mul G. and Moulijn, J.A., Catalysis Communications 3, 19 (2002).

Rebenstrof, B., Larsson L. And Larsson, R., Acta Chim. Scand. A, 32, 461 (1978).

Rega, N.; Iyengar, S. S.; Voth, G. A.; Schlegel, H. B.; Vreven, T.; Frisch, M. J. J. Phys. Chem. B, 108, 4210-4220 (1978).

Reimer, R.A., Slaten, C.S., Seapan, M., Lower M.W. and Tomlinson, P.E., Environ. Progr., 13, 134 (1994).

Reuter, N.; Dejaegere, A.; Maignet, B.; Karplus, M. J. Phys. Chem. A, 104, 1720-1735 (2000).

Riekert, L., Menzel D. And Staib, M., in Proceedings of 3rd International Congress on Catalysis, pp. 387-395 (1965)..

Rodriguez-Mirasol, J., Marbán, G., Kapteijn, F. and Moulijn, J.A., Progress report no. 2 JOU2 project 0229. Report JOU2-0229-2, CPT-TU Delft, Delft (1995).

Ruiz-Lo'pez, M. F.; Rivail, J. L. In Encyclopedia of Computational Chemistry; Schleyer, P. v. R., Allinger, N. L., Kollman, P. A., Clark, T., Schaefer, H. F., III, Gasteiger, J., Schreiner, P. R., Eds.; Wiley: Chichester; Vol. 1. (1998).

Russo, N., Fino, D., Saracco, G. and Specchia, V., Catalysis Today 119, 228 (2007).

Salama T.M., Shido, T., Ohnishi, R., Ichikawa, M., J.Phys.Chem, 100i, pp.3688-3694 (1996).

Santiago, M. and Ramirez, J., Environ. Sci. Technol., 41,1704 (2007).

Scagnelli, A., Di Valentin, C., Pacchioni, G., Surface Science 600, 386 (2006).

Schwaner, A.L., Mahmood, W., and White, J.M., Surf. Sci., vol. 351, p. 228, (1996)

Schwaner, A.L., Mahmood, W., White, J.M., Surf. Sci. 351, 228-232 (1996).

Singh, U. C.; Kollman, P. A. J. Comput. Chem., 7, 718-730 (1986).

Slinkin, A.A., Lavroskaya, T.K., Loktev M.I., Mishin, I.V. and Rubinshtein A.M., Kinet. Katal. (Emgl.) 20, 424 (1979).

- Soete, G.G.d., Rev. Inst. Franc. Petr., 48, 413 (1993).
- Spitzer, A. and Luth, H., Phys. Rev. B: Condens. Matter, vol. 30, p. 3098 (1984)
- Steacie, E.W.R. and McCubbin, J.W., J. Chem. Phys., 2, 585 (1934).
- Stephens, P.J., Devlin, F.J., Chabalowski, C.F., Frisch, M.J. J. Phys. Chem., 98, 11623 (1994).
- Soyer, S., M.Sc. Dissertation, Middle East Technical University, Ankara (2005).
- Stone, F.S., Egerton, T.A. and Vickerman, J.C., J.Catal., 33 (1974) 307
- Stone, F.S., J.Solid State Chem., 12 (1975) 271.
- Strain, M. C.; Scuseria, G. E.; Frisch, M. J. Science, 271, 51 (1996).
- Strajbl, M.; Hong, G.; Warshel, A. J. Phys. Chem. B, 106, 13333-13343 (2002).
- Sugawara, K., Nobukawa, T., Yoshida, M., Sato, Y., Okumura, K., Tomishige, K. and Kunimori, K., Applied Catalysis B: Environmental 69, 154 (2007).
- Sun, K., Xia, H., Hensen, E., van Santen R. and Li, C., Journal of Catalysis 238, 186 (2006).
- Svensson, M.; Humbel, S.; Froese, R. D. J.; Matsubara, T.; Sieber, S.; Morokuma, K. J. Phys. Chem., 100, 19357- 19363 (1996).
- Swamy, C.S., Kannan, S., Li, Y., Armor, J.N. and Braymer, T.A., Patent 5.407.652 (1995).

Swart, M. *Int. J. Quantum Chem.*, 91, 177-183 (2002)

Tai-Quan Wu, T.Q., Tang, J. C.T., Li, H.Y., *Applied Surface Science* 252, 7837–7843 (2006).

Takoudis, C.G. and Schmidt, L.D., *J. Catal.*, 80, 274 (1983).

Tan, S.A., Grant, R.B. and Lambert, R.M., *J.Catal.* 104, 156-163 (1987)

They, V.; Rinaldi, D.; Rivail, J. L.; Maigret, B.; Ferenczy, G. G. *J. Comput. Chem.* 15, 269-282 (1994).

Tomasi, J.; Pomelli, C. S. In *Encyclopedia of Computational Chemistry*; Schleyer, P. v. R., Allinger, N. L., Kollman, P. A., Clark, T., Schaefer, H. F., III, Gasteiger, J., Schreiner, P. R., Eds.; Wiley: Chichester; Vol. 4, pp 2343-2350, (1998).

Ujaque, G.; Maseras, F. *Structure Bonding*, 112, 117- 149 (2004).

Umbach, E.; Menzel, D. *Chem. Phys. Lett.*,84, 491 (1981).

Uriarte, A.K.; *Stud. Surf. Sci. Catal.* 130, 743 (2000).

Vosko, S.J., Wilk, L., Nusair, M., *Can. J. Phys.*, 58, 1200 (1980).

Vreven, T., Byun, K.S., Komáromi, I., Dapprich, S., Montgomery, J.A., Morokuma, K. and Frisch, M.J., *J. Chem. Theory Comput.*, 2, 815-826 (2006).

Vreven, T.; Frisch, M. J.; Kudin, K. N.; Schlegel, H. B.; Morokuma, K. *Mol. Phys.*, 104, 701-714 (2006).

Vreven, T.; Mennucci, B.; da Silva, C. O.; Morokuma, K.; Tomasi, J. J. Chem. Phys., 115, 62-72 (2001).

Vreven, T.; Morokuma, K. J. Comput. Chem., 21, 1419-1432 (2000).

Vreven, T.; Morokuma, K. Theor. Chem. Acc., 109, 125-132 (2003).

Vreven, T.; Morokuma, K.; Farkas, O.; Schlegel, H. B.; Frisch, M. J. J. Comput. Chem., 24, 760-769 (2003).

W. H. J. Vac. Sci. Technol., 1, 1220 (1983).

Wang, G., Jin, X., Chen, M., Zhou, M., Chem. Phys. Lett. 420, 130-134 (2006).

Wang, J., Yasuda, H., Inumaru, K. And Misono M., Bull. Chem. Soc. Jpn., 68, 1226 (1995).

Warshel, A. Annu. Rev. Biophys. Biomol. Struct., 32, 425-443 (2003).

Warshel, A.; Levitt, M. J. Mol. Biol., 103, 227-249 (1976).

Winter, E.R.S., J. Catal., 15, 144, (1969).

Winter, E.R.S., J. Catal., 19, 32 (1970).

Winter, E.R.S., J. Catal., 34, 431 (1974).

Wojtowicz, M.A., Pels, J.R. and Moulijn, J.A., Fuel Proc. Technol., 34, 1 (1993).

Wood, B.R., Reimer, J. A. and Bell, J. A.; Journal of Catalysis 209, 151 (2002).

Wyckoff R.W.G., Crystal Structures, Bookmart, New York, 1(965).

Yamashita, T. And Vannice M.A., J.Catal. submitted (1996)

Yamazoe, N. and Teraoka, Y., Catal. Today, 8 175 (1990).

Zeigarnik, A.V., Kinetics and Catalysis, Vol. 44, No. 2, pp. 233–246 (2003).

Zeng, H.C., Lin, J., Teo, W.K., Wu, J. And Tan, K.L., Mater. Res. Soc. Symp. Proc., 344, 21 (1994).

Zhang, Q., Guo, Q., Wang, X., Shishido, T., Wang, Y., J. Catal. 239, 105-116 (2006).

Zhang, X., Walters, A.B. and Vannice M.A., Appl. Catal. B, 4, 237 (1994).

Zhang, Y. K.; Lee, T. S.; Yang, W. T. J. Chem. Phys., 110, 46-54 (1999).

Zharkova G.I., Baldina I.A., Igumenou, I.K., J.Struct.Chem., 47, pp.1117,1126 (2006).

Zhen, K.J., Khan, M.M., Mak, C.H., Lewis, K.B., Somorjai, G.A., J. Catal. 94 501 (1985).

APPENDIX A

SAMPLE INPUT AND OUTPUT FILES OF GAUSSIAN 2003

Input and output files for coordinate driving of nitrous oxide decomposition over Ag₅₁ cluster representing (111) surface is given in Table A.1 and Table A.2, respectively. It should be indicated that input and output geometries were demonstrated in Figure 4.1 and Figure 4.4, respectively.

Table A.1 Gaussian input file for coordinate driving of nitrous oxide decomposition on Ag₅₁ cluster representing (111) surface

```
%chk=kaanag.chk
%mem=250MW
%nprocshared=4
# opt=(modredundant,maxcycle=1000) oniom(b3lyp/geneadmp:uff) nosymm
geom=connectivity scf=(maxcycle=1000,conver=4)

buyuk ag + O RXN

0 2 0 4 0 4
Ag-      -1  -4.533379  -2.631216  -6.102358 L H-H_   8
Ag-      -1  -2.642916  -0.452035  -6.079561 L H-H_   8
Ag-      -1  -0.752454   1.727146  -6.056763 L H-H_  14
Ag-      -1   1.138009   3.906328  -6.033965 L H-H_  16
Ag-      -1  -4.880570  -6.196760  -1.579178 L H-H_   7
Ag-      -1  -4.706974  -4.413988  -3.840768 L H-H_   8
```

Table A.1 (cont'd)

Ag-	-1	-2.990107	-4.017579	-1.556381	H	
Ag-	-1	-2.816512	-2.234807	-3.817971	H	
Ag-	-1	-5.128406	-2.156958	-2.093939	L H-H ₁	7
Ag-	-1	-1.099644	-1.838397	-1.533583	H	
Ag-	-1	-4.954811	-0.374186	-4.355529	L H-H ₁	8
Ag-	-1	-3.237943	0.022223	-2.071142	L H-H ₁	8
Ag-	-1	-3.064348	1.804995	-4.332732	L H-H ₁	14
Ag-	-1	-0.926049	-0.055625	-3.795173	H	
Ag-	-1	0.790818	0.340784	-1.510786	H	
Ag-	-1	0.964414	2.123556	-3.772375	H	
Ag-	-1	-1.347481	2.201404	-2.048344	L H-H ₁	14
Ag-	-1	2.681281	2.519965	-1.487988	H	
Ag-	-1	-1.173885	3.984176	-4.309934	L H-H ₁	16
Ag-	-1	0.542982	4.380586	-2.025547	L H-H ₁	16
Ag-	-1	2.854876	4.302737	-3.749578	L H-H ₁	16
Ag-	-1	4.571743	4.699147	-1.465190	L H-H ₁	18
Ag-	-1	-3.163703	-5.800350	0.705209	L H-H ₁	7
Ag-	-1	-1.446835	-5.403941	2.989597	L H-H ₁	28
Ag-	-1	-5.302002	-3.939730	0.167650	L H-H ₁	7
Ag-	-1	-3.585134	-3.543321	2.452038	L H-H ₁	28
Ag-	-1	-3.411539	-1.760549	0.190448	L H-H ₁	7
Ag-	-1	-1.273240	-3.621169	0.728007	H	
Ag-	-1	0.443627	-3.224760	3.012394	H	
Ag-	-1	0.617223	-1.441988	0.750804	H	
Ag-	-1	-1.694672	-1.364139	2.474836	L H-H ₁	28
Ag-	-1	2.334090	-1.045578	3.035192	H	
Ag-	-1	-1.521076	0.418633	0.213246	L H-H ₁	10
Ag-	-1	0.195791	0.815042	2.497633	L H-H ₁	30
Ag-	-1	0.369386	2.597814	0.236043	L H-H ₁	15
Ag-	-1	2.507685	0.737193	0.773602	H	
Ag-	-1	4.224552	1.133603	3.057990	H	
Ag-	-1	4.398148	2.916375	0.796400	H	
Ag-	-1	2.086254	2.994223	2.520431	L H-H ₁	36
Ag-	-1	6.115015	3.312784	3.080787	L H-H ₁	37
Ag-	-1	2.259849	4.776995	0.258841	L H-H ₁	18
Ag-	-1	3.976716	5.173405	2.543229	L H-H ₁	38
Ag-	-1	6.288611	5.095556	0.819197	L H-H ₁	38
Ag-	-1	0.270032	-5.007532	5.273984	L H-H ₁	29
Ag-	-1	-1.868267	-3.146911	4.736426	L H-H ₁	29
Ag-	-1	0.022195	-0.967730	4.759223	L H-H ₁	29
Ag-	-1	2.160494	-2.828350	5.296782	L H-H ₁	29
Ag-	-1	4.050957	-0.649169	5.319580	L H-H ₁	32
Ag-	-1	1.912658	1.211452	4.782021	L H-H ₁	32

Table A.1 (cont'd)

Ag-	-1	3.803121	3.390633	4.804819	L H-H_	37
Ag-	-1	5.941420	1.530012	5.342377	L H-H_	37
O-O_R	0	2.703340	-3.160079	-2.532575	H	
N-N_R	0	3.497578	-3.847725	-3.096840	H	
N-N_R	0	4.253072	-4.501828	-3.633580	H	

1 6 1.0 2 1.0 8 1.0 11 1.0
2 8 1.0 3 1.0 14 1.0 11 1.0 13 1.0
3 14 1.0 4 1.0 16 1.0 13 1.0 19 1.0
4 16 1.0 21 1.0 19 1.0
5 6 1.0 7 1.0 23 1.0 25 1.0
6 8 1.0 7 1.0 9 1.0
7 8 1.0 23 1.0 10 1.0 28 1.0 9 1.0 25 1.0 27 1.0
8 14 1.0 10 1.0 11 1.0 9 1.0 12 1.0
9 25 1.0 11 1.0 27 1.0 12 1.0
10 14 1.0 28 1.0 15 1.0 30 1.0 12 1.0 27 1.0 33 1.0
11 12 1.0 13 1.0
12 27 1.0 13 1.0 33 1.0 17 1.0 14 1.0
13 17 1.0 19 1.0 14 1.0
14 16 1.0 15 1.0 17 1.0
15 30 1.0 16 1.0 18 1.0 36 1.0 17 1.0 33 1.0 35 1.0
16 21 1.0 18 1.0 19 1.0 17 1.0 20 1.0
17 33 1.0 19 1.0 35 1.0 20 1.0
18 36 1.0 21 1.0 22 1.0 38 1.0 20 1.0 35 1.0 41 1.0
19 20 1.0
20 35 1.0 41 1.0 21 1.0
21 22 1.0
22 38 1.0 43 1.0 41 1.0
23 28 1.0 24 1.0 25 1.0 26 1.0
24 28 1.0 29 1.0 44 1.0 26 1.0 45 1.0
25 26 1.0 27 1.0
26 27 1.0 45 1.0 31 1.0 28 1.0
27 31 1.0 33 1.0 28 1.0
28 30 1.0 29 1.0 31 1.0
29 44 1.0 30 1.0 32 1.0 47 1.0 31 1.0 45 1.0 46 1.0
30 36 1.0 32 1.0 33 1.0 31 1.0 34 1.0
31 45 1.0 33 1.0 46 1.0 34 1.0
32 47 1.0 36 1.0 37 1.0 48 1.0 34 1.0 46 1.0 49 1.0
33 34 1.0 35 1.0
34 46 1.0 35 1.0 49 1.0 39 1.0 36 1.0
35 39 1.0 41 1.0 36 1.0
36 38 1.0 37 1.0 39 1.0

Table A.1 (cont'd)

37 48 1.0 38 1.0 40 1.0 51 1.0 39 1.0 49 1.0 50 1.0
38 43 1.0 40 1.0 41 1.0 39 1.0 42 1.0
39 49 1.0 41 1.0 50 1.0 42 1.0
40 51 1.0 43 1.0 50 1.0 42 1.0
41 42 1.0
42 50 1.0 43 1.0
43
44 47 1.0 45 1.0
45 46 1.0
46 49 1.0 47 1.0
47 48 1.0
48 51 1.0 49 1.0
49 50 1.0
50 51 1.0
51
52 53 2.0
53 54 2.0
54

B 52 33 S 25 -0.120000

Ag 0
LanL2DZ

N O H 0
3-21g**

Ag 0
LanL2DZ

Table A.2 Gaussian output file for coordinate driving of nitrous oxide decomposition
on Ag₅₁ cluster representing (111) surface

Gaussian, Inc.),
the Gaussian 86(TM) system (copyright 1986, Carnegie Mellon
University), and the Gaussian 82(TM) system (copyright 1983,
Carnegie Mellon University). Gaussian is a federally registered
trademark of Gaussian, Inc.

This software contains proprietary and confidential information,
including trade secrets, belonging to Gaussian, Inc.

This software is provided under written license and may be
used, copied, transmitted, or stored only in accord with that
written license.

The following legend is applicable only to US Government
contracts under FAR:

RESTRICTED RIGHTS LEGEND

Use, reproduction and disclosure by the US Government is
subject to restrictions as set forth in subparagraphs (a)
and (c) of the Commercial Computer Software - Restricted
Rights clause in FAR 52.227-19.

Gaussian, Inc.
340 Quinipiac St., Bldg. 40, Wallingford CT 06492

Warning -- This program may not be used in any manner that
competes with the business of Gaussian, Inc. or will provide
assistance to any competitor of Gaussian, Inc. The licensee
of this program is prohibited from giving any competitor of
Gaussian, Inc. access to this program. By using this program,
the user acknowledges that Gaussian, Inc. is engaged in the

Table A.2 (cont'd)

business of creating and licensing software in the field of computational chemistry and represents and warrants to the licensee that it is not a competitor of Gaussian, Inc. and that it will not use this program in any manner prohibited above.

Cite this work as:

Gaussian 03, Revision D.01,
M. J. Frisch, G. W. Trucks, H. B. Schlegel, G. E. Scuseria,
M. A. Robb, J. R. Cheeseman, J. A. Montgomery, Jr., T. Vreven,
K. N. Kudin, J. C. Burant, J. M. Millam, S. S. Iyengar, J. Tomasi,
V. Barone, B. Mennucci, M. Cossi, G. Scalmani, N. Rega,
G. A. Petersson, H. Nakatsuji, M. Hada, M. Ehara, K. Toyota,
R. Fukuda, J. Hasegawa, M. Ishida, T. Nakajima, Y. Honda, O. Kitao,
H. Nakai, M. Klene, X. Li, J. E. Knox, H. P. Hratchian, J. B. Cross,
V. Bakken, C. Adamo, J. Jaramillo, R. Gomperts, R. E. Stratmann,
O. Yazyev, A. J. Austin, R. Cammi, C. Pomelli, J. W. Ochterski,
P. Y. Ayala, K. Morokuma, G. A. Voth, P. Salvador, J. J. Dannenberg,
V. G. Zakrzewski, S. Dapprich, A. D. Daniels, M. C. Strain,
O. Farkas, D. K. Malick, A. D. Rabuck, K. Raghavachari,
J. B. Foresman, J. V. Ortiz, Q. Cui, A. G. Baboul, S. Clifford,
J. Cioslowski, B. B. Stefanov, G. Liu, A. Liashenko, P. Piskorz,
I. Komaromi, R. L. Martin, D. J. Fox, T. Keith, M. A. Al-Laham,
C. Y. Peng, A. Nanayakkara, M. Challacombe, P. M. W. Gill,
B. Johnson, W. Chen, M. W. Wong, C. Gonzalez, and J. A. Pople,
Gaussian, Inc., Wallingford CT, 2004.

Gaussian 03: IA32L-G03RevD.01 13-Oct-2005
21-Mar-2007

%chk=kaanag.chk

%mem=250MW

%nprocshared=4

Will use up to 4 processors via shared memory.

opt=(modredundant,loose,maxcycle=1000) oniom(b3lyp/genecp:uff) nosym
m geom=connectivity scf=(maxcycle=1000,conver=4)

1/6=1000,7=-1,14=-1,18=1000120,38=1,52=2,56=1,57=2,64=2/1,3;

2/9=110,15=1,17=6,18=5,40=1/2;

1/6=1000,14=-1,18=1000120,38=1,52=2,53=3172,64=2/20;

Table A.2 (cont'd)

$3/5=30, 11=9, 16=1, 25=1, 30=1/1;$
 $4/20=10, 22=1, 23=1000, 24=3, 28=4, 68=-1/2;$
 $7/7=1, 30=1, 33=-1, 44=-1/16;$
 $1/6=1000, 14=-1, 18=1000120, 52=2, 53=2032/20;$
 $3/5=7, 11=2, 16=1, 17=8, 25=1, 30=1, 74=-5/1, 2, 3;$
 $4/1;$
 $5/5=2, 6=4, 7=1000, 38=5, 94=2/2;$
 $6/7=2, 8=2, 9=2, 10=2, 28=1/1;$
 $7/7=1, 30=1, 33=-1/1, 2, 3, 16;$
 $1/6=1000, 14=-1, 18=1000120, 52=2, 53=1022, 64=2/20;$
 $3/5=30, 11=9, 16=1, 25=1, 30=1/1;$
 $4/20=10, 22=1, 23=1000, 24=3, 28=4, 68=-1/2;$
 $7/7=1, 30=1, 33=-1, 44=-1/16;$
 $1/6=1000, 14=-1, 18=1000120, 52=2, 53=3015, 64=2/20;$
 $7/9=1, 44=-1/16;$
 $1/6=1000, 14=-1, 18=1000020, 52=2, 64=2/3(2);$
 $2/9=110, 15=1/2;$
 $99/99;$
 $2/9=110, 15=1/2;$
 $1/6=1000, 14=-1, 18=1000020, 52=2, 53=3173, 64=2/20;$
 $3/5=30, 11=9, 16=1, 25=1, 30=1/1;$
 $4/16=2, 20=10, 22=1, 23=1000, 24=3, 28=4, 68=-1/2;$
 $7/7=1, 30=1, 33=-1, 44=-1/16;$
 $1/6=1000, 14=-1, 18=1000020, 52=2, 53=2033/20;$
 $3/5=7, 6=1, 11=2, 16=1, 17=8, 25=1, 30=1, 74=-5, 82=7/1, 2, 3;$
 $4/5=5, 16=3/1;$
 $5/5=2, 6=4, 7=1000, 38=5, 94=2/2;$
 $7/7=1, 30=1, 33=-1/1, 2, 3, 16;$
 $1/6=1000, 14=-1, 18=1000020, 52=2, 53=1023, 64=2/20;$
 $3/5=30, 11=9, 16=1, 25=1, 30=1/1;$
 $4/16=2, 20=10, 22=1, 23=1000, 24=3, 28=4, 68=-1/2;$
 $7/7=1, 30=1, 33=-1, 44=-1/16;$
 $1/6=1000, 14=-1, 18=1000020, 52=2, 53=3015, 64=2/20;$
 $7/9=1, 44=-1/16;$
 $1/6=1000, 14=-1, 18=1000020, 52=2, 64=2/3(-16);$
 $2/9=110, 15=1/2;$
 $99/99;$

 buyuk ag + O RXN

Symbolic Z-matrix:

Charge = 0 Multiplicity = 2 for low level calculation on real system.

Charge = 0 Multiplicity = 4 for high level calculation on model system.

Table A.2 (cont'd)

Charge = 0 Multiplicity = 4 for low level calculation on model system.

Ag-	-1	-4.53338	-2.63122	-6.10236	L	H-H ₂	8	0.	0.
Ag-	-1	-2.64292	-0.45204	-6.07956	L	H-H ₂	8	0.	0.
Ag-	-1	-0.75245	1.72715	-6.05676	L	H-H ₂	14	0.	0.
Ag-	-1	1.13801	3.90633	-6.03397	L	H-H ₂	16	0.	0.
Ag-	-1	-4.88057	-6.19676	-1.57918	L	H-H ₂	7	0.	0.
Ag-	-1	-4.70697	-4.41399	-3.84077	L	H-H ₂	8	0.	0.
Ag-	-1	-2.99011	-4.01758	-1.55638	H				
Ag-	-1	-2.81651	-2.23481	-3.81797	H				
Ag-	-1	-5.12841	-2.15696	-2.09394	L	H-H ₂	7	0.	0.
Ag-	-1	-1.09964	-1.8384	-1.53358	H				
Ag-	-1	-4.95481	-0.37419	-4.35553	L	H-H ₂	8	0.	0.
Ag-	-1	-3.23794	0.02222	-2.07114	L	H-H ₂	8	0.	0.
Ag-	-1	-3.06435	1.805	-4.33273	L	H-H ₂	14	0.	0.
Ag-	-1	-0.92605	-0.05563	-3.79517	H				
Ag-	-1	0.79082	0.34078	-1.51079	H				
Ag-	-1	0.96441	2.12356	-3.77238	H				
Ag-	-1	-1.34748	2.2014	-2.04834	L	H-H ₂	14	0.	0.
Ag-	-1	2.68128	2.51997	-1.48799	H				
Ag-	-1	-1.17389	3.98418	-4.30993	L	H-H ₂	16	0.	0.
Ag-	-1	0.54298	4.38059	-2.02555	L	H-H ₂	16	0.	0.
Ag-	-1	2.85488	4.30274	-3.74958	L	H-H ₂	16	0.	0.
Ag-	-1	4.57174	4.69915	-1.46519	L	H-H ₂	18	0.	0.
Ag-	-1	-3.1637	-5.80035	0.70521	L	H-H ₂	7	0.	0.
Ag-	-1	-1.44684	-5.40394	2.9896	L	H-H ₂	28	0.	0.
Ag-	-1	-5.302	-3.93973	0.16765	L	H-H ₂	7	0.	0.
Ag-	-1	-3.58513	-3.54332	2.45204	L	H-H ₂	28	0.	0.
Ag-	-1	-3.41154	-1.76055	0.19045	L	H-H ₂	7	0.	0.
Ag-	-1	-1.27324	-3.62117	0.72801	H				
Ag-	-1	0.44363	-3.22476	3.01239	H				
Ag-	-1	0.61722	-1.44199	0.7508	H				
Ag-	-1	-1.69467	-1.36414	2.47484	L	H-H ₂	28	0.	0.
Ag-	-1	2.33409	-1.04558	3.03519	H				
Ag-	-1	-1.52108	0.41863	0.21325	L	H-H ₂	10	0.	0.
Ag-	-1	0.19579	0.81504	2.49763	L	H-H ₂	30	0.	0.
Ag-	-1	0.36939	2.59781	0.23604	L	H-H ₂	15	0.	0.
Ag-	-1	2.50769	0.73719	0.7736	H				
Ag-	-1	4.22455	1.1336	3.05799	H				
Ag-	-1	4.39815	2.91638	0.7964	H				
Ag-	-1	2.08625	2.99422	2.52043	L	H-H ₂	36	0.	0.
Ag-	-1	6.11501	3.31278	3.08079	L	H-H ₂	37	0.	0.
Ag-	-1	2.25985	4.777	0.25884	L	H-H ₂	18	0.	0.
Ag-	-1	3.97672	5.1734	2.54323	L	H-H ₂	38	0.	0.

Table A.2 (cont'd)

Ag-	-1	6.28861	5.09556	0.8192	L	H-H_	38	0.	0.
Ag-	-1	0.27003	-5.00753	5.27398	L	H-H_	29	0.	0.
Ag-	-1	-1.86827	-3.14691	4.73643	L	H-H_	29	0.	0.
Ag-	-1	0.0222	-0.96773	4.75922	L	H-H_	29	0.	0.
Ag-	-1	2.16049	-2.82835	5.29678	L	H-H_	29	0.	0.
Ag-	-1	4.05096	-0.64917	5.31958	L	H-H_	32	0.	0.
Ag-	-1	1.91266	1.21145	4.78202	L	H-H_	32	0.	0.
Ag-	-1	3.80312	3.39063	4.80482	L	H-H_	37	0.	0.
Ag-	-1	5.94142	1.53001	5.34238	L	H-H_	37	0.	0.
O-O_R	0	2.70334	-3.16008	-2.53258	H				
N-N_R	0	3.49758	-3.84773	-3.09684	H				
N-N_R	0	4.25307	-4.50183	-3.63358	H				

The following ModRedundant input section has been read:

B 33 52 S 25 -0.120

I= 53 IAn= 7 Valence= 4.

JB= 1 J= 54 IAn= 7 IBT= 2 Dist= 1.13D+00

JB= 2 J= 52 IAn= 8 IBT= 2 Dist= 1.19D+00

Include all MM classes

MMInit generated parameter data with length LenPar= 21574.

“THE PART HERE IS CUT IN ORDER TO SAVE PLACE”

Variable	Old X	-DE/DX (Linear)	Delta X (Quad)	Delta X (Total)	Delta X	New X
X1	-8.56684	-0.21065	0.00000	0.00000	0.00000	-8.56684
Y1	-4.97228	-0.49222	0.00000	0.00000	0.00000	-4.97228
Z1	-11.53179	-0.74042	0.00000	0.00000	0.00000	-11.53179
X2	-4.99439	-0.11516	0.00000	0.00000	0.00000	-4.99439
Y2	-0.85422	-1.21604	0.00000	0.00000	0.00000	-0.85422
Z2	-11.48871	-0.78581	0.00000	0.00000	0.00000	-11.48871
X3	-1.42193	0.19643	0.00000	0.00000	0.00000	-1.42193
Y3	3.26383	-0.86066	0.00000	0.00000	0.00000	3.26383
Z3	-11.44562	-0.76499	0.00000	0.00000	0.00000	-11.44562
X4	2.15053	0.80138	0.00000	0.00000	0.00000	2.15053
Y4	7.38189	0.69805	0.00000	0.00000	0.00000	7.38189
Z4	-11.40254	-0.73938	0.00000	0.00000	0.00000	-11.40254
X5	-9.22294	-0.29386	0.00000	0.00000	0.00000	-9.22294
Y5	-11.71018	-1.15592	0.00000	0.00000	0.00000	-11.71018
Z5	-2.98421	0.09842	0.00000	0.00000	0.00000	-2.98421
X6	-8.89489	0.12217	0.00000	0.00000	0.00000	-8.89489

Table A.2 (cont'd)

Y6	-8.34123	0.05986	0.00000	0.00000	0.00000	-8.34123
Z6	-7.25800	-1.08826	0.00000	0.00000	0.00000	-7.25800
X7	-5.65048	-2.24432	0.00000	0.00000	0.00000	-5.65048
Y7	-7.59212	-2.41181	0.00000	0.00000	0.00000	-7.59212
Z7	-2.94113	-0.23627	0.00000	0.00000	0.00000	-2.94113
X8	-5.32244	-1.49116	0.00000	0.00000	0.00000	-5.32244
Y8	-4.22317	-0.91735	0.00000	0.00000	0.00000	-4.22317
Z8	-7.21492	-2.64019	0.00000	0.00000	0.00000	-7.21492
X9	-9.69128	-0.98110	0.00000	0.00000	0.00000	-9.69128
Y9	-4.07606	-0.88746	0.00000	0.00000	0.00000	-4.07606
Z9	-3.95697	0.92243	0.00000	0.00000	0.00000	-3.95697
X10	-2.07803	0.03717	0.00000	0.00000	0.00000	-2.07803
Y10	-3.47407	-0.05609	0.00000	0.00000	0.00000	-3.47407
Z10	-2.89805	-0.12618	0.00000	0.00000	0.00000	-2.89805
X11	-9.36324	-1.49971	0.00000	0.00000	0.00000	-9.36324
Y11	-0.70711	0.21212	0.00000	0.00000	0.00000	-0.70711
Z11	-8.23076	-0.61441	0.00000	0.00000	0.00000	-8.23076
X12	-6.11883	-0.90127	0.00000	0.00000	0.00000	-6.11883
Y12	0.04200	-0.16385	0.00000	0.00000	0.00000	0.04200
Z12	-3.91389	-1.03386	0.00000	0.00000	0.00000	-3.91389
X13	-5.79078	-0.33876	0.00000	0.00000	0.00000	-5.79078
Y13	3.41095	1.50411	0.00000	0.00000	0.00000	3.41095
Z13	-8.18768	-0.21175	0.00000	0.00000	0.00000	-8.18768
X14	-1.74998	-0.19767	0.00000	0.00000	0.00000	-1.74998
Y14	-0.10512	0.29668	0.00000	0.00000	0.00000	-0.10512
Z14	-7.17184	-1.05703	0.00000	0.00000	0.00000	-7.17184
X15	1.49443	0.18441	0.00000	0.00000	0.00000	1.49443
Y15	0.64399	0.07422	0.00000	0.00000	0.00000	0.64399
Z15	-2.85497	-0.04262	0.00000	0.00000	0.00000	-2.85497
X16	1.82248	0.94422	0.00000	0.00000	0.00000	1.82248
Y16	4.01294	2.60237	0.00000	0.00000	0.00000	4.01294
Z16	-7.12876	-1.68544	0.00000	0.00000	0.00000	-7.12876
X17	-2.54637	-0.56121	0.00000	0.00000	0.00000	-2.54637
Y17	4.16005	-0.00188	0.00000	0.00000	0.00000	4.16005
Z17	-3.87081	-0.71431	0.00000	0.00000	0.00000	-3.87081
X18	5.06689	0.59125	0.00000	0.00000	0.00000	5.06689
Y18	4.76204	0.89649	0.00000	0.00000	0.00000	4.76204
Z18	-2.81189	-0.38638	0.00000	0.00000	0.00000	-2.81189
X19	-2.21832	0.32352	0.00000	0.00000	0.00000	-2.21832
Y19	7.52900	2.20817	0.00000	0.00000	0.00000	7.52900
Z19	-8.14459	-0.26658	0.00000	0.00000	0.00000	-8.14459
X20	1.02609	-0.04383	0.00000	0.00000	0.00000	1.02609
Y20	8.27811	1.47464	0.00000	0.00000	0.00000	8.27811

Table A.2 (cont'd)

Z20	-3.82773	-0.93886	0.00000	0.00000	0.00000	-3.82773
X21	5.39493	0.03896	0.00000	0.00000	0.00000	5.39493
Y21	8.13099	-0.04304	0.00000	0.00000	0.00000	8.13099
Z21	-7.08568	-0.76903	0.00000	0.00000	0.00000	-7.08568
X22	8.63934	0.39600	0.00000	0.00000	0.00000	8.63934
Y22	8.88010	-0.00956	0.00000	0.00000	0.00000	8.88010
Z22	-2.76881	-0.36618	0.00000	0.00000	0.00000	-2.76881
X23	-5.97853	-0.09418	0.00000	0.00000	0.00000	-5.97853
Y23	-10.96107	-1.03698	0.00000	0.00000	0.00000	-10.96107
Z23	1.33265	-1.05623	0.00000	0.00000	0.00000	1.33265
X24	-2.73412	0.23537	0.00000	0.00000	0.00000	-2.73412
Y24	-10.21197	-0.99972	0.00000	0.00000	0.00000	-10.21197
Z24	5.64952	-0.66748	0.00000	0.00000	0.00000	5.64952
X25	-10.01933	-1.51776	0.00000	0.00000	0.00000	-10.01933
Y25	-7.44501	-0.12419	0.00000	0.00000	0.00000	-7.44501
Z25	0.31681	-0.17556	0.00000	0.00000	0.00000	0.31681
X26	-6.77492	-0.46761	0.00000	0.00000	0.00000	-6.77492
Y26	-6.69591	0.16984	0.00000	0.00000	0.00000	-6.69591
Z26	4.63368	1.47981	0.00000	0.00000	0.00000	4.63368
X27	-6.44687	-0.97927	0.00000	0.00000	0.00000	-6.44687
Y27	-3.32696	-0.76248	0.00000	0.00000	0.00000	-3.32696
Z27	0.35989	-0.40081	0.00000	0.00000	0.00000	0.35989
X28	-2.40607	-0.38658	0.00000	0.00000	0.00000	-2.40607
Y28	-6.84302	-0.89819	0.00000	0.00000	0.00000	-6.84302
Z28	1.37573	0.58343	0.00000	0.00000	0.00000	1.37573
X29	0.83833	0.55284	0.00000	0.00000	0.00000	0.83833
Y29	-6.09391	-0.99738	0.00000	0.00000	0.00000	-6.09391
Z29	5.69260	3.06812	0.00000	0.00000	0.00000	5.69260
X30	1.16638	0.07965	0.00000	0.00000	0.00000	1.16638
Y30	-2.72496	-0.03508	0.00000	0.00000	0.00000	-2.72496
Z30	1.41881	0.07730	0.00000	0.00000	0.00000	1.41881
X31	-3.20247	-0.69095	0.00000	0.00000	0.00000	-3.20247
Y31	-2.57785	-0.65727	0.00000	0.00000	0.00000	-2.57785
Z31	4.67676	0.02650	0.00000	0.00000	0.00000	4.67676
X32	4.41079	0.50406	0.00000	0.00000	0.00000	4.41079
Y32	-1.97586	-0.28404	0.00000	0.00000	0.00000	-1.97586
Z32	5.73568	1.01583	0.00000	0.00000	0.00000	5.73568
X33	-2.87442	-0.08161	0.00000	0.00000	0.00000	-2.87442
Y33	0.79110	-0.03962	0.00000	0.00000	0.00000	0.79110
Z33	0.40298	-0.07349	0.00000	0.00000	0.00000	0.40298
X34	0.36999	-0.11432	0.00000	0.00000	0.00000	0.36999
Y34	1.54021	0.00415	0.00000	0.00000	0.00000	1.54021
Z34	4.71984	-0.01290	0.00000	0.00000	0.00000	4.71984

Table A.2 (cont'd)

X35	0.69804	-0.08854	0.00000	0.00000	0.00000	0.69804
Y35	4.90916	0.03554	0.00000	0.00000	0.00000	4.90916
Z35	0.44606	-0.04933	0.00000	0.00000	0.00000	0.44606
X36	4.73884	0.09857	0.00000	0.00000	0.00000	4.73884
Y36	1.39309	-0.01068	0.00000	0.00000	0.00000	1.39309
Z36	1.46190	0.00154	0.00000	0.00000	0.00000	1.46190
X37	7.98325	1.67446	0.00000	0.00000	0.00000	7.98325
Y37	2.14220	-0.09739	0.00000	0.00000	0.00000	2.14220
Z37	5.77876	1.74790	0.00000	0.00000	0.00000	5.77876
X38	8.31130	1.15964	0.00000	0.00000	0.00000	8.31130
Y38	5.51115	1.80508	0.00000	0.00000	0.00000	5.51115
Z38	1.50498	-0.23901	0.00000	0.00000	0.00000	1.50498
X39	3.94245	-0.12057	0.00000	0.00000	0.00000	3.94245
Y39	5.65826	-0.01187	0.00000	0.00000	0.00000	5.65826
Z39	4.76292	-0.01768	0.00000	0.00000	0.00000	4.76292
X40	11.55570	0.91441	0.00000	0.00000	0.00000	11.55570
Y40	6.26025	-1.04740	0.00000	0.00000	0.00000	6.26025
Z40	5.82184	0.57233	0.00000	0.00000	0.00000	5.82184
X41	4.27050	0.31253	0.00000	0.00000	0.00000	4.27050
Y41	9.02721	1.52707	0.00000	0.00000	0.00000	9.02721
Z41	0.48914	-0.50861	0.00000	0.00000	0.00000	0.48914
X42	7.51490	0.50978	0.00000	0.00000	0.00000	7.51490
Y42	9.77632	2.33043	0.00000	0.00000	0.00000	9.77632
Z42	4.80601	-0.07696	0.00000	0.00000	0.00000	4.80601
X43	11.88375	1.13234	0.00000	0.00000	0.00000	11.88375
Y43	9.62921	0.77021	0.00000	0.00000	0.00000	9.62921
Z43	1.54806	-0.29979	0.00000	0.00000	0.00000	1.54806
X44	0.51029	0.67222	0.00000	0.00000	0.00000	0.51029
Y44	-9.46286	-0.60996	0.00000	0.00000	0.00000	-9.46286
Z44	9.96639	0.92120	0.00000	0.00000	0.00000	9.96639
X45	-3.53051	0.18277	0.00000	0.00000	0.00000	-3.53051
Y45	-5.94680	0.31149	0.00000	0.00000	0.00000	-5.94680
Z45	8.95055	2.29479	0.00000	0.00000	0.00000	8.95055
X46	0.04194	-0.25560	0.00000	0.00000	0.00000	0.04194
Y46	-1.82874	-0.59636	0.00000	0.00000	0.00000	-1.82874
Z46	8.99363	1.64343	0.00000	0.00000	0.00000	8.99363
X47	4.08274	0.02821	0.00000	0.00000	0.00000	4.08274
Y47	-5.34481	-0.80567	0.00000	0.00000	0.00000	-5.34481
Z47	10.00947	0.10275	0.00000	0.00000	0.00000	10.00947
X48	7.65520	0.37136	0.00000	0.00000	0.00000	7.65520
Y48	-1.22675	-0.39900	0.00000	0.00000	0.00000	-1.22675
Z48	10.05255	0.10563	0.00000	0.00000	0.00000	10.05255
X49	3.61440	0.10993	0.00000	0.00000	0.00000	3.61440

Table A.2 (cont'd)

Y49	2.28931	-0.19444	0.00000	0.00000	0.00000	2.28931
Z49	9.03671	1.66553	0.00000	0.00000	0.00000	9.03671
X50	7.18686	0.44291	0.00000	0.00000	0.00000	7.18686
Y50	6.40737	0.70351	0.00000	0.00000	0.00000	6.40737
Z50	9.07979	1.94161	0.00000	0.00000	0.00000	9.07979
X51	11.22766	1.05911	0.00000	0.00000	0.00000	11.22766
Y51	2.89130	0.13957	0.00000	0.00000	0.00000	2.89130
Z51	10.09563	0.51725	0.00000	0.00000	0.00000	10.09563
R1	3.52511	0.02749	-0.00006	-0.00197	-0.00203	3.52309
R2	6.00939	0.09329	0.00000	0.00000	0.00000	6.00939
R3	6.30750	0.00003	0.00004	-0.00295	-0.00291	6.30459
R4	2.09858	0.00124	0.00001	0.00083	0.00084	2.09942
A1	0.67448	0.01014	0.00000	0.00070	0.00070	0.67518
A2	1.56239	0.08135	-0.00001	0.00067	0.00066	1.56306
A3	2.45377	0.19000	-0.00001	0.00037	0.00036	2.45412
A4	2.23392	-0.08792	0.00000	0.00064	0.00064	2.23457
A5	2.46711	0.06180	0.00000	-0.00070	-0.00070	2.46641
A6	0.68783	-0.01116	0.00001	-0.00037	-0.00036	0.68747
A7	1.41310	-0.02379	0.00001	0.00028	0.00029	1.41338
A8	2.24463	-0.02242	0.00001	-0.00021	-0.00020	2.24443
A9	1.57920	-0.02356	0.00001	-0.00067	-0.00066	1.57854
A10	1.40595	0.00041	0.00001	0.00157	0.00157	1.40752
A11	2.65604	0.00006	-0.00013	0.00087	0.00074	2.65678
A12	5.18812	-0.00002	0.00010	-0.00087	-0.00077	5.18735
D1	0.45778	0.14811	0.00001	0.00028	0.00029	0.45806
D2	1.41309	0.26404	0.00001	0.00028	0.00029	1.41338
D3	-2.35539	0.09256	0.00002	-0.00031	-0.00029	-2.35567
D4	2.97248	-0.23083	0.00002	-0.00031	-0.00029	2.97219
D5	0.78621	-0.24271	0.00002	-0.00031	-0.00029	0.78592
D6	2.01717	0.09599	0.00002	-0.00031	-0.00029	2.01688
D7	-2.35539	0.07581	0.00002	-0.00031	-0.00029	-2.35567
D8	2.97248	0.11152	0.00002	-0.00031	-0.00029	2.97219
D9	2.01717	0.04787	0.00002	-0.00031	-0.00029	2.01688
D10	0.78621	-0.00976	0.00002	-0.00031	-0.00029	0.78592
D11	-2.68382	0.16785	0.00001	0.00028	0.00029	-2.68353
D12	0.45778	-0.10710	0.00001	0.00028	0.00029	0.45806
D13	1.41309	-0.08317	0.00001	0.00028	0.00029	1.41338
D14	2.36841	-0.03331	0.00001	0.00028	0.00029	2.36870
D15	0.76998	-0.15691	0.00000	0.00098	0.00099	0.77097
D16	2.00094	0.05618	0.00000	0.00098	0.00099	2.00193
D17	2.95626	-0.05659	0.00000	0.00098	0.00099	2.95725
D18	-2.37161	0.27088	0.00000	0.00098	0.00099	-2.37062
D19	-0.13377	0.02741	0.00001	-0.00043	-0.00041	-0.13418

Table A.2 (cont'd)

D20	-1.08909	-0.07889	0.00001	-0.00043	-0.00041	-1.08950
D21	-2.32005	-0.46155	0.00001	-0.00043	-0.00041	-2.32046
D22	3.00782	0.10217	0.00001	-0.00043	-0.00041	3.00741
D23	-2.97248	-0.11343	-0.00002	0.00031	0.00029	-2.97219
D24	2.35539	-0.12122	-0.00002	0.00031	0.00029	2.35567
D25	-0.78621	-0.08052	-0.00002	0.00031	0.00029	-0.78592
D26	-2.01717	-0.11018	-0.00002	0.00031	0.00029	-2.01688
D27	-0.78621	-0.04360	-0.00002	0.00031	0.00029	-0.78592
D28	-0.76998	-0.01622	0.00000	-0.00098	-0.00099	-0.77097
D29	-2.00094	0.14602	0.00000	-0.00098	-0.00099	-2.00193
D30	2.37161	-0.03503	0.00000	-0.00098	-0.00099	2.37062
D31	-2.95626	0.01862	0.00000	-0.00098	-0.00099	-2.95725
D32	-1.56229	-0.02021	0.00001	-0.00068	-0.00067	-1.56296
D33	-0.60697	-0.07850	0.00001	-0.00068	-0.00067	-0.60764
D34	0.62399	-0.12409	0.00001	-0.00068	-0.00067	0.62332
D35	1.57930	-0.00450	0.00001	-0.00068	-0.00067	1.57863
D36	-2.99132	0.03225	0.00000	-0.00089	-0.00089	-2.99220
D37	0.15028	0.03435	0.00000	-0.00089	-0.00089	0.14939
D38	1.10559	0.04482	0.00000	-0.00089	-0.00089	1.10470
D39	2.33655	0.19573	0.00000	-0.00089	-0.00089	2.33566
D40	-0.45778	0.01387	-0.00001	-0.00028	-0.00029	-0.45806
D41	-1.41309	0.00120	-0.00001	-0.00028	-0.00029	-1.41338
D42	2.68382	0.05597	-0.00001	-0.00028	-0.00029	2.68353
D43	-2.36841	0.02000	-0.00001	-0.00028	-0.00029	-2.36870
D44	2.68382	-0.08508	-0.00001	-0.00028	-0.00029	2.68353
D45	-0.45778	-0.02207	-0.00001	-0.00028	-0.00029	-0.45806
D46	-1.41309	0.00461	-0.00001	-0.00028	-0.00029	-1.41338
D47	-2.36841	0.08831	-0.00001	-0.00028	-0.00029	-2.36870
D48	3.09838	0.01892	0.00006	-0.00147	-0.00141	3.09697
D49	2.43867	0.00692	0.00005	-0.00123	-0.00118	2.43749
D50	1.79156	-0.10688	0.00004	-0.00199	-0.00195	1.78961
D51	-2.96958	-0.09017	0.00004	-0.00097	-0.00093	-2.97051
D52	-0.04321	0.11166	0.00006	-0.00147	-0.00141	-0.04462
D53	-1.35003	0.02447	0.00004	-0.00199	-0.00195	-1.35198
D54	-2.27238	0.01194	0.00005	-0.00134	-0.00129	-2.27367
D55	-1.58809	-0.01252	0.00005	-0.00068	-0.00063	-1.58872
D56	-0.70292	0.03508	0.00005	-0.00123	-0.00118	-0.70411

Table A.2 (cont'd)

Item	Value	Threshold	Converged?
Maximum Force	0.001241	0.002500	YES
RMS Force	0.000189	0.001667	YES
Maximum Displacement	0.006192	0.010000	YES
RMS Displacement	0.000817	0.006667	YES

Predicted change in Energy=-3.764102D-06
Optimization completed.
-- Stationary point found.

“THE PART HERE IS CUT IN ORDER TO SAVE PLACE”

C1

Z-Matrix orientation:

Center Number	Atomic Number	Atomic Type	Coordinates (Angstroms)		
			X	Y	Z
1	47	10471001	-4.533379	-2.631216	-6.102358
2	47	10471001	-2.642916	-0.452035	-6.079561
3	47	10471001	-0.752454	1.727146	-6.056763
4	47	10471001	1.138009	3.906328	-6.033965
5	47	10471001	-4.880570	-6.196760	-1.579178
6	47	10471001	-4.706974	-4.413988	-3.840768
7	47	10471001	-2.990107	-4.017579	-1.556381
8	47	10471001	-2.816512	-2.234807	-3.817971
9	47	10471001	-5.128406	-2.156958	-2.093939
10	47	10471001	-1.099644	-1.838397	-1.533583
11	47	10471001	-4.954811	-0.374186	-4.355529
12	47	10471001	-3.237943	0.022223	-2.071142
13	47	10471001	-3.064348	1.804995	-4.332732
14	47	10471001	-0.926049	-0.055625	-3.795173
15	47	10471001	0.790818	0.340784	-1.510786
16	47	10471001	0.964414	2.123556	-3.772375
17	47	10471001	-1.347481	2.201404	-2.048344
18	47	10471001	2.681281	2.519965	-1.487988
19	47	10471001	-1.173885	3.984176	-4.309934
20	47	10471001	0.542982	4.380586	-2.025547
21	47	10471001	2.854876	4.302737	-3.749578
22	47	10471001	4.571743	4.699147	-1.465190
23	47	10471001	-3.163703	-5.800350	0.705209
24	47	10471001	-1.446835	-5.403941	2.989597

Table A.2 (cont'd)

25	47	10471001	-5.302002	-3.939730	0.167650
26	47	10471001	-3.585134	-3.543321	2.452038
27	47	10471001	-3.411539	-1.760549	0.190448
28	47	10471001	-1.273240	-3.621169	0.728007
29	47	10471001	0.443627	-3.224760	3.012394
30	47	10471001	0.617223	-1.441988	0.750804
31	47	10471001	-1.694672	-1.364139	2.474836
32	47	10471001	2.334090	-1.045578	3.035192
33	47	10471001	-1.521076	0.418633	0.213246
34	47	10471001	0.195791	0.815042	2.497633
35	47	10471001	0.369386	2.597814	0.236043
36	47	10471001	2.507685	0.737193	0.773602
37	47	10471001	4.224552	1.133603	3.057990
38	47	10471001	4.398148	2.916375	0.796400
39	47	10471001	2.086254	2.994223	2.520431
40	47	10471001	6.115015	3.312784	3.080787
41	47	10471001	2.259849	4.776995	0.258841
42	47	10471001	3.976716	5.173405	2.543229
43	47	10471001	6.288611	5.095556	0.819197
44	47	10471001	0.270032	-5.007532	5.273984
45	47	10471001	-1.868267	-3.146911	4.736426
46	47	10471001	0.022195	-0.967730	4.759223
47	47	10471001	2.160494	-2.828350	5.296782
48	47	10471001	4.050957	-0.649169	5.319580
49	47	10471001	1.912658	1.211452	4.782021
50	47	10471001	3.803121	3.390633	4.804819
51	47	10471001	5.941420	1.530012	5.342377
52	8	10081000	0.658635	-1.477509	-1.115709
53	7	10071000	3.895724	-1.006705	-0.452064
54	7	10071000	4.401227	-1.803720	-1.037294

 Rotational constants (GHZ): 0.0066979 0.0048476 0.0030807

1\1\GINC-

OAR41\Scan\ONIOM(B3LYP/GenECP:UFF/ZDO)\Mixed\Ag51N2O1(2)\EVRE
 NT\03-Apr-2007\0\# opt=(modredundant,loose,maxcycle=1000)
 oniom(b3lyp/genecp:uff) nosymm geom=connectivity
 scf=(maxcycle=1000,conver=4)\\buyuk ag + O RXN\0,2\Ag,-4.533379,-2.631216,-
 6.102358\Ag,-2.642916,-0.452035,-6.079561\Ag,-0.752454,1.727146,-
 6.056763\Ag,1.138009,3.906328,- 6.033965\Ag,-4.88057,-6.19676,-1.579178\Ag,-
 4.706974,-4.413988,-3.8407 68\Ag,-2.990107,-4.017579,-1.556381\Ag,-2.816512,-
 2.234807,-3.817971\A g,-5.128406,-2.156958,-2.093939\Ag,-1.099644,-1.838397,-
 1.533583\Ag,-4 .954811,-0.374186,-4.355529\Ag,-3.237943,0.022223,-

Table A.2 (cont'd)

2.071142\Ag,-3.0643 48,1.804995,-4.332732\Ag,-0.926049,-0.055625,-
3.795173\Ag,0.790818,0.3
40784,-1.510786\Ag,0.964414,2.123556,-3.772375\Ag,-1.347481,2.201404,-
2.048344\Ag,2.681281,2.519965,-1.487988\Ag,-1.173885,3.984176,-
4.309934\Ag,0.542982,4.380586,-2.025547\Ag,2.854876,4.302737,-
3.749578\Ag,4.571743,4.699147,-1.46519\Ag,-3.163703,-5.80035,0.705209\Ag,-
1.446835,-5.403941,2.989597\Ag,-5.302002,-3.93973,0.16765\Ag,-3.585134,-
3.543321,2.452038\Ag,-3.411539,-1.760549,0.190448\Ag,-1.27324,-
3.621169,0.728007\Ag,0.443627,-3.22476,3.012394\Ag,0.617223,-
1.441988,0.750804\Ag,-1.694672,-1.364139,2.474836\Ag,2.33409,-
1.045578,3.035192\Ag,-
1.521076,0.418633,0.213246\Ag,0.195791,0.815042,2.497633\Ag,0.369386,2.59781
4,0.236043\Ag,2.507685,0.737193,0.773602\Ag,4.224552,1.133603,3.05799\Ag,4.39
8148,2.916375,0.7964\Ag,2.086254,2.994223,2.520431\Ag,6.115015,3.312784,3.080
787\Ag,2.259849,4.776995,0.258841\Ag,3.976716,5.173405,2.543229\Ag,6.288611,
5.095556,0.819197\Ag,0.270032,-5.007532,5.273984\Ag,-1.868267,-
3.146911,4.736426\Ag,0.022195,-0.96773,4.759223\Ag,2.160494,-
2.82835,5.296782\Ag,4.050957,-
0.649169,5.31958\Ag,1.912658,1.211452,4.782021\Ag,3.803121,3.390633,4.804819\
Ag,5.94142,1.530012,5.342377\O,0.6586349609,-1.4775092577,-
1.1157092383\N,3.8957237137,-1.0067049399,-0.4520635161\N,4.4012268154,-
1.8037200902,
1.0372939164\\Version=IA32LG03RevD.01\HF=250.1256427,250.1304829,250.136
0735,250.1435652,256.2610874,256.1601911,256.3232399,256.7301028,256.830170
8,257.2501913\S2=5.835392,5.832932,5.834611,5.841645,6.971662,7.010367,7.0467
39,7.089714,7.132487,7.169028\S2-
1=0.,0.,0.,0.,0.,0.,0.,0.,0.,0.\S2A=6.708786,6.699065,6.703652,6.731994,11.710652,1
1.897845,12.073301,12.280982,12.485221
,12.657284\RMSD=4.541e-05,4.904e-05,7.782e-05,4.185e-05,5.046e-05,3.704e-
05,4.601e-05,8.613e-05,7.038e-05,2.745e-
05\Thermal=0.,0.,0.,0.,0.,0.,0.,0.,0.,0.\PG=C01 [X(Ag51N2O1)]\@
ORIGINALITY CONSISTS NOT IN SAYING WHAT NO ONE HAS EVER SAID
BEFORE,BUT IN SAYING WHAT YOU THINK YOUR SELF.-- JAMES F.
STEPHEN
Job cpu time: 5 days 3 hours 33 minutes 4.6 seconds.
File lengths (MBytes): RWF= 305 Int= 0 D2E= 0 Chk= 45 Scr=1 Normal
termination of Gaussian 03 at Tue Apr 3 23:08:58 2007.

APPENDIX B

DENSITY FUNCTIONAL THEORY

Over the last fifteen years density functional theory (DFT) has strongly influenced the evolution of quantum chemistry. In contrast to the Hartree-Fock picture, which begins conceptually with a description of individual electrons interacting with the nuclei and all other electrons in the system, density functional theory allows one to replace the complicated n -electron wave function, $\Psi (r_1, r_2, \dots, r_n)$, and the associated Schrödinger equation by the much simpler electron density, $\rho(r)$, and its associated calculation scheme. It is important to note that the charge density is a function of only three variables, while the wave function contains for an n -electron system $3n$ coordinates. The rigorous foundation of density functional theory is given by Hohenberg and Kohn (1964) who proved that in essence an exact representation of the ground state properties of a stationary, non-relativistic many-body system in terms of the ground state density is possible. The theorem ensures that the exact ground state density can be calculated without resort to the Schrödinger equation from a variational principle involving only the electron density. In other words, the electron correlation energy is at least in principle included in density-functional theory. For a given system of Coulomb-interacting particles moving in an external potential, $V^{ext}(r)$, the exact ground state density and energy are obtained by minimization of the energy functional:

$$E[\rho] = T[\rho] + V_{el-el}[\rho] + \int d^3r V^{ext}(r)\rho(r) \quad (\text{B.1})$$

where $T[\rho]$ is the kinetic contribution and $V_{el-el}[\rho]$ is the electron-electron interaction functional of the electron density. These two functionals do not depend on the external potential $V^{ext}(r)$ of the system and are therefore universal (e.g. the same functional can be used for Br_2 , H_2O , Cu or Fe). The problem of DFT is that although it has been proven that each different density yields a different ground-state energy, the Hohenberg-Kohn functional, $F_{HK}[\rho] = T[\rho] + V_{el-el}[\rho]$, connecting these two quantities is not known (Heyden, 2005).

B.1.1. Kohn-Sham Equations

The Hohenberg-Kohn theorems set the foundations of density functional theory, but owing to the unknown Hohenberg-Kohn functional, in particular the kinetic energy functional, $T[\rho]$, an efficient scheme to obtain the ground state density and energy was missing. Kohn and Sham (1965) turned DFT from a theory to a practical tool for quantum chemical calculations by the introduction of the concept of a non-interacting reference system. Kohn and Sham invented an indirect approach to the kinetic energy functional, $T[\rho]$, by separating it into the kinetic energy T_S of a system of non-interacting electrons, which can be calculated exactly using orbitals:

$$T_S = \sum_{i=1}^n \int dr \phi_i^*(r) \left(-\frac{\hbar^2}{2mi} \nabla_i^2 \right) \phi_i(r) \quad (\text{B.2})$$

and a small unknown component T_C , which contains the corrections resulting from the electronic interaction. The single-particle Kohn-Sham orbitals ϕ_i , in Eqn. (B.2) are determined under the constraint to reproduce the density of the fully interacting many-body system in a self-consistent way from the Kohn-Sham equations,

$$f_{KS} \phi_i(r) = \varepsilon_i \phi_i(r) \quad (\text{B.3})$$

The Kohn-Sham operator f_{KS} is an effective one-electron operator and is given by

$$f_{KS} = -\frac{\hbar^2}{2m} \nabla^2 + V^{ext}[\rho] + E_H[\rho] + V_{XC}[\rho] \quad (\text{B.4})$$

$V^{ext}[\rho]$ is the external potential due to the nuclei, $E_H[\rho]$ is the classical Hartree potential, which is essentially the known classical part of the universal electron-electron interaction functional:

$$E_H[\rho] = V_{el-el}[\rho] - E_{non-classical}[\rho] = \frac{1}{2} \frac{e^2}{4\pi\varepsilon_0} \iint dr dr' \frac{\rho(r)\rho(r')}{|r-r'|} \quad (\text{B.5})$$

and $V_{XC}[\rho]$ is the exchange-correlation potential. The density constructed from the Kohn-Sham orbitals ϕ_i is the same as the density of the interacting system:

$$\rho(r) = \sum_{i=1}^n |\phi_i(r)|^2 \quad (\text{B.6})$$

The ϕ_i are functionals of the density, ρ , and hence, the kinetic energy, Eqn. (B.2), is also given as a functional of the density. The remaining kinetic energy part owing to the electron interaction T_C is combined with the non-classical contributions to the electron-electron interaction in the exchange-correlation functional $E_{XC}[\rho]$. As a result, the exchange-correlation functional contains everything unknown. The exchange-correlation functional is related to the exchange-correlation potential V_{XC} in Eqn. (B.4)

in that the latter is the exchange-correlation functionals derivative with respect to the density:

$$V_{xc}[\rho(r)] = \frac{\delta E_{xc}[\rho(r)]}{\delta \rho(r)} \quad (\text{B.7})$$

In summary, the essence of the Kohn-Sham scheme is the existence of an auxiliary system of a non-interacting classical electron gas, with kinetic energy T_S , subject to two external potentials: one due to the nuclei, V^{ext} , and one due to the exchange and correlation effects, V_{xc} , such that the ground-state density, $\rho(r)$, of the interacting system equals the ground-state density of the auxiliary system. The price to be paid for this scheme is the appearance of orbitals instead of just the ground-state density, $\rho(r)$. The Kohn-Sham equations, Eqn. (B.4), are one-electron equations, just as the Hartree-Fock equations, that have to be solved iteratively. The incorporation of electron correlation in these equations appears with the exchange correlation potential, $V_{xc}[\rho(r)]$, the form of which is unknown and for which no systematic strategy for improvement is available (Heyden, 2005).

B.1.2. Exchange-Correlation Functionals

With the introduction of the Kohn-Sham formalism most contributions to the total energy can be calculated exactly. The remaining unknown parts are assembled in the exchange-correlation functional. Good approximations to $E_{xc}[\rho]$ are crucial to obtain reliable results in a DFT calculation. The first attempt to find an expression for $E_{xc}[\rho]$ was based on the homogeneous electron gas for which the exact exchange-correlation energy is known. In this local density approximation (LDA) the exchange-correlation energy for the homogeneous electron gas is used for the non-homogeneous system. The basic assumption is that exchange and correlation depend only on the local value of the density. One approximates the real inhomogeneous electron density as a

sum of small cells each of which has a homogeneous electron density. It is assumed that $E_{XC}[\rho(r)]$ at position r is identical to $E_{XC}^{LDA}[\rho(r)]$ of the homogeneous electron gas of the same density. The exchange-correlation functional is then given by

$$E_{XC}^{LDA}[\rho(r)] = \int dr \rho(r) \varepsilon_{XC}(\rho(r)) \quad (\text{B.8})$$

where ε_{XC} is the exchange-correlation energy per particle of the homogeneous electron gas. $E_{XC}^{LDA}[\rho(r)]$ can be split into an exchange and a correlation contribution E_X^{LDA} and E_C^{LDA} . The exchange part can be given analytically:

$$E_X^{LDA}[\rho] = -\frac{3}{4} \left(\frac{3}{\pi} \right)^{\frac{1}{3}} \int dr \rho^{\frac{4}{3}} \quad (\text{B.9})$$

while the correlation energy is only known numerically from quantum Monte Carlo calculations from Ceperley and Alder (1980). The correlation part was parameterized by Vosko et al. (1980) and by Perdew and Wang (1992). Both parameterizations give usually very similar results.

Although the local density approximation is a rather unrealistic model for real systems, it gives for slowly varying electron densities as in simple crystalline metals very accurate results. Even for other systems it is, due to a fortunate error cancellation, often comparable to the Hartree-Fock method. However, the LDA approximation typically overestimates binding energies and underestimates bond lengths. An improvement on LDA can be achieved by including the first derivative of the electron density, $\nabla\rho$, in the exchange-correlation functional.

The exchange-correlation functional can then be written in this generalized gradient approximation (GGA) as:

$$E_{XC}^{GGA}[\rho(r)] = \int dr f(\rho(r), \nabla\rho(r)) \quad (\text{B.10})$$

Hybrid density functional theory is based on the adiabatic connection theory which states that more accurate results can be obtained by replacing some DFT exchange by Hartree-Fock exchange. Hartree-Fock exchange does not suffer from the self-interaction error of DFT, but does not include static and dynamic correlation which is inseparable from the DFT exchange. As a result, a fraction of the Hartree-Fock exchange is added to the exchange-correlation functional. The hybrid B3LYP density functional (Stephens et al., 1994) can be written as:

$$E_{XC} = (1 - a_o)E_X^{LSDA} + a_o E_X^{HF} + a_X \Delta E_X^{B88} + E_C^{LSDA} + a_C \Delta E_C^{PW91} \quad (\text{B.11})$$

Here ΔE_X^{B88} is Becke's (1988) gradient correction to the exchange functional, ΔE_C^{PW91} is the Perdew-Wang gradient correction to the correlation functional (Perdew, 1991), E_X^{HF} is the exact Hartree-Fock exchange, and E_X^{LSDA} and E_C^{LSDA} are the local spin density approximation to the exchange and correlation functional, respectively. The coefficients $a_o = 0.2$, $a_X = 0.72$, and $a_C = 0.81$ were fitted to heats of formation of small molecules.

B.1.4. Applications of DFT

There are two general approaches for modeling surface chemistry with quantum mechanics: the cluster approach and the extended band surface (or slab) approach. In the cluster approach, the local molecular fragment orbitals are explicit, thus making the local chemical interaction, chemical bonding, and charge transfer mechanism

between the adsorbate and the metal surface orbitals very easy to elucidate. This detailed level of focus, however, makes it difficult to treat the bulk electronic structure. The extended band surface approach provides a more accurate representation of the materials electronic structure. The cluster approach, instead of a continuous conduction and valance bands, is based on discrete orbitals which have specific energy gaps.

Both cluster, as well as the slab approaches, will likely to play invaluable roles in the future toward the quantitative prediction of transition metal surface chemistry (Soyer, 2005).

B.1.5. Assessment of DFT methods

The status of density functional calculations for solids, surfaces, and molecules can be described as follows.

B.1.5.1. Capability

Like Hartree-Fock methods, density functional calculations provide structural, energetic, and vibration properties. More than Hartree-Fock calculations, density functional calculations enable also the prediction of electronic, optical, and magnetic properties of condensed phases (Soyer, 2005).

B.1.5.2. Generality

The density functional approach is applicable to all atoms of the periodic table, provided relativistic effects are taken into account for heavier elements such as third-row transition metals, rare-earths, and actinides. The approach can be used for

metallic, covalent, and ionic bonds. Its greatest strength is metallic condensed systems, yet its range also includes organic molecules. With the inclusion of gradient corrections for the exchange-correlation term, even weaker interactions such as hydrogen bonds can be reasonably well described. Furthermore, so-called “difficult” molecules such as ozone seem to be treated by density functional methods with the same level of accuracy as other molecules. Within molecular applications, the approach is particularly useful for organometallic systems. Thus, in terms of generality and robustness, density functional theory seems to be superior to the Hartree-Fock approach. Local density functional calculations do encounter problems for narrow-gap insulators and certain oxides. The LDA tends to overemphasize the metallic character and one needs to be careful in the interpretation of the density functional one-electron energies. Furthermore, weaker bonds such as hydrogen bonds are significantly overestimated in the LDA. The primary results of density functional calculations are the electron density, the spin density, the total energy, and the one-particle energies and wave functions. From these quantities, one can derive important electronic, optic and magnetic properties including dipole (and higher) moments, polarizabilities and hyperpolarizabilities, and magnetic moments. LDA calculations for systems in their electronic ground state can be used to estimate electronic excitation energies including work functions, optical and UV spectra, and core level spectra for solids, surfaces, and molecules (Soyer, 2005).

B.1.5.3. Accuracy

Quite consistently, for a great number of strong bonds in solids, molecules, and surfaces, interatomic equilibrium distances are predicted by precise density functional calculations to within about 0.02 Å of experiment; bond angles and dihedral angles are found within a few degrees of their experimental values. Within the local density approximation, binding energies are typically overestimated, sometimes by as much

as a factor of two. Inclusion of non-local gradient corrections improves the values of binding energies and brings them to within about 10 kJ/mol of experiment. The results obtained at this level of theory are comparable with sophisticated correlated quantum mechanical methods such as coupled cluster theory. Vibration frequencies are predicted to be within 10-50 cm^{-1} (Soyer, 2005).

At present, there is no clear theoretical path that would allow the systematic improvement of the accuracy of density functional methods. This is a major conceptual difference to Hartree-Fock based methods, where at least in principle there is a way for systematic improvements. Practical density functional calculations involve numerical integrations in addition to the evaluation of analytical expressions. These numerical integrations introduce a numerical noise that can be noticed, for example, in geometry optimizations of highly flexible molecules. By increasing the size of the numerical grid, this numerical noise can be controlled, though at the expense of computational effort. This is in contrast to Hartree-Fock methods, which are usually implemented in a completely analytical way. Thus, the numerical precision of Hartree-Fock calculations is limited by the machine precision (typically 14 decimal figures) whereas the precision of density functional calculations is governed by the grid resolution. One could argue that if a theory has a certain inherent error compared with experiment, any computational approach that gives results within that error range is acceptable and any improvement in numerical precision has no physical meaning. On the other hand, it can be desirable, for example in the investigation of subtle trends, to have a high numerical precision (Soyer, 2005).

B.1.5.4. System Size

Density functional calculations are possible for systems of the order of 100 atoms. By exploring point-group symmetry, calculations for clusters of over 1000 atoms have been demonstrated for fixed geometries. While the self-consistent-field procedure

converges typically in 10-20 iterations for organic materials and semiconductors, metallic systems and especially magnetic transition metals such as Fe and Ni are very difficult to converge. In practice, this limits the size of systems that can be treated to perhaps less than 60 atoms per unit cell or cluster (Soyer, 2005).

B.1.5.5. Tractable Time Scale

Recently, density functional calculations have become possible for studying dynamic phenomena. However, for a system with about 100 atoms, accurate density functional calculations are about 1000 times slower than force field calculations, thus reducing the accessible time scales to the range of picoseconds. In practice, the Car-Parrinello method is presently used for structure optimizations by simulated annealing rather than for dynamic simulations, which has been done so far only for a few cases (Soyer, 2005).

B.1.5.6. Computational Efficiency

Depending on the system under investigation, for example a metallic alloy or a molecular crystal, density functional theory can be implemented in quite different ways thus leading to efficient methods for particular materials. On the other hand, practical Hartree-Fock methods require the use of Gaussian basis functions, which can be fairly inefficient, for example for close-packed systems. Thus, in general, density functional theory tends to be computationally more efficient than Hartree-Fock calculations. Without doubt, compared with correlated post-Hartree-Fock methods, density functional calculations are by far more efficient computationally, scaling at worst with a third power in the number of basis functions. In fact, significant effort is dedicated to the development of so-called order-N methods, i.e. methods for which the computational effort increases linearly with system size. Such methods have been successfully demonstrated, yet the pre-factor is rather large so that these methods are

competitive with conventional density functional implementations only for systems with several hundred atoms. In molecular calculations it can be important to calculate vibration frequencies in order to determine ground state structures, transition states, and to predict infrared spectra (Soyer, 2005).

In Hartree-Fock theory, this approach is well established, whereas the evaluation of vibration frequencies (i.e. the calculation of the second derivatives of the total energy with respect to nuclear displacements) for molecular density functional is been done by a finite difference technique using analytic first derivatives. This is computationally not very efficient compared with analytical methods. While this type of calculation has been used for density functional methods within the pseudopotential plane wave approach for some time, the implementation of analytic second derivatives in localized orbital density functional calculations is a fairly recent development. However, this type of calculation is quite time consuming and may require supercomputer resources for larger molecules (Soyer, 2005).